

Aus der Fakultät für Medizin
der Universität Regensburg
Prof. Tobias Pukrop
Hämatologie/Onkologie

Targeting the ROS-defense of tumor cells as a therapeutic strategy against brain
metastasis

Inaugural – Dissertation
zur Erlangung des
Doktorgrades der Medizin

der
Fakultät für Medizin der
Universität Regensburg

vorgelegt von
Ellinor Görgen

2023

Aus der Fakultät für Medizin
der Universität Regensburg
Prof. Tobias Pukrop
Hämatologie/Onkologie

Targeting the ROS-defense of tumor cells as a therapeutic strategy against brain
metastasis

Inaugural – Dissertation
zur Erlangung des
Doktorgrades der Medizin

der
Fakultät für Medizin der
Universität Regensburg

vorgelegt von
Ellinor Görgen

2023

Dekan: Prof. Dr. Dirk Hellwig

1. Berichterstatter: Prof. Dr. Tobias Pukrop

2. Berichterstatter: PD Dr. Katja Dettmer-Wilde

Tag der mündlichen Prüfung: 23.06.2023

List of Contents

List of Contents	I
List of Figures.....	III
List of Tables	III
Abbreviations.....	IV
1 Introduction.....	1
1.1 Brain metastasis.....	1
1.1.1 Definition, prevalence and epidemiology.....	1
1.1.2 Therapy options	1
1.2 Steps of metastatic cascade.....	4
1.2.1 Colonization	6
1.3 Immune defense.....	7
1.3.1 ROS metabolism.....	9
1.4 Aim of the study.....	12
2 Materials and Methods	13
2.1 Materials.....	13
2.1.1 Cell lines	13
2.1.2 Cell culture media and additives	13
2.1.3 Chemicals, enzymes and other reagents	14
2.1.4 Kits	17
2.1.5 crRNA	18
2.1.6 Antibodies	19
2.1.7 Oligonucleotides.....	19
2.1.8 Consumables	23
2.1.9 Equipment and software	25
2.2 Methods.....	26
2.2.1 Cell culture methods	27
2.2.2 Protein biochemistry.....	31
2.2.3 Gene expression analysis	34
2.2.4 Flow cytometry methods	37
2.2.5 T7 Endonuclease 1 Assay	38

2.2.6 Sequencing	41
2.2.7 XO Activity measurement.....	45
2.2.8 Statistical analysis.....	46
3 Results.....	46
3.1 Xdh and BlvrB are highly expressed in the more aggressive cell lines.	46
3.2 Pharmacological inhibition of XDH and BLVRB.....	48
3.1.2 Effect of Xdh inhibition on EO771-LG and CT26 in vitro	48
3.1.3 Effect of BlvrB inhibition on EO771-LG and CT26 in vitro	51
3.2 Genetic inhibition of Xdh and BlvrB	53
3.2.1 CRISPR/Cas9- transfection is more efficient in CT26 than in EO771-LG .	53
3.2.2 Xdh-knockout via CRISPR/Cas9 is more efficient than BlvrB-knockout	55
3.2.3. Sanger Sequencing of Xdh-KO clones.....	59
3.2.4. Next-Generation-Sequencing of Xdh-KO clones.....	59
3.3. Functional characterization of Xdh-KO clones.....	61
3.3.1 RNA	61
3.3.2 Protein.....	61
3.3.3 The CRISPR/Cas9-treated cells show no difference in morphology and cell metabolic activity.....	62
3.3.3 Xanthine oxidase assay shows no difference in KO cells compared to controls	64
3.3.4 ROS-measurement	64
4 Discussion	65
4.1 Xdh and BlvrB confirmed as targets	66
4.2 CRISPR/Cas9 knock-out as a stable model for Xdh-deprivation.....	66
4.3 XDH expression – survival advantage or highway to hell?	68
4.4 XDH as ROS quencher or ROS producer?	69
4.5 Pharmacological inhibition of BLVRB still uncertain	73
4.6 Outlook.....	74
5 Summary and conclusions	75
6 Literaturverzeichnis.....	77
Acknowledgements.....	84
Curriculum Vitae.....	86
Supplemental material	88

List of Figures

Figure 1: Model of metastatic colonization.....	5
Figure 2: Organ defense in metastatic colonization.....	8
Figure 3: Reaction of BVR.....	10
Figure 4: Reactions of XOR.....	11
Figure 5: Model of catalytic sites of XOR.....	12
Figure 6: Model of Xdh and Blvrb with gRNAs targeting genes.	29
Figure 7: T7 Endonuclease Assay to confirm transfection efficiency.....	39
Figure 8: Sanger Sequencing.....	42
Figure 9: Colonization Index of breast and colon cancer.....	47
Figure 10: Western Blot of Xdh and Blvrb.....	47
Figure 11: Analysis of EO771-LG and CT26 treated with Xdh-i.....	49
Figure 12: Influence of Febuxostat on protein and gene expression of Xdh.	50
Figure 13: ROS-measurement after Febuxostat inhibition.....	51
Figure 14: Analysis of EO771-LG and CT26 treated with Blvrb-i.....	52
Figure 15: Influence of Phloxine B on protein and gene expression of Blvrb.....	53
Figure 16: FACS results of EO771-LG and CT26 after transfection.....	54
Figure 17: Summary of T7 Endonuclease 1 Assay for Blvrb-KO.....	56
Figure 18: Summary of T7 Endonuclease 1 Assay for Xdh-KO.....	58
Figure 19: Sanger Sequencing results of CRISPR/Cas9 samples.	59
Figure 20: Summary of NGS.	60
Figure 21: qRT-PCR of CT26 Xdh-KO clones.....	61
Figure 22: Western Blot and quantification comparing the CRISPR-treated CT26 KO cells with the controls.....	62
Figure 23: Morphology of CT26 Xdh-KO cells.....	63
Figure 24: MTT analysis of CT26 Xdh-KO and controls.....	63
Figure 25: XO activity assay of CT26 Xdh-KO cells.....	64
Figure 26: Analysis of ROS production through DCFDA assay.....	65

List of Tables

Table 1: Cell lines.....	13
Table 2: Media and additives.....	13

Table 3: Chemicals, enzymes and other reagents.....	14
Table 4: Kits.....	17
Table 5: cRNAs	18
Table 6: Antibodies	19
Table 7: Oligonucleotides	19
Table 8: Consumables.....	23
Table 9: Equipment and software	25
Table 10: Nomenclature of CT26 Xdh-KO cells.....	30

Abbreviations

5-FU	5-fluorouracil
ALK	anaplastic lymphoma kinase
APS	ammonium persulfate
BBB	blood-brain-barrier
Blv, Blvr	biliverdin reductase
Blvra	biliverdin reductase A
Blvrb	biliverdin reductase B
BRAF	B-rapidly growing fibrosarcoma
BrdU	bromodeoxyuridine
BSA	bovine serum albumin
BTB	blood-tumor-barrier
cDNA	complementary deoxyribonucleic acid
CNS	central nervous system
CRC	colorectal cancer
CRISPR	clustered regularly interspaced short palindromic repeats
crRNA	crispr ribonucleic acid
CTLA-4	cytotoxic T-lymphocyte-associated protein 4
DCF	2',7'-dichlorofluorescein
DCFDA	2',7'-dichlorofluorescein diacetate
ddNTP	dideoxyribonucleoside triphosphate
DEP	differentially expressed protein
DMEM	Dulbecco's modified eagle medium
DMSO	dimethyl sulfoxide
DNA	deoxyribonucleic acid
dNTP	deoxyribonucleoside triphosphate

dsRNA	double-stranded deoxyribonucleic acid
EDTA	ethylenediaminetetraacetic acid
EGFR	epidermal growth factor receptor
ER	estrogen receptor
FACS	fluorescence-activated cell sorting
FAD	flavin adenine dinucleotide
FCS	fetal calf serum
Gapdh	glyceraldehyde 3-phosphate dehydrogenase
GOI	gene of interest
gRNA	guide ribonucleic acid
GSH	glutathione
HER2	human epidermal growth factor receptor 2
HO-1	heme oxygenase 1
HPRT	hypoxanthine-guanine-phosphoribosyltransferase
HRP	horseradish peroxidase
HSP90	heat shock protein 90
INDEL	insertion or deletion
KO	knock-out
KRAS	Kirsten rat sarcoma viral oncogene
LEF1	lymphoid enhancer-binding factor 1
MAPK	mitogen-activated protein kinase
MFI	mean fluorescence intensity
MMLV	Moloney murine leukemia virus
MMP	milk powder
MMPI	macro-metastasis/organ parenchyma interface
Mo	molybdopterin
MRI	magnetic resonance imaging
mRNA	messenger ribonucleic acid
MTT	3-(4,5-dimethylthiazol-2-yl)-2,5-diphenyltetrazolium bromide
n.s.	non-significant
NC	negative control
NGS	next generation sequencing
NHEJ	non-homologous end joining
NRAS	neuroblastoma-rat sarcoma viral oncogene

NSCLC	non-small cell lung cancer
OAS	overall survival
PAGE	polyacrylamide gel electrophoresis
PAM	prototype adjacent motif
PBS	phosphate-buffered saline
PCR	polymerase chain reaction
PD-1	programmed cell death protein 1
PD-L1	programmed cell death 1 ligand 1
Pgk1	phosphoglycerate kinase 1
PR	progesterone receptor
QoL	quality of life
qRT-PCR	quantitative real-time polymerase chain reaction
RMS	rhabdomyosarcoma
RNA	ribonucleic acid
RNP	ribonucleoprotein
ROS	reactive oxygen species
SCLC	small cell lung cancer
SD	standard deviation
SDS	sodium dodecyl sulfate
SEM	standard error of the mean
SOD	superoxide dismutase
SRS	stereotactical radiosurgery
ssDNA	single-stranded deoxyribonucleic acid
T7E1	T7 endonuclease 1
tBHP	tert-butyl-hydroperoxide
TBST	tris-buffered saline with Tween 20
TEMED	tetramethylethylenediamine
TKI	tyrosine kinase inhibitors
TME	tumor microenvironment
tracrRNA	trans-activating CRISPR ribonucleic acid
Uox	uricase
VEGF	vascular endothelial growth factor
WBRT	whole-brain radiation therapy
WT	wildtype

Xdh	xanthine dehydrogenase
Xo	xanthine oxidase
Xor	xanthine oxidoreductase

1 Introduction

1.1 Brain metastasis

1.1.1 Definition, prevalence and epidemiology

Brain metastasis occurs when a malignant cancer, often melanoma, breast, lung or colon cancer, spreads to the brain. Brain metastases are the most common malignancy in the brain (Focusing on brain tumours and brain metastasis 2020). Approximately 10 – 40% of patients with cancer develop brain metastases in the course of their disease (D'Andrea et al. 2017). Unfortunately, to this day, the prognosis is still very poor, with a mean 2-year and 5-year survival rate for all primary tumor types of 8.1% and 2.4%, respectively (Achrol et al. 2019). The incidence of brain metastasis in breast cancer is 5-20%, and that of colorectal cancer has significantly increased in the last years to approximately 13% (Nieder et al. 2011). The unique immune microenvironment, anatomical prerequisites (e.g., blood-brain-barrier) and metabolic demands make the brain a challenging target for antitumor therapy (Boire et al. 2020). The treatment options for melanoma and NSCLC brain metastasis have evolved over the last years, partly through the therapeutic use of immunotherapies (Achrol et al. 2019). To date, such results have not been reached for the treatment of colon and breast cancer brain metastasis. These facts highlight the urgent need for further research in the field of brain metastasis.

1.1.2 Therapy options

The standard care of brain metastasis to date is highly dependent on the number of metastases, the location, the primary tumor, the performance status of the patient and of course individual factors as the patients wish. In the following, the most commonly used and most promising therapies are briefly explained.

1.1.2.1 Surgical resection

Upon the first symptoms of brain metastasis, including nausea, vertigo, headache, hemi symptomatic paralysis, and overall signs of intracranial pressure, patients are often in a state of disease that is far advanced. However, the clinical impression and performance status of the patient might still be incongruent with the progress of the disease. In those cases, to relieve the symptomatic burden of brain metastasis, surgery

is often considered. The amount of resected tissue can make it possible to analyze the tumor microenvironment and the Macro-metastasis brain parenchyma interface (MMPI), which is of increasing interest. Both are especially important for further targeted therapies, immunotherapies and clinical decision making.

Overall, surgical methods have evolved to very minimally invasive surgery with a low risk for the patient (depending on the performance status and other prognostic indices) and significant developments in guided neurosurgery (i.e., MRI guided), increasing the importance of the field for treatment of brain metastasis.

1.1.2.2 Radiotherapy

1.1.2.2.1 Whole Brain Radiation Therapy (WBRT)

The WBRT used to be the standard procedure to treat patients with brain metastasis, mainly because of the advantages of quick initiation of therapy after the diagnosis, extensive availability, and the idea of treating possible disseminated cancer cells in addition to the known tumor site. However, this frequent use reduced in the last years, although being the most frequently used radiation therapy for brain metastasis (Kann et al. 2017). This reduction is mostly due to many impairments for the treated patients concerning their neurological development. The overall cognitive function is often worsening, which also reduces the quality of life for patients with an advanced cancerous disease. On top of that, there is inconsistent data as to whether WBRT is significantly changing the OS compared to the more evolving local application of radiation (described below).

1.1.2.2.2 Stereotactical Radiosurgery (SRS)

In order to reduce the toxic effects of radiation on the brain, a technique sparing most of the healthy brain tissue has come to attention, the so-called stereotactical radiosurgery (SRS). The treatment minimizes the amounts of radiation on all other regions than the metastatic lesion by working in a three-dimensional manner with several radiation beams, all focused on the region of interest. SRS is commonly used for the treatment of multiple brain lesions (up to 10), compromising cognitive function to a lesser extent than WBRT. SRS has also been functioning as adjuvant therapy after surgical metastasis resection (Brown et al. 2017).

1.1.2.3 Systemic therapies

1.1.2.3.1 Chemotherapy

In the systemic treatment of brain metastasis, conventional chemotherapies like cisplatin, etoposide, paclitaxel, pemetrexed, temozolomide have been tested alone or in combination for different types of primary tumors. One difficulty with conventional chemotherapies in brain metastasis is the BBB and the blood-tumor-barrier (BTB). Most drugs used are not able to penetrate the brain, nor are they penetrating the tumor sufficiently when having reached it. However, temozolomide, for instance, has shown rather promising results for other tumor types (e.g. glioma) that are located in the brain and is, therefore, one of the more often used chemotherapeutic drugs in metastatic brain lesions in studies, alone or in combination (Christodoulou et al. 2005). Among the therapy of NSCLC, triple-negative breast cancer, melanoma and SCLC, the latter has shown to be a rather good candidate for chemotherapy, likely due to its highly aggressive character. For ER-, PR-, and Her2-positive breast cancer, there are more specialized therapies available in clinical use aiming at the hormonal overexpression, which increased OS (Yap et al. 2012; Le Scodan et al. 2011). To this day, treating melanoma brain metastasis with standard chemotherapy regimens has not proven to be successful (Larkin et al. 2007). However, for melanoma patients, the new findings regarding targeted and immunotherapies have massively increased therapy response and OS (mentioned below).

Not to be forgotten, chemotherapy includes many adverse effects, including hair loss, bone marrow suppression, stomatitis, nausea, amongst others. Thus, the need for better treatment strategies has become apparent in the last years. More personalized therapy options are explained in the following.

1.1.2.3.2 Targeted therapy

As for new therapeutic options, targeted therapy approaches have arisen in the last few years. These therapies aim at specific mutations in the tumor with the goal to enhance the anti-tumor effect by reaching all tumor cells with that specific mutation and subsequently reduce adverse effects in healthy cells not carrying the mutation. This strategy has proven to work for tyrosine kinase inhibitors (TKI), commonly used to treat solid tumors and their metastases with an EGFR mutation, like NSCLC. Another important application of targeted therapy has been the malignant melanoma,

which previously had no good treatment options, especially in an advanced stage of the disease with brain metastases present. BRAF, KRAS, EGFR and NRAS mutations have come to attention for several tumors, colorectal cancer (CRC) being one of them. In addition to the mutations mentioned above, numerous tumor entities often have an altered VEGF-status in common, enabling treatment options with VEGF-inhibitors such as bevacizumab.

However, there are limitations to targeted therapy as well. First, the BBB penetration is as much of a problem as with conventional chemotherapy. Second, there is the challenge of the tumor and its metastases continually changing and accumulating mutations and epigenetic variations. This complicates treatment, making it necessary to change a previously well-tolerated therapy regimen. However, recent studies have reported that a certain time pause in tumor treatment can reverse epigenetic alterations possibly responsible for drug resistance (Obenauf et al. 2015).

1.1.2.3.3 Immunotherapy

The importance of tumor microenvironment (TME) and consequently, the possibility of therapeutic strategies targeting the individual TME, has come to attention in research in the last years. Checkpoint inhibition has shown to be a very promising strategy in the treatment of not only the primary tumor, which is often NSCLC or melanoma, but also brain metastases. This therapy targets the tumor-induced immunosuppression through T-cells expressing PD-1/PD-L1 and CTLA-4 (Quail und Joyce 2017). By inhibiting the immunosuppression mediated by the tumor with antibodies for PD-1/PD-L1 (e.g. pembrolizumab and atezolizumab, respectively) alone or in combination with CTLA-4-targeted inhibition (ipilimumab), therapy response has increased immensely from previously 4 – 5 months OS to a 1-year survival rate of 81.5 % and 2-year-survival of approximately 70 % for melanoma patients with brain metastases (Tawbi et al. 2018).

1.2 Steps of metastatic cascade

To get closer to the establishment of a promising therapy against brain metastasis, it is crucial to understand how tumor cells get to metastasize. Several steps enable the tumor cells to intravasate into lymph and/or blood vessels. The cells that survive this intravasation start to colonize the target organ. During colonization, micro-metastases

(< 2 mm) grow to macro-metastases (2 – 10 mm). Usually, the lesions are detected in the last step when the target lesion (≥ 10 mm) becomes discernible (Blazquez et al. 2020a)) (Figure 1).

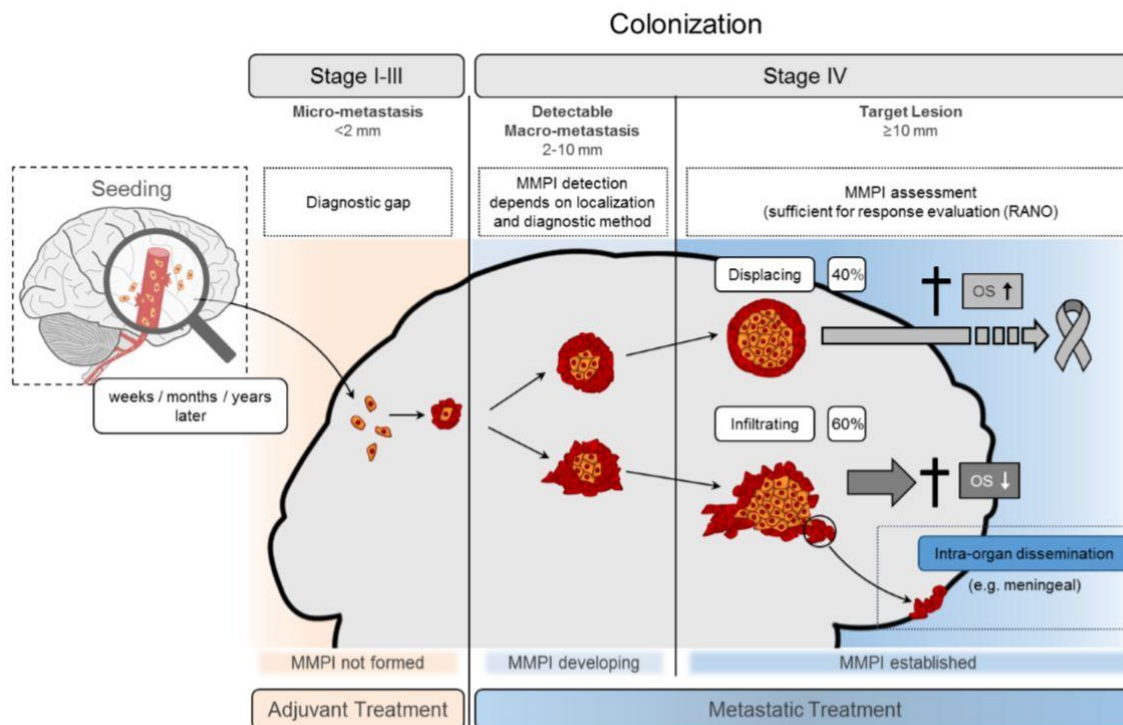


Figure 1: Model of metastatic colonization

After having intravasated into surrounding vessels, the tumor cells start to seed throughout the organism. The re-proliferation process can take place weeks, months, years or even not at all after the initial seeding. If cells are proliferating, the MMPI can generally be assessed after the metastasis has developed from micro- (<2 mm) to macro-metastasis (2–10 mm) or even to a target lesion (≤ 10 mm). The general subtype of MMPI varies from displacing (40%) to infiltrating (60%), with displacing MMPIs reporting a longer OAS in patients. Infiltrating MMPI patterns can then disseminate throughout the complete organ (Taken from (Blazquez et al. 2020a)).

According to the current understanding of metastasis formation, a tumor needs to present a certain genetic variation, known as heterogeneity, in order to metastasize (Marusyk and Polyak 2010). There are two main theories to explain tumor development. The “branched evolution” theory, stating that the tumor continuously gains several mutations throughout its development; and the “punctuated evolution” theory, meaning a massive burst of mutations was acquired in the beginning of tumor development are the predominant theories (Davis et al. 2017). However, the main belief at the time consists of multiple evolutions taking place at different times of the

tumor development, i.e. a starting burst of mutations followed by continuously accumulating point mutations. The consequence of this understanding is that the seeding of the tumor cell does not necessarily happen after the primary tumor becomes apparent. More likely, the seeding happens at any time point during tumor development, making it an unlikely target for metastasis prevention.

Every cell of the primary tumor can potentially mutate in a way that makes it possible for the cell to lose adherence to the primarius, intravasate and disseminate through hematogenic or lymphogenic pathways. Fortunately, most tumor cells do not survive this process (van Zijl et al. 2011). Moreover, even if the cells arrive at the target organ, they still have to survive the attack the organ defense and adapt to the foreign microenvironment (Steeg 2006; Kienast et al. 2010). Thus, the colonization is the most inefficient step of the metastatic cascade (Ganesh und Massagué 2021).

Still, if this step is successful, the intra-organ dissemination can take place, and the metastases can become clinically apparent. Importantly, since by that time, every other step of the metastatic cascade has already taken place, the colonization is the only therapeutically targetable step.

1.2.1 Colonization

As already mentioned, the colonization process is the most inefficient of the steps in metastasis formation. However, it is one of the most important steps concerning therapeutical targeting. Here, it is determined whether a micro-metastasis develops into a macro-metastasis, which pattern of macro-metastasis/organ-parenchyma interface (MMPI) develops and subsequently the impact on clinical deterioration through further dissemination in the affected organ is established. A prerequisite for a micro-metastasis to develop into a macro-metastasis is the overcoming of the organ immune response. It has been described very early that malignant cells need to express a defense mechanism against the host immune defense, i.e. by expression of matrix metalloproteinases, to metastasize and survive (Fidler und Kozlowski 1984). If the previously seeded tumor cells have no established defense mechanism, they will not be able to overcome the host immune response, which in part works through generation of ROS by macrophages/microglia in the brain (Jay Forman 2001). The majority of tumor cells don't express a sufficient coping mechanism against this respiratory burst and then die in the process of colonization (Fidler 1970). Very few

cells, however, do manage to survive. These few cells then excel in colonization of the brain parenchyma and even manage to misuse the local defense to their advantage (Hohensee et al. 2017; Chuang et al. 2013; Pukrop et al. 2010).

The respiratory burst the tumor cells must face occurs not only through the host immune defense. The high proliferation also serves as a source of ROS (e.g., superoxide, nitric oxide, hydroperoxide), mainly through ROS production in mitochondria, during the electron transfers in complex I, III and IV in the respiratory chain (Balaban et al. 2005; Valko et al. 2006; Andreyev et al. 2015), and also in the peroxisome and the cytosol (Forrester et al. 2018). The produced ROS may then harm the genetic material of the cell. This renders it likely that there is an evolutionary advantage for highly proliferating tumor cells with a good ROS coping mechanism.

In addition to that, many systemic and local cancer therapies enhance cell death by inducing ROS (Chung et al. 2020). The different types of ROS-mediated cell death may include, e.g., apoptosis or ferroptosis (Dixon und Stockwell 2014; Li et al. 2020). In accordance with these observations, chemoresistance was found to be partly mediated by ROS quenching mechanisms (Xue et al. 2020; Patel et al. 2017) .

These findings highlight the importance of ROS in the colonization process. The ROS defense in tumor cells is therefore an important target in further therapeutic strategies, which could reduce tumor burden and inhibit further dissemination before it becomes clinically apparent.

1.3 Immune defense

In recent years, the role of macrophages has been studied more extensively, especially in inflammatory states and their respective role in immune defense. Among others, brain metastasis and brain injury have been investigated (Larger und Felding-Habermann 2010; Davalos et al. 2005) and macrophages/microglia have shown to rapidly migrate to places of attack, containing the intruder or inflammation via several mechanisms. In the case of metastatic brain colonization, the tumor cells have shown to interact in four different ways with the immune cells. For one thing, a very highly

investigated mechanism is the so-called shielding, which relies on immune cells (microglia, neutrophils) containing the cancer cells and dampening the immune response (Uderhardt et al. 2019; Culemann et al. 2019)). Another way is the induction of apoptosis as has been observed by our group (Chuang et al. 2013). We have already described another important mechanism, in which the tumor cells misuse the immune cells to their advantage with the result of improved colonization (Pukrop et al. 2010). However, there is also the possibility of the immune cells to attack cancer cells by producing a respiratory burst which functions through ROS release. Tumor cells escaping this mechanism have been proposed to colonize better and therefore have a survival advantage, which will be elaborated in the following (Blazquez et al. 2018).

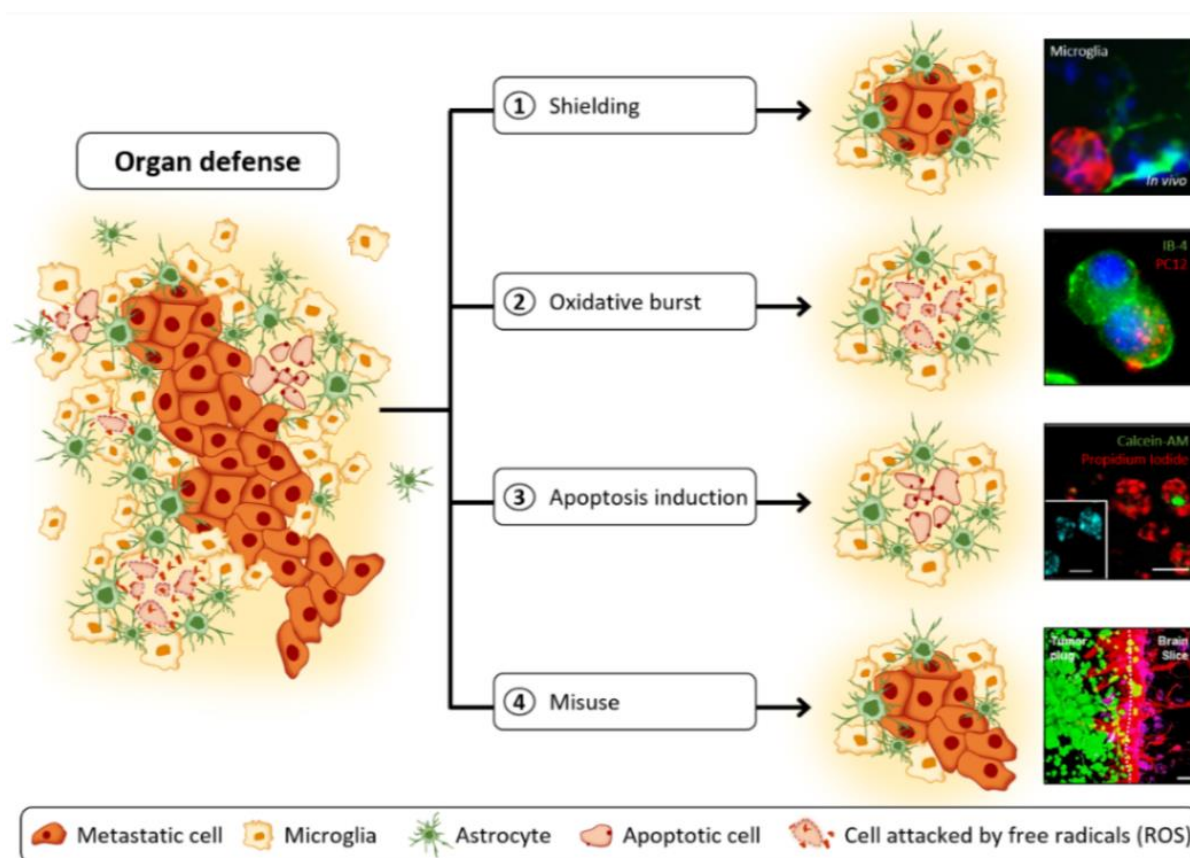


Figure 2: Organ defense in metastatic colonization

Immune cells interact with cancer cells by (1) shielding, (2) producing an oxidative burst with ROS, (3) induction of apoptosis or by being misused by the tumor cells to facilitate colonization (4). Taken from Blazquez et al., unpublished data.

1.3.1 ROS metabolism

Previous work of our group has established that the EMT transcription factor LEF1 enhances colonization in brain tissue. Interestingly, it was seen that it does not do so by stimulating epithelial-to-mesenchymal transition (EMT) as it is generally thought, but by enhancing the ROS metabolism of the cells (Blazquez et al. 2020b) Through a proteomic comparison, several proteins related to GSH metabolism were identified in the high colonizing LEF-overexpressing cancer cells. This led us to believe, that metabolic and detoxifying properties played an important role in the improved colonization capacity of the LEF1-overexpressing cells. Among these ROS-related proteins that were higher expressed in the highly colonizing cells, *Xdh* and *Blvrb* seemed to be promising targets.

1.3.1.1 *Blvrb* and *Xdh* as potential therapeutic targets

The biliverdin reductase exists in two forms, biliverdin reductase α (BVR-A or BLVRA) and biliverdin reductase β (BVR-B or BLVRB). The BLVRB is mostly involved in the reduction of biliverdin-IX β , -IX γ and -IX δ , while BLVRA also catalyzes the reduction of the biliverdin-Ix α isomer (Franklin et al. 2009). Biliverdin is reduced into bilirubin, which acts as a ROS quencher, especially in the lipid peroxidation (Stocker et al. 1987), as displayed in Figure 3.

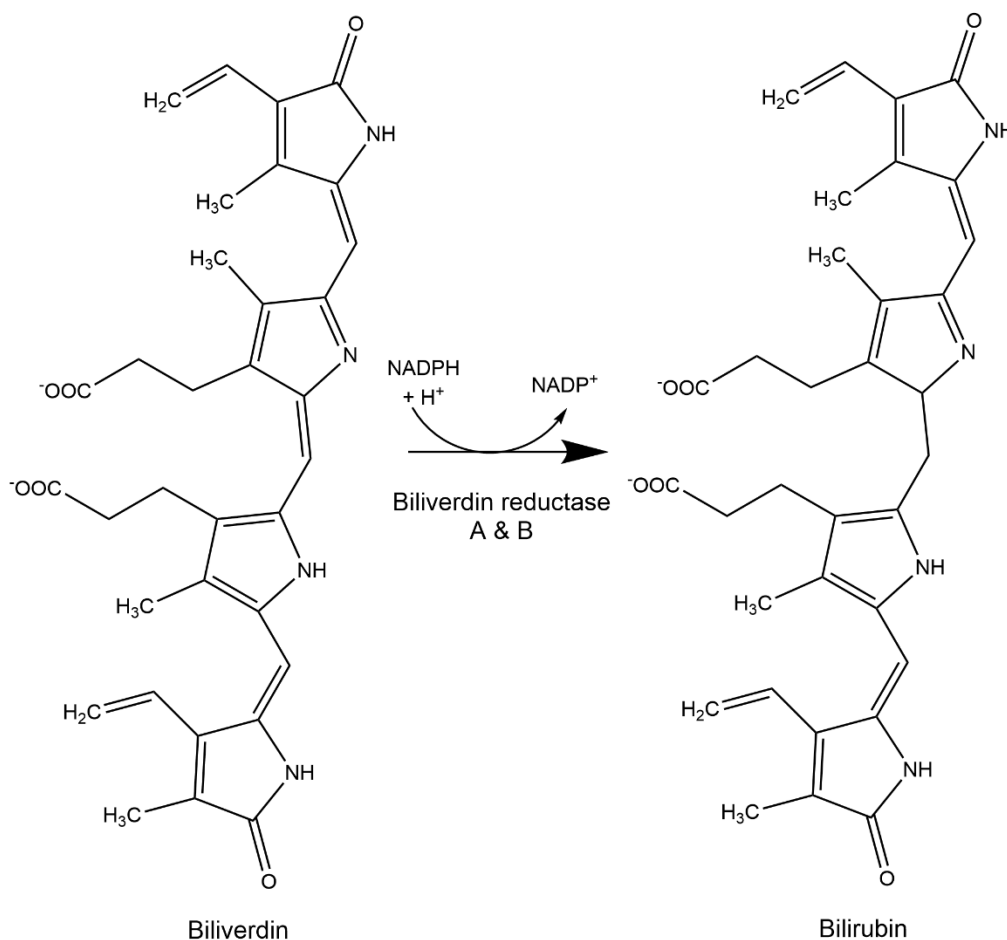


Figure 3: Reaction of BVR.

Biliverdin reductase isoforms A & B are catalyzing the conversion of biliverdin-IX α , - β , - γ , - δ to bilirubin, an endogenous ROS quencher, by using NADPH and H⁺ and converting it to NADP⁺.

The role of XDH concerning the ROS metabolism and its oxidant or antioxidant capacities is widely discussed in literature. On the one hand, in the primary reaction catalyzed by the enzyme XDH, one of the byproducts is uric acid. Uric acid has been known for a long time to be an effective antioxidant (Ames et al. 1981). XDH is connected to the GSH metabolism through the superoxide dismutase, linking the two possible ROS scavenging mechanisms in the tumor cell.

On the other hand, XDH is one isoform of the enzyme xanthine oxidoreductase (XOR), xanthine oxidase (XO) being the other isoform. XO is generally seen as the isoform reacting with oxygen, resulting in superoxide and hydroxyl peroxide, while XDH seems to be mostly involved in the NAD⁺/NADH-dependent mechanism (Fig. 4). However, it is known that XDH can also produce reactive oxygen species in a hypoxic environment

(Battelli et al. 2016b). The isoforms can convert into each other either irreversibly through proteolysis or reversibly through the oxidation of sulfhydryl groups. XOR contains three important cofactor binding sites, one binding 2 [2Fe-S2] clusters and the other two binding molybdenum-molybdopterin and FAD (Amaya et al. 1990) (Fig. 5).

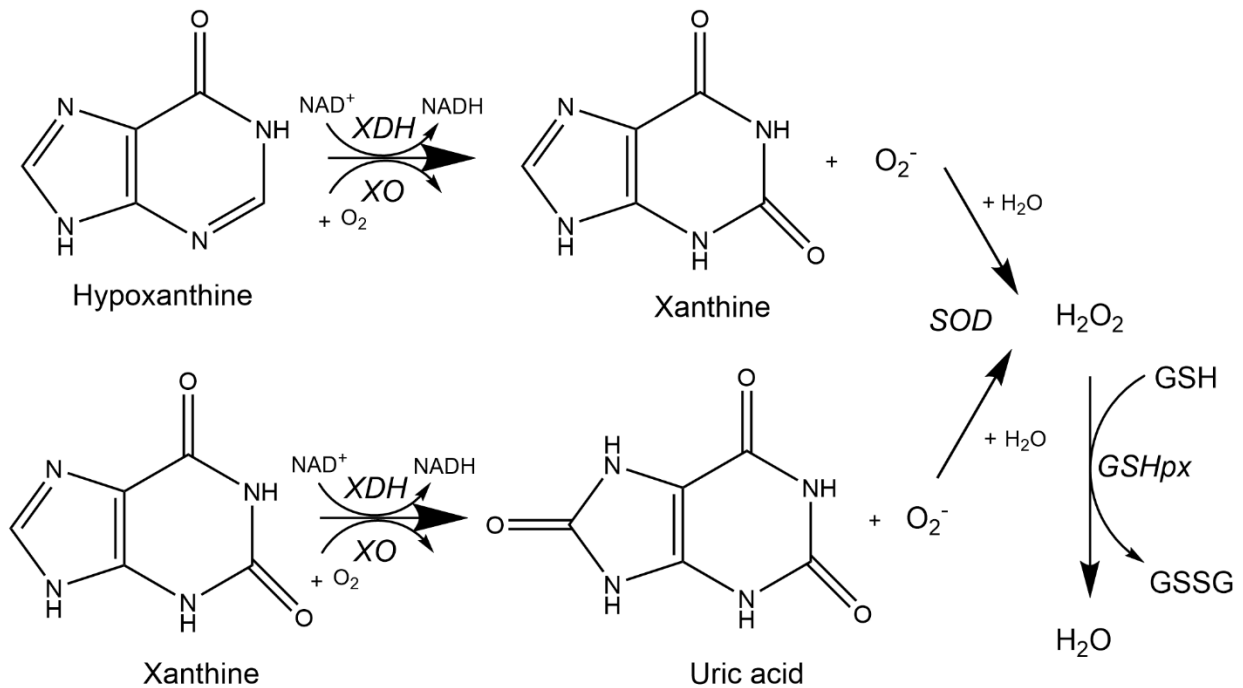


Figure 4: Reactions of XOR.

Brief description of reactions linking XDH and XO to GSH metabolism through superoxide dismutase (SOD) and GSH peroxidase (GSHpx). The byproduct superoxide (O₂⁻) is rapidly converted by SOD to the highly reactive hydroxyl peroxide (H₂O₂), which is in turn processed by GSH peroxidase (among others) to H₂O.

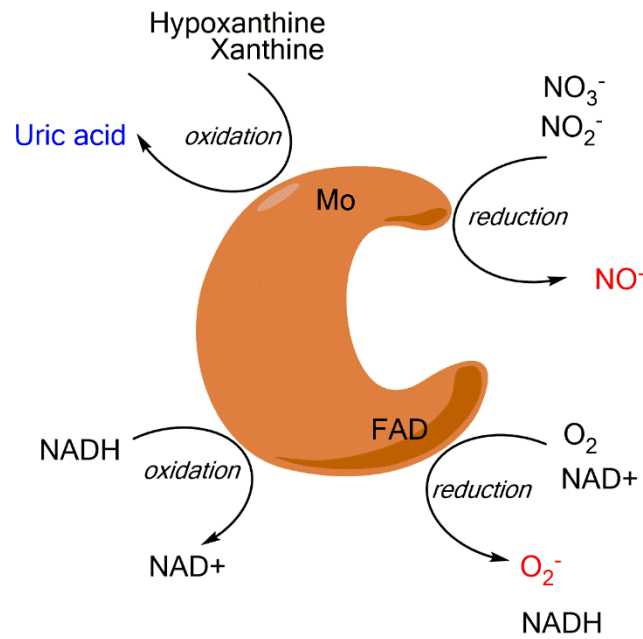


Figure 5: Model of catalytic sites of XOR.

Depicted are the most important reaction sites of the enzyme in the context of ROS metabolism. The molybdopterin-containing site is catalyzing the oxidation of hypoxanthine to xanthine and xanthine to uric acid, as well as the reduction of nitrate and nitrite to nitric oxide. The FAD site is mostly responsible for the oxidation of NADH to NAD⁺ and the reduction of oxygen to superoxide. ROS-scavengers (blue) and ROS (red) are produced in the process. XDH is mostly active at the molybdopterin site and the NADH-dependent FAD site, while XO is active at the molybdopterin site and the O₂-dependent FAD site.

1.4 Aim of the study

The goal of this project is to generate Xdh and Blvrb deprived cell lines and to evaluate the influence on ROS metabolism and cell viability. This will be achieved through pharmacological inhibition of the enzymes of interest and through a genetic knock-out of the genes of interest in a CRISPR/Cas9-mediated approach in the colon and breast cancer cell lines CT26 and EO771-LG, respectively.

2 Materials and Methods

2.1 Materials

2.1.1 Cell lines

The cell lines used in this thesis are listed in Table 1.

Table 1: Cell lines

Name	Cell type / Species	Background	Origin / Obtained from	Reference
EO771-LG	mouse breast cancer	C57BL/6N	Prof. J. Pollard (Edinburgh, UK)	(Kitamura et al., 2019)
410.4	mouse breast cancer	BALB/c	Prof. F. Balkwill (London)	(Miller, Miller, & Heppner, 1983)
4T1	mouse breast cancer	BALB/c	Prof. F. Balkwill (London)	(Aslakson & Miller, 1992)
CT26	mouse colon cancer	BALB/c	ATCC (Wesel)	(Brattain et al., 1980)
CMT93 Var	mouse colon cancer	C57BL/6N	Dr. med. C. Hackl (Regensburg)	(Franks et al., 1978)
CMT93 ATCC	mouse colon cancer	C57BL/6N	ATCC, Manassas, USA	(Franks et al., 1978)

2.1.2 Cell culture media and additives

All media and additives used in this thesis are listed in Table 2.

Table 2: Media and additives

Product	Company
DMEM medium with stable glutamine (1 g/l glucose)	Merck/Biochrom

Dulbecco's Phosphate buffered saline (PBS)	Sigma-Aldrich
Fetal calf serum (FCS)	PAN-Biotech
Opti-MEM I, Reduced Serum Medium	Thermo Fisher Scientific
Trypsin-EDTA Solution	Sigma-Aldrich

2.1.3 Chemicals, enzymes and other reagents

All chemicals, enzymes and other reagents used in this thesis are listed in Table 3.

Table 3: Chemicals, enzymes and other reagents

Product	Company
2-Mercaptoethanol	Sigma-Aldrich
Acrylamide	Carl Roth
Agarose	Thermo Fisher Scientific
Albumin Fraction V	Carl Roth
Alt-R HPRT PCR Primer Mix	IDT
Ammonium persulfate (APS)	Merck Millipore
Blotting buffer	25 mM Tris-Base/Tris-HCl 192 mM glycine 20% (v/v) methanol ad 1 l H ₂ O

Bromophenol blue	Carl Roth, Pharmacia Biotech
Bovine serum albumin (BSA)	Carl Roth
Dimethyl sulfoxide (DMSO)	Sigma-Aldrich
DNase I	Bio-Rad
dNTPs	New England Biolabs
dNTPs	IDT
dNTPs	Roche
Ethanol	Merck Millipore, Carl Roth
Ethidium bromide (EtBr)	Sigma-Aldrich
Febuxostat	MedChemExpress
Formic acid	Carl Roth
Gel Loading Dye Purple (6x), no SDS	New England Biolabs
GeneRule 1 kilo bases (kb) DNA ladder	Thermo Fisher Scientific
Glycerol	Sigma-Aldrich
Glycine	Sigma-Aldrich
HiFi Cas9 Nuclease V3	IDT
Isopropanol 70%	B.Braun
iTaq Universal SYBR Green Supermix	Bio-Rad
Kapa HiFi Fidelity Buffer (5X)	IDT
Kapa HiFi HotStart Polymerase	IDT
Laemmli buffer (4x)	2 g/5 ml SDS in H ₂ O 10 mg bromophenol blue 40% (v/v) glycerol 20% (v/v) stacking gel buffer 20% (v/v) 2-mercaptoethanol
Lipofectamine CRISPRMAX	Thermo Fisher Scientific
Lipofectamine RNAiMAX Transfection Reagent	Thermo Fisher Scientific
Methanol	Merck
Milk powder (MMP)	Carl Roth

MTT lysis buffer	(v/v) 5% formic acid in isopropanol (B. Braun)
Nuclease Free Duplex Buffer	IDT
Nucleofector Solution	Amaxa
Orange DNA loading dye (6x)	Thermo Fisher Scientific
1 kb Plus DNA Ladder	New England BioLabs
Phloxine B	Cayman Chemical Company
Phosphatase Inhibitor PhosSTOP	Roche
Phusion HF Buffer (5X)	New England Biolabs
Phusion Polymerase	New England Biolabs
Ponceau-Red	AppliChem
Protease Inhibitor Cocktail	Sigma-Aldrich
Protease inhibitor cocktail tablets, EDTA free	Roche
Protein Assay Reagent S	Bio-Rad
RIPA Buffer	50 mM Tris-Base/Tris-HCl (pH 7.2) 150 mM NaCl 0.1% (w/v) SDS 0.5% (w/v) Na-deoxycholate 1% Triton X-100 added fresh: 10x phosphatase inhibitor 100x protease inhibitor
Rotiphorese Gel 30 (30% (v/v) acrylamide/bisacrylamide solution)	Carl Roth
SDS	Carl Roth, Merck
Signal Fire Elite ECL Reagent	Cell Signaling
Sodium Chloride (NaCl)	Carl Roth, Thermo Fisher Scientific
Stacking gel buffer	0.5 M Tris-Base/Tris-HCl 2% (w/v) SDS pH 6.8

Supplement 1	Amaxa
T7 Endonuclease	New England Biolabs
T7 Endonuclease Buffer (10X)	New England Biolabs
TBS-T (1X)	20 mM Tris 137 mM NaCl H ₂ O bidest.: ad 1 l 0,1% (v/v) Tween 20 pH 7,6
Tetramethylethylendiamin (TEMED)	Sigma-Aldrich
Thiazolyl Blue Tetrazolium Bromide	Sigma-Aldrich
tracrRNA-ATT0550	IDT
Tris wash buffer (pH 6)	Merck Millipore
Tris-Base/Tris-HCl (pH 7.2)	Sigma-Aldrich
Tris-buffered saline (TBS)	Sigma-Aldrich
Triton X-100	Sigma-Aldrich
Tween 20	Sigma-Aldrich
UltraPure DNase/RNase-free distilled water	Invitrogen/Thermo Fisher Scientific
Water, DEPC-treated	Sigma-Aldrich

2.1.4 Kits

All Kits used in this thesis are listed in Table 4.

Table 4: Kits

Product	Company
Clarity Western ECL substrate	Bio-Rad
CRISPR-Cas9 Control Kit Mouse	IDT
DC (detergent compatible) protein assay	Bio-Rad

DCFDA Cellular ROS Detection Assay Kit	Abcam
DNA Isolation Kit QIAmp	QIAGEN
ECL Prime Detection Reagent	GE Healthcare
Genome Editing Detection Kit	IDT
High Pure RNA Isolation Kit	Roche
iScript cDNA synthesis Kit	Bio-Rad
Kapa HiFi HotStart PCR Kit	Kapa Biosystems
Monarch PCR & DNA Clean-Up Kit	New England Biolabs
Nucleofection Kit V	Amaxa
SignalFire™ Elite ECL Reagent	Cell Signaling
Xanthine Oxidase Assay Kit	Abcam

2.1.5 crRNA

All crRNAs used in this thesis are listed in Table 5.

Table 5: crRNAs

Organism	Gene Name	Chromosome	Exon	Name ID	Sequence
Mus musculus	Xdh	17qE2	1 out of 36	XDH#1	GAGGACAACGGTAGATGAGT
Mus musculus	Xdh	17qE2	1 out of 36	XDH#2	CGTCACGATGACGAGGACAA
Mus musculus	Xdh	17qE2	1 out of 36	XDH#3	CGTTGTCCTCGTCATCGTGA
Mus musculus	Blvrb	7qA3	3 out of 5	BLVRB#1	ACATGGAGTGGACAAGGTCCG
Mus musculus	Blvrb	7qA3	3 out of 5	BLVRB#2	CCCACTACAGTAATGTCCGA
Mus musculus	Blvrb	7qA3	1 out of 5	BLVRB#3	TCGGTGCCACCGGCAGGACC

2.1.6 Antibodies

All antibodies used in this thesis are listed in Table 4.

Table 6: Antibodies

Name	Source	Application Dilution	Company / Cat. No.
Xdh	Rabbit	WB / 1:300	Thermo Fisher / PA5-26285
Blvrb	Rabbit	WB / 1:1000	NovusBio / NBP1-83435
HSP90	Mouse	WB / 1:10000	Santa Cruz / sc#13119
anti-rabbit IgG-HRP	Mouse	WB / 1:2000	Santa Cruz / sc#2357
m-IgGk BP-HRP	Mouse	WB / 1:2000	Santa Cruz / sc#516102

2.1.7 Oligonucleotides

All oligonucleotides used in this thesis are listed in table 7.

Table 7: Oligonucleotides

Name	Description	Direction	Sequence (5'-3')
mmXDH- 961	XDH#1/#2/# 3	Forward	ACAACGCCAGAAACAATACAC
		Reverse	CACTTTGACTAGGAGGACAGAG

mmXDH- 894	XDH#1/#2/# 3	Forward	TCTCCCTGCACCGAGTTGACCT
		Reverse	TGGATTGGCTGTCTGGTCCTTCT
mmXDH- 1553	XDH#1/#2/# 3	Forward	GAGATGGTGATGGAGGAGTC
		Reverse	TGTGAAGATGGGTGGAATGG
mmBlvr_b_E xon3-1122	BLVRB#1/# 2	Forward	CTAATCCCAGCTTCATTCAGTC
		Reverse	ACAAAGCTGCATCACATTCTC
mmBlvr_b_E xon3-1320	BLVRB#1/# 2	Forward	CAGGTTATGAGGTGACGGTG
		Reverse	CTGTGTTGGGAGGATTAAGTG
mmBlvr_b_E xon3- fw1115	BLVRB#1/# 2	Forward	TCCACTAATTACCCAGAAGGCTCC
		Reverse	TCAACCACGGATCTGTTTGTAC
mmBlvr_b_E xon1-1253	BLVRB#3	Forward	TCCCAAACCTTCCCAATCC
		Reverse	TTCAAATCCCGACACAGCC
mmBlvr_b_E xon1-1517	BLVRB#3	Forward	CACCACCAATAGCACATACAG
		Reverse	GAGTTCAAATCCCGACACAG
mmBlvr_b_E xon1-945	BLVRB#3	Forward	GCAATTTGACTCCTCCGCCT
		Reverse	CCCAAAGCTCAATGTCCTTCCC

mmXdh-172 NGS	Next Generation Sequencing	Forward	G TTCAGAGTTCTACAGTCCGACGATCCCCT TTCAGACAGCAGAATCTC
	Primer XDH#1/#2/# 3	Reverse	TCCTTGGCACCCGAGAATTCCAAGGCGTA TCTTTCAAGTTGCAG
mmXdh_99	qRT-PCR Xanthine dehydrogen ase	Forward	AACACAAGTAACCTCATCCT
		Reverse	TTTGTTTGTTCCTCACCTC
mmBlvrb_7 5	qRT-PCR Biliverdin reductase β	Forward	TAAGATTCTGCAAGAGTCAGG
		Reverse	CCAGTTAGTGGTTGGTCTC
mmGapdh_ 146	qRT-PCR Glyceralde hyde 3- phosphate dehydrogen ase	Forward	CATCTTGGGCTACACTGAG
		Reverse	CTGTAGCCGTATTCATTGTC
mmPgk1_1 37	qRT-PCR Phosphogly cerate kinase 1	Forward	TGTCCAAACTAGGAGATGTC
		Reverse	CCTTGGCAAAGTAGTTCAG
5' Primer "C20"	PCR Next Generation Sequencing	Forward	AATGATACGGCGACCACCGAGATCTACAC GGCCACGTTTCAGAGTTCTACAGTCCGA
3' Primer Index 10	PCR Next Generation Sequencing	Reverse	CAAGCAGAAGACGGCATACTAGATAAGCT AGTGACTGGAGTTCCTTGGCACCCGAGAA TTCCA
3' Primer Index 11	PCR Next Generation Sequencing	Reverse	CAAGCAGAAGACGGCATACTAGATAAGCT CGTGACTGGAGTTCCTTGGCACCCGAGAA TTCCA

3' Primer Index 12	PCR Next Generation Sequencing	Reverse	CAAGCAGAAGACGGC ATACGAGATTACAA GGTGACTGGAGTTC CTTGGCACCCGAGAA TTCCA
3' Primer Index 13	PCR Next Generation Sequencing	Reverse	CAAGCAGAAGACGGC ATACGAGATTTGAC TGTGACTGGAGTTC CTTGGCACCCGAGAA TTCCA
3' Primer Index 14	PCR Next Generation Sequencing	Reverse	CAAGCAGAAGACGGC ATACGAGATGGAAC TGTGACTGGAGTTC CTTGGCACCCGAGAA TTCCA
3' Primer Index 15	PCR Next Generation Sequencing	Reverse	CAAGCAGAAGACGGC ATACGAGATTGACA TGTGACTGGAGTTC CTTGGCACCCGAGAA TTCCA
3' Primer Index 16	PCR Next Generation Sequencing	Reverse	CAAGCAGAAGACGGC ATACGAGATGGACG GGTGACTGGAGTTC CTTGGCACCCGAGAA TTCCA
3' Primer Index 17	PCR Next Generation Sequencing	Reverse	CAAGCAGAAGACGGC ATACGAGATCTCTA CGTGACTGGAGTTC CTTGGCACCCGAGAA TTCCA
3' Primer Index 18	PCR Next Generation Sequencing	Reverse	CAAGCAGAAGACGGC ATACGAGATGCGGA CGTGACTGGAGTTC CTTGGCACCCGAGAA TTCCA
3' Primer Index 19	PCR Next Generation Sequencing	Reverse	CAAGCAGAAGACGGC ATACGAGATTTTCA CGTGACTGGAGTTC CTTGGCACCCGAGAA TTCCA
3' Primer Index 20	PCR Next Generation Sequencing	Reverse	CAAGCAGAAGACGGC ATACGAGATGGCCA CGTGACTGGAGTTC CTTGGCACCCGAGAA TTCCA
3' Primer Index 21	PCR Next Generation Sequencing	Reverse	CAAGCAGAAGACGGC ATACGAGATCGAAA CGTGACTGGAGTTC CTTGGCACCCGAGAA TTCCA
3' Primer Index 22	PCR Next Generation Sequencing	Reverse	CAAGCAGAAGACGGC ATACGAGATCGTAC GGTGACTGGAGTTC CTTGGCACCCGAGAA TTCCA

3' Primer Index 23	PCR Next Generation Sequencing	Reverse	CAAGCAGAAGACGGCATACGAGATCCACT CGTGACTGGAGTTCCTTGGCACCCGAGAA TTCCA
3' Primer Index 24	PCR Next Generation Sequencing	Reverse	CAAGCAGAAGACGGCATACGAGATGCTAC CGTGACTGGAGTTCCTTGGCACCCGAGAA TTCCA
3' Primer Index 25	PCR Next Generation Sequencing	Reverse	CAAGCAGAAGACGGCATACGAGATATCAG TGTGACTGGAGTTCCTTGGCACCCGAGAA TTCCA
3' Primer Index 26	PCR Next Generation Sequencing	Reverse	CAAGCAGAAGACGGCATACGAGATGCTCA TGTGACTGGAGTTCCTTGGCACCCGAGAA TTCCA
3' Primer Index 27	PCR Next Generation Sequencing	Reverse	CAAGCAGAAGACGGCATACGAGATAGGAA TGTGACTGGAGTTCCTTGGCACCCGAGAA TTCCA
3' Primer Index 28	PCR Next Generation Sequencing	Reverse	CAAGCAGAAGACGGCATACGAGATCTTTT GGTGACTGGAGTTCCTTGGCACCCGAGAA TTCCA

2.1.8 Consumables

All consumables used in this thesis are listed in Table 8.

Table 8: Consumables

Product	Company
12-well plates	Sarstedt
24-well plates	Sarstedt
384-well plates (FrameStar384)	4titude
5ml Round bottom tube (FACS tubes)	Falcon
6-well plates	Sarstedt
96-well plates	Falcon

Cell culture flasks (25 cm ² , 75 cm ²)	Sarstedt
Cell scraper 25 cm	Sarstedt
Combitips advanced (0,1 ml)	Eppendorf
FilterTips (qRT-PCR) (10µl/100µl/1000µl)	STARLAB
Glass Pasteur Pipettes (230 mm)	VWR
Hemocytometer Neubauer Improved C-Chip	NanoEntek
Micro tubes & falcons (0,2 ml; 0,5 ml; 1,5 ml; 2,0 ml; 15 ml; 50 ml)	Sarstedt
Nitrocellulose blotting membrane (0.45 µm)	GE Healthcare Life Sciences
Pipette tips (10 µl, 100 µl, 200 µl, 1000 µl)	Eppendorf
Pipettes "Research Plus" (0.5µl -10 µl; 2µl - 20 µl; 10µl -100 µl; 20µl - 200 µl; 30µl - 300 µl; 100µl - 1000 µl)	Eppendorf
Rotilabo blotting papers (1.5 mm)	Carl Roth
Sealing foil (AMPLIseal, transparent)	Greiner Bio-One
Serological pipettes (10 ml; 50 ml)	Greiner Bio-One
Serological pipettes (25 ml)	Nerbe Plus
Serological pipettes (5 ml)	Corning
Trans-Blot Turbo mini nitrocellulose transfer pack	Bio-Rad
Trans-Blot Turbo mini-size nitrocellulose membranes	Bio-Rad
Trans-Blot Turbo mini-size transfer stacks	Bio-Rad

2.1.9 Equipment and software

All lab equipment and software used in this thesis are listed in Table 8.

Table 9: Equipment and software

Product	Company
Accu-jet pro	Brand
Amersham Typhoon Imager 9200	GE Healthcare
Applied Biosystems TaqMan	Thermo Fisher Scientific
BD FACSAria IIu Cell Sorter	BD Biosciences
BD FACSCalibur	BD Biosciences
Biofuge fresco	Heraeus Instruments
Electrophoresis power supply EPS 301	Amersham Pharmacia Biotech
Electrophoresis power supply LKB GPS200/400	Pharmacia
Electrophoresis system Mini-PROTEAN Tetra cell	Bio-Rad
ELISA reader TECAN Sunrise Infinite F50	Tecan Group
EVOS FL Cell Imaging System	Thermo Fisher Scientific
Gassed incubator for cell culture - B6120	Heraeus Instruments
Gel imaging system Gel Doc XR+	Bio-Rad
GraphPad Prism v.6.04.	GraphPad Software
GuW 1213 Freezer (-20°C)	Liebherr
H600 Microscope	HUND Wetzlar
Heating and drying table MEDAX	Medax
Heating/shaking block Thermomixer 5436	Eppendorf
Heating/shaking block Thermomixer R	Eppendorf
Hemocytometer Neubauer-improved	Marienfeld
ImageJ (win64) (version 1.51s)	Wayne Rasband
ImageQuant LAS-4000	GE Healthcare
Integrative Genomics Viewer (version 2.7.2 for Windows)	Broad Institute

KuW 1740 Refrigerator (4°C-8°C)	Liebherr
Megafuge 1.0	Heraeus Sepatech
Megafuge 3.0R	Heraeus Sepatech
MiSeq	Illumina
NanoDrop ND-1000 spectrophotometer	PEQLAB
Outknocker v.2.0 beta	Outknocker.org
PerlPrimer Software (version 1.1.21 for Windows)	SourceForge.net
SnapGene Viewer (version 4.3.10 for Windows)	SnapGene.com
Thermal cycler DNA Engine	MJ Research
U725-G Ultra Low Freezer (-80°C)	Eppendorf / New Brunswick
Water purification system MilliQ	Millipore
Western blot transfer system Trans-Blot SD Semi-Dry	Bio-Rad
Western blot transfer system Trans-Blot Turbo	Bio-Rad

2.2 Methods

2.2.1 Cell culture methods

2.2.1.1 Maintenance of tumor cell lines

The tumor cells were grown at 37°C and 5% CO₂ in a humidified incubator. To passage the cells, media was aspirated, they were once washed with 6 ml of PBS, and then 1 ml of Trypsin EDTA (1x) was added to the 75 cm² flask. They were then incubated for 5-10 min and resuspended with DMEM with 10% FCS. They were split in ratios of 1:10 or 1:20. To maintain the cell lines for longer, cells were frozen in DMSO and 90% FCS and stored in liquid nitrogen.

2.2.1.2 Generation of stable knock-out cell lines via CRISPR/Cas9

2.2.1.2.1 Lipofection with cationic lipid reagent Lipofectamine™

The clustered regularly interspaced short palindromic repeats (CRISPR)/Caspase9-mediated approach is based on the ability of bacteria to specifically recognize, remember and cut the viral genome of a bacteriophage, inserted by the phage into the genome of the host cell. The site where the viral DNA is integrated is called CRISPR-site. After translating this part of the genome to RNA, it is called crRNA or crRNA. The cell then uses a specific marker, the tracrRNA, to bind to the crRNA. Together, they bind to the Cas9 enzyme and use its capability to cut the crRNA as a defense mechanism against this virus - once the viral DNA is again recognized in the cell, the crRNA can bind to exactly this virus DNA and the Cas9 enzyme cuts the DNA strands, leaving the virus damaged. However, to prevent the Cas9 from falsely cutting the bacteria itself, the Cas9 only cuts at sites where there is a "prototype adjacent motif", a PAM, following the crRNA. This motif, typically consisting of the base sequence NGG for the Cas9, is only present in the virus DNA and therefore the bacterial DNA, containing the crRNA of previously survived virus attacks, is not harmed in the process. In genome editing, we use this system to precisely cut DNA sites in the cell. In order to do that, we only have to design a crRNA that contains the sequence of the genome we want to cut and is adjacent to a PAM.

The construction of a knock-out with the CRISPR system is based on the ability of a cell to repair double-stranded breaks in the DNA like those inserted by CRISPR, but to repair them falsely. This system is also called non-homologous end joining (NHEJ) and generates insertions or deletions (INDELS), which can be the cause of a knock-out. (Hille et al. 2018)

We have developed three different guided sequences (gRNA) per gene of interest to increase the probability of a positive knock-out and tested each of them in the cells by forming ribonucleoprotein (RNP) complexes with the Cas9 enzyme. Each of those RNP complexes is linked with a fluorescent tracrRNA (ATTO550) and can be detected in the FACS.

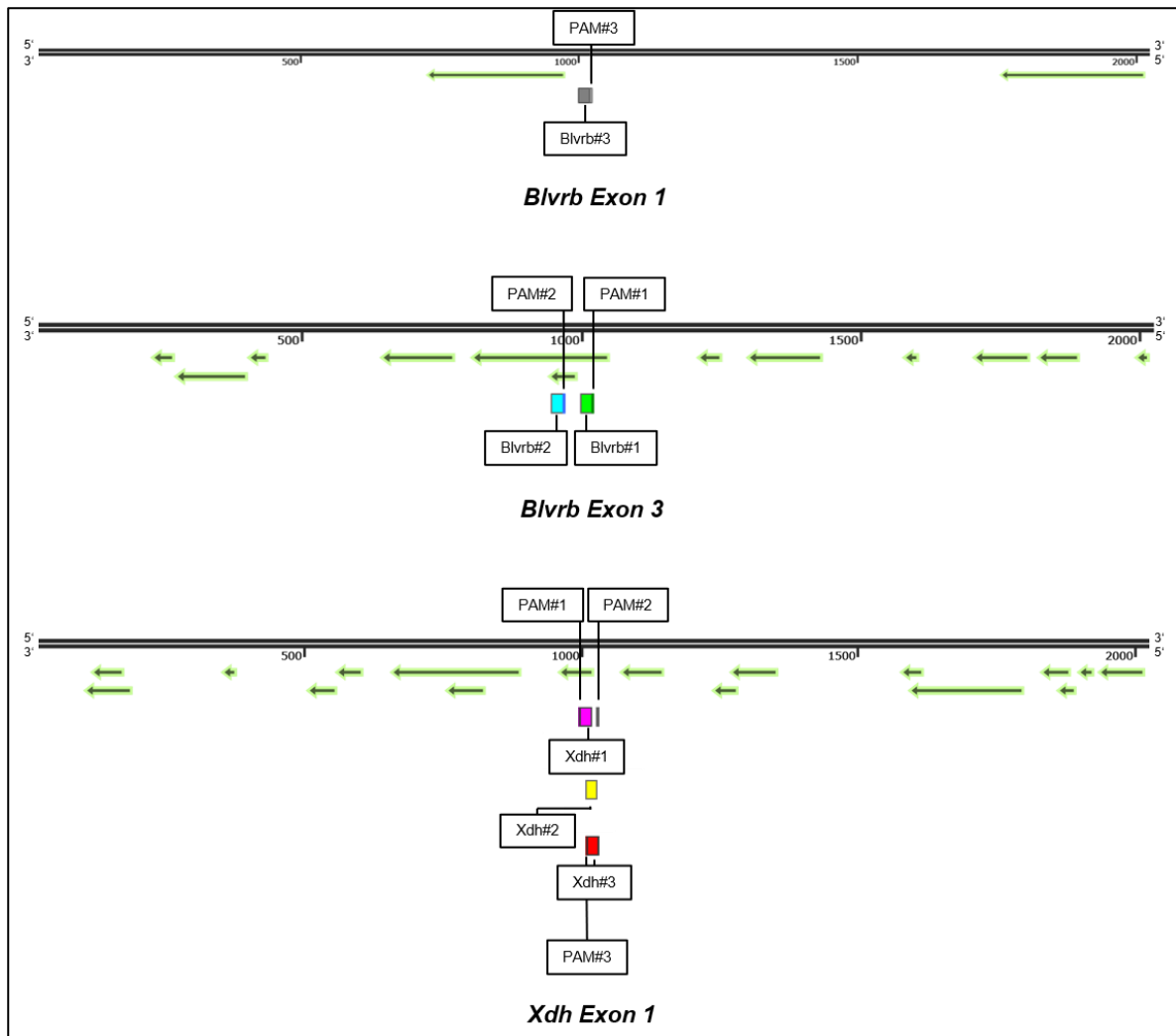


Figure 6: Model of Xdh and Blvr with gRNAs targeting genes.

Xdh: The three gRNAs are depicted as Xdh#1 (purple), Xdh#2 (red) and Xdh#3 (yellow) with their respective PAMs. Blvr Exon 3: gRNAs Blvr#1 (green) and Blvr#2 (blue) on Exon 3 of the Blvr gene with corresponding PAMs. Blvr Exon 1: gRNA Blvr#3 (gray) with corresponding PAM. Green arrows depict translated regions of bottom strand.

The transfection was performed with 4.8 μ L Lipofectamine Transfection Reagent and 1.6×10^5 cells of CT26 or less per well in 24 MW with 1 ml of DMEM medium without FCS, after 2 hours of incubation 60 μ L of DMEM with 10% FCS were added.

The CT26 Xdh-KO clones derived from the transfection with the three gRNAs were labelled KO-1 to KO-12 with KO-1 carrying the lowest amount of unimpaired Xdh

alleles to KO-12 carrying the highest amount, based on below discussed results in Next-Generation-Sequencing. KO-13 to KO-21 were not tested further due to weaker performance in the WB (see Table 10).

Table 10: Nomenclature of CT26 Xdh-KO cells

clone	suspected percentage of uninfluenced XDH	simplified nomenclature	continued with
#1	not tested	KO-13	
#2	not tested	KO-14	
#3	56%	KO-9	
#4	46%	KO-5	#3
#5	40%	KO-3	
#6	51%	KO-8	
#7	not tested	KO-15	
#1	1%	KO-1	#1
#2	46%	KO-6	
#3	26%	KO-2	
#4	not tested	KO-16	
#5	not tested	KO-17	
#6	not tested	KO-18	
#1	67%	KO-10	
#3	46%	KO-7	
#4	43%	KO-4	#2
#5	67%	KO-11	
#6	73%	KO-12	
#7	not tested	KO-19	
#8	not tested	KO-20	
#9	not tested	KO-21	

2.2.1.3 Assessment of cell viability and proliferation

2.2.1.3.1 MTT Assay

To determine cell viability, we performed a 3-(4,5-dimethylthiazol-2-yl)-2,5-diphenyltetrazolium bromide (MTT) assay (Mosmann, 1983). The MTT assay is a metabolic colorimetric assay measuring cell viability. It is based on the ability of NAD(P)H-dependent cellular enzymes to reduce the water-soluble MTT reagent to the insoluble formazan of purple color, that can be detected in a spectrophotometer. The assay was performed with 5×10^4 cells of the cell lines CT26, CMT93 Var, CMT93

ATCC, EO771-LG, 410.4, 4T1, CT26 X1.4, CT26 X1.6, CT26 X2.1, CT26 X2.3, CT26 X3.4 and CT26 X3.6 per well in a 24-well-plate were seeded and incubated overnight to become adherent. They were then either treated with several concentrations in a range from 1 nM to 100 μ M of the Xdh-inhibitor Febuxostat or the BlvrB-inhibitor Phloxine B over 72 h. The CRISPR/Cas9 treated cell lines were not treated with an inhibitor but incubated for 24 h. Subsequently, the cells were incubated with 500 μ L medium with 10% MTT-solution for 4 h at 37°C and 5% CO₂ in the dark. The medium was aspirated, and the formed formazan crystals were dissolved in 200 μ L MTT lysis buffer. The extinction of the samples was then measured in triplicates in a 96-well-plate at 550 nm in a photometer (Tecan) and related to the extinction values of the untreated control to determine survival.

MTT-Solution

- Thiazolyl Blue Tetrazolium Bromide: 0.25 g
- PBS: 50 ml

2.2.1.3.2 Cell counting (for MTT and proliferation)

Cells were counted manually in a standardized reusable Neubauer improved chamber or a C-CHIP standardized Neubauer improved chamber. To determine the cell number, 10 μ l of the cell suspension were pipetted into the hemocytometer. The total number of cells per ml was calculated by multiplying the average of the cell numbers of 4 squares with the chamber factor of 10⁴.

2.2.2 Protein biochemistry

2.2.2.1 Protein isolation

1x10⁶ of the in 2.2.1.3.1 mentioned cells were seeded in a 6-well-plate and allowed to adhere overnight. The cells were then either treated with 10 μ M of XDH-i, of BLVRB-i or not treated at all. They were then incubated for 0, 4, 24, 48 or 72 h at 37°C and 5% CO₂. The cells were once washed with ice-cold PBS and detached with a cell scraper in 150 μ L of RIPA solution. Protease and phosphatase inhibitors were freshly added to the RIPA solution. The suspension was then transferred into 1,5 ml Eppendorf cups and, after being vortexed thoroughly, incubated on ice for 30 min. Subsequently, the

suspension was centrifuged at 4°C and 13.000 rpm for 10 min. The supernatant was collected and transferred into new cups and stored at -20°C.

2.2.2.2 Protein quantification by Lowry assay

The DC (detergent compatible) assay is a colorimetric protein quantification assay based on the reaction in the well-documented Lowry assay (Lowry, 1951), but is adjusted in the reaction kinetics.

As in the Lowry assay, the color production is based on two reactions, the first one being the reaction of the peptide bonds of the protein with copper-(III)-ions in an alkaline environment, and the second one leading to reduced Folin products by the reaction of the copper-treated proteins with Folin. The generated Folin product is reduced in 1, 2 or 3 oxygen atoms and produces a color signal that can be measured at 700 nm with a photometer (Tecan) in relation to the BSA standard curve. The samples were diluted 1:10 with ddH₂O, and the assay was carried out according to the manufacturer's instructions.

2.2.2.3 SDS-PAGE

The discontinuous sodium dodecyl sulfate-polyacrylamide gel electrophoresis (SDS-PAGE) (Laemmli, 1970) was performed to separate and visualize proteins on a gel according to their molecular masses for further Western Blotting (2.2.2.4). The SDS-Page consists of two different gels, one resolving (8% or 10%) and one stacking gel (5%), cast at different pH values. First, the resolving gel was prepared and polymerized before layering the stacking gel on top. A comb with 15 wells was introduced in the stacking gel and removed once the gel was polymerized. The protein samples (20-30 µg) were prepared with 4x Laemmli Buffer and H₂O before being incubated at 95°C for 5 min. Respectively, the Laemmli Buffer contains 2-mercaptoethanol and SDS, that reduce the disulphide bonds in proteins and quantitatively bind to proteins whilst charging them negatively in proportion to their mass, which therefore renders it possible to evaluate only the protein mass as an influence of the mobility in the resolving gel during the electrophoresis. The samples were then loaded onto the wells and focused in the stacking gel at 90 V for 30 min. Subsequently, they were resolved

at 130 V for 90 min. For the determination of the protein size, a standard ladder of Thermo Fisher Scientific was also loaded.

Stacking gel (5%):

- 1.5 M Tris + 2% SDS (pH 6.8): 630 μ l
- Acrylamide/Bisacrylamide (30%): 830 μ l
- APS (10% w/v): 50 μ l
- TEMED: 5 μ l
- H₂O bidest.: 3,45 ml

Resolving gel (8%/10%):

- 1.5 M Tris + 2% SDS (pH 6.8): 5 ml/5 ml
- Acrylamide/Bisacrylamide (30%): 5,4 ml/6,7 ml
- APS (10% w/v): 200 μ L/200 μ l
- TEMED: 20 μ L/20 μ l
- H₂O bidest.: 9,4 ml/7,9 ml

Electrophoresis buffer:

- 25 mM Tris: 3g
- 192 mM Glycine: 14,4 g- SDS 0,1% (w/v): 1 g
- H₂O bidest.: ad 1 l

2.2.2.4 Western Blot

After electrophoresis, the proteins were blotted onto a nitrocellulose membrane (Bio-Rad), allowing detection by specific antibodies. In order to transfer the proteins, several layers of filter paper, a nitrocellulose membrane following the gel and another block of several layers of filter paper were put together after being incubated in blotting buffer for 1-2 min and then transferred onto a high-performance western blotting transfer system (Bio-Rad) at 25 V for 7 min. To ensure efficient protein transfer, the membrane was stained in Ponceau-Red for 3-5 min. After confirming the transfer process, the Ponceau-Red was washed off with 1x TBST-T. The membrane was blocked in 5% MMP or 5% BSA in 1x TBS-T for 1 h at room temperature to ensure no unspecific binding of the antibody would take place. Subsequently, the membrane was incubated with the specific primary antibody, that was either dissolved in MMP or BSA, at 4°C overnight. After incubation, the primary antibody was discarded or stored for reuse.

This process was followed by 3 washing steps with 1x TBS-T for 5 min, 15 min and 5 min, respectively. Then, the secondary antibody conjugated with horseradish peroxidase (HRP) was added to the membrane and incubated for 1 h. HRP is an enzyme that catalyzes a reaction to form luminol, a product forming a chemiluminescent signal, which can be detected in a biomolecular imager. Another three washing steps followed before the membrane was developed with ECL Clarity (Bio-Rad) or ECL Signal Fire (Cell Signaling) in the LAS-4000 Imager (GE Healthcare).

TBS-T (1x):

- 20 mM Tris: 2,4 g
- 137 mM NaCl 8 g
- H₂O bidest.: ad 1 l (adjust to pH 7,6)
- 0,1% (v/v) Tween-20: 1 ml

Blotting buffer (10x):

- 20 mM Tris: 30,28 g
- Glycin: 144,14 g
- H₂O bidest.: ad 1 l

Blotting buffer (1x):

- 1x Blotting buffer: 100 ml
- H₂O bidest.: 700 ml
- Methanol: 200 ml

2.2.3 Gene expression analysis

2.2.3.1 Isolation of mRNA from murine cancer cells

The isolation of mRNA from cultured cells was carried out with the High Pure RNA isolation kit (Roche) according to the manufacturer's instructions. 1×10^6 cells per well in a 6-well-plate were seeded the day before the isolation and allowed to adhere overnight at 37°C and 5% CO₂. The medium was aspirated, and the cells were washed once with 1 ml PBS. The PBS was removed, and another 200 µl of PBS were added.

Subsequently, 400 μL of lysis/binding buffer were added to the cells, and the cells were detached with a cell scraper, put in 1,5 ml Eppendorf cups and vortexed thoroughly to ensure efficient cell lysis. The lysis/binding buffer contains guanidine hydrochloride, a chaotropic salt, that destroys hydrogen bonds and therefore activates protein denaturation. The suspension was transferred to a spin column consisting of glass fiber fleece with a collection tube. The spin column was centrifuged at 8000 g for 15 sec to ensure binding of the nucleic acids, whereas proteins and other cell debris could be collected and discarded. The containing DNA was enzymatically digested during the following incubation with DNase I for 15 min. The remaining RNA was washed three times and eluted with the provided elution buffer. The concentration and purity were established with the NanoDrop ND-1000 spectrophotometer (PEQLAB), and the RNA was stored at -80°C .

2.2.3.2 Reverse transcription

In order to properly analyze the gene expression of a specific gene with qRT-PCR, the generated mRNA needs to be transcribed to complementary DNA (cDNA). The reverse transcription of the samples was performed with the iScript Reverse Transcription Kit (Bio-Rad). The enzyme used was the Moloney murine leukemia virus (MMLV) transcriptase with RNase H activity, to ensure degradation of the transcribed RNA. The primers provided by the kit were oligo(dT) primers that are complementary to the poly-A tail of eukaryotic mRNA and therefore produce a full-length cDNA.

The reaction setup was prepared as follows:

5x iScript reaction mix	4 μl
iScript reverse transcriptase	1 μl
RNA template (1 μg)	x μl
Nuclease-free water	y μl
<hr/>	
Total volume	20 μl

The cDNA was synthesized in a thermal cycler (DNA Engine, MJ Research) with the following conditions:

Time	Temperature
<hr/>	

5 min	25°C
30 min	42°C
5 min	85°C
Hold	4°C

2.2.3.3 Quantitative real-time PCR (qRT-PCR)

To examine gene expression, a quantitative real-time PCR (qRT-PCR) with SYBR green detection was used. The qRT-PCR follows the basic principle of common PCR, including activation of a polymerase, a denaturation step and an annealing and elongation step, which is being repeated 40 times. The SYBR green that was added to the sample is an intercalating dye which binds to ssDNA as well as to dsDNA but shows a much higher fluorescence when binding to dsDNA. The intensity of fluorescence is therefore indicating the amount of elongated DNA and progression of the reaction. After each cycle, the fluorescence of SYBR green was being measured. Once the fluorescence reached a threshold, which was defined as a fluorescent signal measurable over background, the number of cycles was defined as the Ct value. This value was being normalized by the expression of two housekeeping genes (=ΔCt value).

The primers used in this experiment are listed in 2.1.7 under Table 7. Samples were normalized by *Gapdh* and *Pgk1* expression. To each well of a 384-well-plate (4tituide) 8 µl of the prepared PCR reaction mix were pipetted, 2 µl of cDNA were added, the plate was sealed and centrifuged at 1500 rpm at room temperature for 5 min. The plate was measured according to the following protocol in a QuantStudio Design & Analysis (version 1.5.0) (Thermo Fisher Scientific):

Standard qRT-PCR program:

Activation of Taq polymerase:	95°C	12 min	
Denaturation:	95°C	15 sec	40 cycles
Annealing and elongation:	60°C	1 min	

Melting curve analysis:	95°C	15 sec
	60-95°C	0,075°C/s

2.2.4 Flow cytometry methods

2.2.4.1 FACS Sort of CRISPR Cells

To evaluate the CRISPR/Cas9 transfection and to grow single clones of the transfected cells, the ATTO550 positive cells were sorted one cell per well in a 96-well-plate (Falcon) with the FACS Aria IIu cell sorter (BD Biosciences). The flow cytometry is based on the distribution of cells by their size and granularity. A laser can measure the fluorescent signal emitted by a cell; in this case, the fluorescent ATTO550 dye caused the signal. The ATTO550 positive cells were then marked with a charge and removed by an electrostatic deflection system that sorts the cell droplet in a particular container. The cells were sorted 24 h after transfection and then kept in culture. Once cell count was enough, DNA was isolated as mentioned in 2.2.5.2, and the cells were frozen in liquid nitrogen as mentioned in 2.2.1.1.

2.2.4.2 ROS-measurement of CT26 cells treated with Febuxostat

The cells treated with the Xdh-inhibitor Febuxostat were analyzed for their potential to produce reactive oxygen species (ROS). The day before the measurement, 4×10^6 and $2,5 \times 10^6$ cells were seeded to allow adherence overnight. The cells were then incubated with $10 \mu\text{M}$ XDH-i for 1 h (4×10^6 cells), 4 h (4×10^6 cells) and 24 h ($2,5 \times 10^6$ cells). 5×10^5 cells were subsequently collected in FACS tubes, stained with $20 \mu\text{M}$ 2',7'-dichlorofluorescein diacetate (DCFDA) for 30 min and then either stimulated with $200 \mu\text{M}$ tert-butyl-hydroperoxide (tBHP) (included in the kit), which is a ROS stimulator and served as a positive control and to determine the maximum amount of ROS produced in the samples, or not stimulated. The FACS tubes were incubated at 37°C and 5 % CO_2 for either 1 h or 4 h and shook continuously each 30 min to ensure non-adherence. DCFDA is a fluorogenic dye that measures intracellular ROS. Cellular esterases later deacetylate it to a non-fluorescent product, which is then again oxidized by ROS to

2',7'-dichlorofluorescein (DCF). DCF is then measured by flow cytometry with excitation/emission at 495 nm/529 nm.

2.2.4.3 ROS-measurement of CT26-CRISPR/Cas9 cells

The method was conducted similarly to the ROS-measurement of CT26 cells treated with XDH-i as mentioned in 2.2.4.2, although cells were not stimulated with XDH-i and 4×10^6 cells were seeded the day before measurement.

2.2.5 T7 Endonuclease 1 Assay

2.2.5.1 Primer design

The T7 Endonuclease I (T7E1) assay is a confirmation method for the successful cutting of the CRISPR machinery, visible on a standard agarose gel. It is premised on the T7 endonuclease's ability to cut mismatches between the two DNA strands (Fig. 7). Primers were designed with PerlPrimer, amplifying the gRNA at about 2/3 of the total amplicon. All the primers used in this experiment are listed in table 7.

Since we know the size of the amplicon that the primers generate and the expected site of CRISPR induced mismatches (at the specific guide sequence), we were able to compare the actual results of the T7 products on the agarose gel with the expected results.

2.2.5.2 DNA isolation and PCR amplification of target

DNA of the murine cells was isolated in a spin-column procedure with the QIAamp DNA Mini Kit (QIAGEN). Cells were cultured in a 75 cm² flask. The medium was aspirated, and the cells were washed with 6 ml of PBS and detached with 1 ml of Trypsin EDTA (1x). 5×10^6 cells were transferred into a 1,5 ml microcentrifuge cup and centrifuged at 300 g for 5 min. The supernatant was discarded. The cell pellet was resuspended in 200 μ l PBS, 20 μ l proteinase K were added to the samples to ensure efficient cell lysis. 200 μ l of the provided Buffer AL were added, and the samples were mixed thoroughly by pulse-vortexing for 15 sec. The samples were incubated at 56°C for 5 min. Subsequently, the mixture was applied into the provided spin columns, the

released DNA binding specifically to the silica-gel membrane. The spin-column was put in a 2 ml collection tube and centrifuged at 8000 rpm for 1 min, and the collected supernatant was discarded. Two washing steps were carried out to clean the DNA from contaminants that could inhibit PCR, such as divalent cations or proteins, with the provided washing buffers. The DNA was eluted in Buffer AE. The concentration and purity were established with the NanoDrop ND-1000 spectrophotometer (PEQLAB), and the DNA was stored at -20°C.

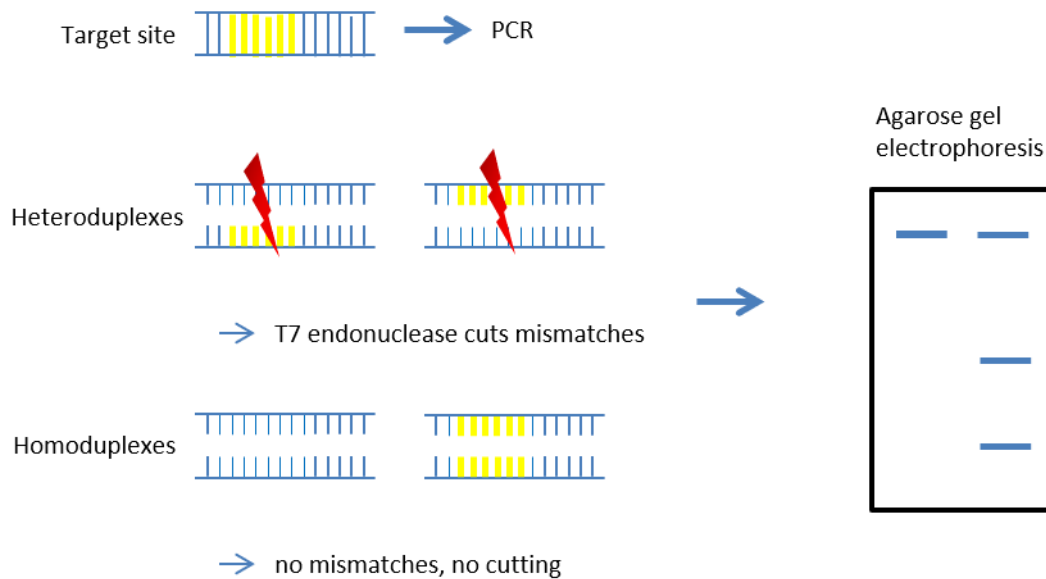


Figure 7: T7 Endonuclease Assay to confirm transfection efficiency.

The T7 Endonuclease 1 cuts the mismatched DNA strands but does not affect non-mismatched homoduplexes, resulting in three bands if digested by T7E1 and one band if not digested.

The PCR for the further experimental procedure was carried out under the following conditions:

DNA (4ng)	x µl
Primer mix (fw / rv)	5 µl (2,5 µl / 2,5 µl)
Phusion Polymerase / Kapa Hifi Hotstart	0,5 µl / 1 µl
Polymerase	
Phusion Polymerase Buffer 5x / Kapa Hifi	10 µl / 10 µl
Fidelity Buffer 5x	
dNTP's (10mM)	1 µl
DEPC H ₂ O	ad 50 µl

with the standard program:

95 °C	5 min	30 cycles
95 °C	20 sec	
Primer-specific annealing temperature (57 °C – 64 °C)	15 sec	
72 °C	30 sec	
72 °C	2 min	
4 °C	Hold	

2.2.5.3 Clean-up and T7E1 digestion

The PCR amplicon was cleaned-up before continuing with the T7E1 digestion to provide the best quality for the further experiment. The purification was carried out with the Monarch™ PCR & DNA Cleanup Kit (New England Biolabs) according to the manufacturer's instructions. The concentration and purity were established with the NanoDrop ND-1000 spectrophotometer (PEQLAB), and the product was stored at -20°C.

The T7E1 is an enzyme that detects mismatched DNA and induces a double-stranded cut at the site of the mismatch (Sentmanat et al. 2018) can be visualized in gel electrophoresis. The CRISPR/Cas9 complex induces a cut at the gRNA which is repaired incorrectly through NHEJ. The T7E1 assay uses this principle. By denaturing and reannealing the DNA strands present in the sample through PCR, either homoduplexes or heteroduplexes are formed, the latter being cut by the enzyme.

The PCR building the homo- and heteroduplexes was performed under the following conditions:

95 °C	5 min
95 – 85 °C	-2 °C / sec
85 – 25 °C	-0.3 °C / sec
4 °C	Hold

In order to compare the reaction before and after the T7E1 digestion, the same reaction mix, consisting of 200 ng of PCR product, 2 µl of T7E1 reaction buffer and nuclease-free water ad 19 µl and 20 µl, respectively, was treated or not treated with 1 µl of the enzyme after the PCR forming the DNA duplexes. The prepared samples were incubated at 37°C for 20 min.

2.2.5.4 Gel electrophoresis

A 1 % (w/v) agarose gel was cast with 10 µl ethidium bromide in 200 ml of gel. 4 µl of loading dye 6x was added to the samples before loading them on the gel. For the determination of the DNA size, a 1 kb plus DNA ladder of New England Biolabs was also loaded. The samples were resolved in the gel at 110 V for 1 h. The gel was imaged on the Amersham Typhoon Imager 9200 (GE Healthcare).

2.2.5.5 Analysis

The quantitative analysis of the bands was done with ImageJ. The gene-editing efficiency E was calculated with the following formula:

$$E = 100 \times [1 - (1 - \textit{fraction cleaved})^{\frac{1}{2}}]$$

where fraction cleaved = concentration of digested products / (concentration of digested products + concentration of undigested bands).

2.2.6 Sequencing

2.2.6.1 Sanger Sequencing

Sanger Sequencing (Sanger, 1977) is a commonly used method to analyze the exact sequence of a DNA strand. It is based on standard PCR techniques, whereas in Sanger sequencing, apart from regular dNTPs, ddNTPs that lack the 3' hydroxyl group are added to the reaction mix. Therefore, once the DNA polymerase builds in a ddNTP, the elongation stops at that site. The reaction is done several times with dNTPs of all

four bases and one ddNTP. This ensures when done sufficiently often, that every base on the template strand is at least once paired with its complementary ddNTP. The produced DNA can then be run on a gel, with each ddNTP running in a separate lane. The smallest DNA will be at the bottom of the gel, whereas the longest products will be at the top. Thus, it is possible to read the complementary DNA sequence from the bottom to the top.

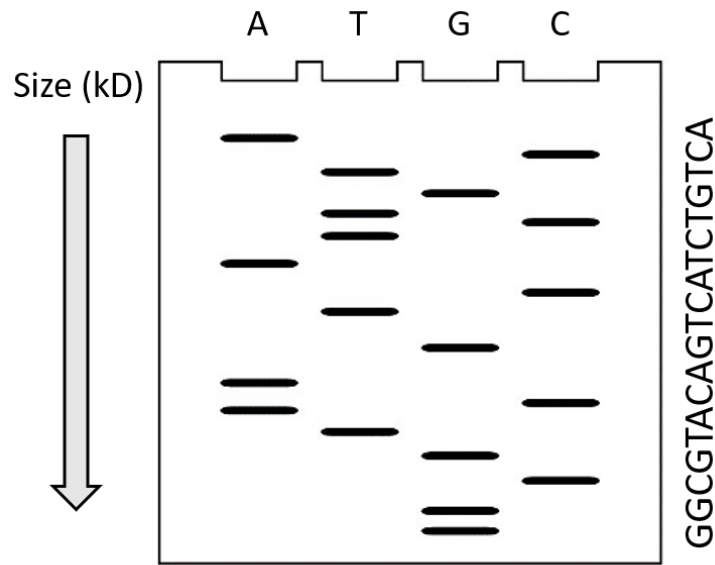


Figure 8: Sanger Sequencing.

The products of the PCR with ddNTPs are run on a gel, each in a separate lane. Based on the nature of the gel, they distribute by size, the smallest molecule running the farthest in the gel, making it possible to draw conclusions on

The samples were sequenced by a company service (Thermo Fisher). In preparation of the sequencing, the sequence of interest was amplified with PCR. The primers used are listed in table 7. The PCR was carried out under the following conditions:

DNA (4ng)	X μ l
Primer mix (fw / rv)	5 μ l (2,5 μ l / 2,5 μ l)
Phusion Polymerase / Kapa Hifi Hotstart	0,5 μ l / 1 μ l
Polymerase	
Phusion Polymerase Buffer 5x / Kapa Hifi	10 μ l / 10 μ l
Fidelity Buffer 5x	
dNTP's (10mM)	1 μ l

DEPC H₂O

ad 50 µl

with the standard program:

95 °C	5 min	30 cycles
95 °C	20 sec	
Primer-specific annealing temperature (57 °C – 64 °C)	15 sec	
72 °C	30 sec	
72 °C	2 min	
4 °C	Hold	

The amplicon was purified with the Monarch™ PCR & DNA Cleanup Kit (New England Biolabs) according to the manufacturer's instructions. The concentration and purity were established with the NanoDrop ND-1000 spectrophotometer (PEQLAB). For further preparation of the samples, 10 ng / 100 bp of the purified PCR product were added to a reaction mix of 10 pMol of primer and DEPC-H₂O ad 8 µl. The product was stored at -20°C.

2.2.6.2 Next Generation Sequencing

To further evaluate the samples, Next Generation Sequencing (NGS) (Balasubramanian, Klenerman, 1998), was necessary. This method consists of 4 basic parts, including sample preparation, cluster generation, sequencing and data analysis. For sample preparation, the DNA containing the gRNA was amplified with specifically designed primers (Table 7). They contain one sequence specific to the amplicon and one sequence, which is complementary to the sequence of the primers comprising indices used for the next steps (Adapter). PCR was performed under the following conditions:

Primer mix (fw / rv)	5 µl (2,5 µl / 2,5 µl)
Phusion Polymerase / Kapa Hifi Hotstart Polymerase	0,5 µl / 1 µl

Phusion Polymerase Buffer 5x / Kapa Hifi	10 μ l / 10 μ l
Fidelity Buffer 5x	
dNTP's (10mM)	1 μ l
DEPC H ₂ O	ad 50 μ l

with the standard program:

95 °C	5 min	30 cycles
95 °C	20 sec	
52 °C	15 sec	
72 °C	30 sec	
72 °C	2 min	
4 °C	Hold	

The samples were cleaned with the Monarch™ PCR & DNA Cleanup Kit (New England Biolabs) according to the manufacturer's instructions. The concentration and purity were established with the NanoDrop ND-1000 spectrophotometer (PEQLAB). The purified PCR product was then processed in the following PCR. During this step, several important attachments were added. For one, the MiSeq sequencer (Illumina) needs to recognize a motif where it can start the sequence – the sequencing binding site. Equally important in the cluster generation are the introduced regions complementary to the flow cell oligos. To identify the samples in the data output, special 5-nt-indices were added, one on the 5'-primer and one on the 3'-primer (Table 7). The PCR was performed under the following conditions:

5' PCR primer	1 μ l
3' PCR primer (index differing)	1 μ l
Phusion Polymerase	0,5 μ l
Phusion Polymerase Buffer 5x	10 μ l
dNTP's (10 mM)	1,25 μ l
DNA (20 ng)	x μ l
DEPC H ₂ O	ad 50 μ l

with the following program:

98°C	1 min	11 cycles
98°C	10 sec	
60°C	10 sec	
72°C	40 sec	
72°C	10 min	
4°C	Hold	

The clustering took place on a flow cell, to which multiple oligonucleotides were adjacent. The adapters added during the sample prep then enabled a stable binding of single-stranded DNA to the flow cell, still facilitating access to enzymes. Enzymes and non-labeled nucleotides were added, producing double-stranded DNA in a bridge confirmation. Denaturation was initiated, leaving single-stranded templates attached to the flow cell. This process was repeated multiple times, resulting in several million clusters of single-stranded copies of the template. Primers, DNA polymerase, and four labeled reversible terminators were added to initiate the sequencing by determination of the first base. After laser excitation, a fluorescent signal was emitted by the binding of the labeled terminators, which was captured by the machine. This procedure was repeated to sequence the total DNA template.

The data output format was FASTQ, and the data were analyzed with IGV v.2.7.2 (Robinson et al. 2011) and Outknocker v.2.0 beta (Schmid-Burgk et al. 2014) on a Windows 10 system with Mozilla Firefox.

2.2.7 XO Activity measurement

The XO activity was determined with the Xanthine Oxidase Activity Assay Kit (abcam), an enzymatic, colorimetric assay kit. The assay is based on the reaction of xanthine to uric acid in which hydrogen peroxide is being produced, catalyzed by xanthine oxidase present in the sample. By adding the dye OxiRed™, hydrogen peroxide is then stoichiometrically converted to a fluorescent product, emitting a signal at 570 nm.

2x10⁶ cells were counted and centrifuged at 1300 rpm for 7 min. The supernatant was discarded. The cells were resuspended with 1 ml of PBS and centrifuged again at 1300 rpm for 7 min. The supernatant was again discarded. The cell pellet was homogenized with 300 µl of the provided assay buffer and transferred into 1,5 ml Eppendorf cups.

The suspension was centrifuged at 13 000 rpm for 10 min. The supernatant containing the xanthine oxidase present in the sample was used for further measuring according to the manufacturer's protocol. The signal produced after 0 min and 40 min of incubation was then measured at 570 nm in a photometer (Tecan).

XO activity was calculated according to the manufacturer's protocol.

2.2.8 Statistical analysis

All data was received at least in biological triplicates. Data are shown as means \pm SD of the mean (SEM). The significance was tested with the two-sided student's t-test unless marked otherwise. A p-value under 0,05 indicated statistical significance (*p < 0,05; **p < 0,01; ***p < 0,001). Data were plotted with the GraphPad Prism software v.6.04.

3 Results

3.1 Xdh and Blvrb are highly expressed in the more aggressive cell lines.

Previous work of our group led us to believe that *Xdh* and *Blvrb* are interesting target genes for brain colonization. To verify the hypothesis, that the highly metastasizing cells also express high levels of Xdh and Blvrb, we assessed the protein levels of these target enzymes in a series of murine breast and colon cancer cell lines with different colonization potentials. The colonization potential of each cell line was analyzed in vivo with the colony index. This equation evaluates the parameters 'Successful Colonization', 'Injected cells' and 'Median OS' (Figure 9). The Western Blot confirmed that the highly metastasizing cell lines of breast and colon cancer (Figure 10), show higher protein expression of Xdh and Blvrb than the lower metastasizing ones.

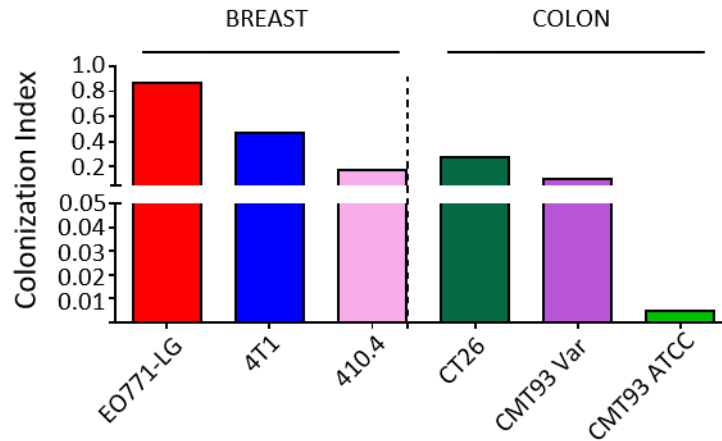


Figure 9: Colonization Index of breast and colon cancer

Colonization Index (CI) of breast and colon cancer metastasis models. Higher CI indicates more aggressive brain colonization. $CI = \frac{\text{Successful Colonization (\%)}}{\text{Injected cells (n)} \times \text{Median OS (d)}} \times 100$. Unpublished data.

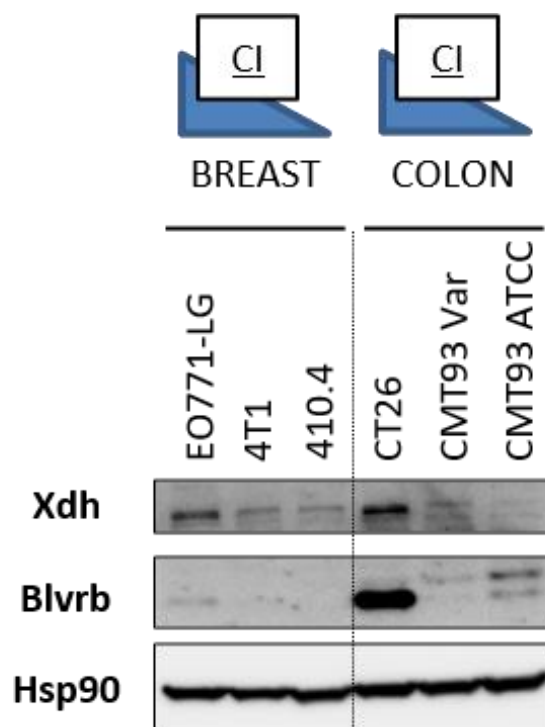


Figure 10: Western Blot of Xdh and Blvrb.

Representative Western Blot analysis of Xdh and Blvrb expression in examined breast (EO771-LG, 4T1, 410.4) and colon (CT26, CMT93 Var, CMT93 ATCC) cancer cell lines. Hsp90 serves as a housekeeping protein.

3.2 Pharmacological inhibition of XDH and BLVRB

3.1.2 Effect of Xdh inhibition on EO771-LG and CT26 in vitro

Having confirmed the high expression of the two target proteins in the highly metastasizing cell lines, we were aiming for a functional blockade of the protein activity to check the impact of the proteins which are important for ROS-quenching through different methods.

To evaluate whether Febuxostat, an Xdh inhibitor (Xdh-i), has a cytotoxic effect on the cells compared to cells treated only with the solvent dimethyl sulfoxide (DMSO), we performed an MTT assay.

The assay showed that the inhibitor has a significant effect on the metabolic activity and therefore the survival of the CT26 cells only at high concentrations of 100 μM . At lower concentrations, we did not see a significant effect (see Figure 11). The EO771-LG cells weren't affected at all by the Xdh-i. In fact, the mean inhibitory values (IC50) were not reached with the concentrations used in this experiment. Since we were aiming for a comparable cell count in the following experiments with the Xdh-i, we chose the highest concentration of inhibitor possible that is not cytotoxic to the cells. Therefore, we decided to continue the experiments with a concentration of 10 μM .

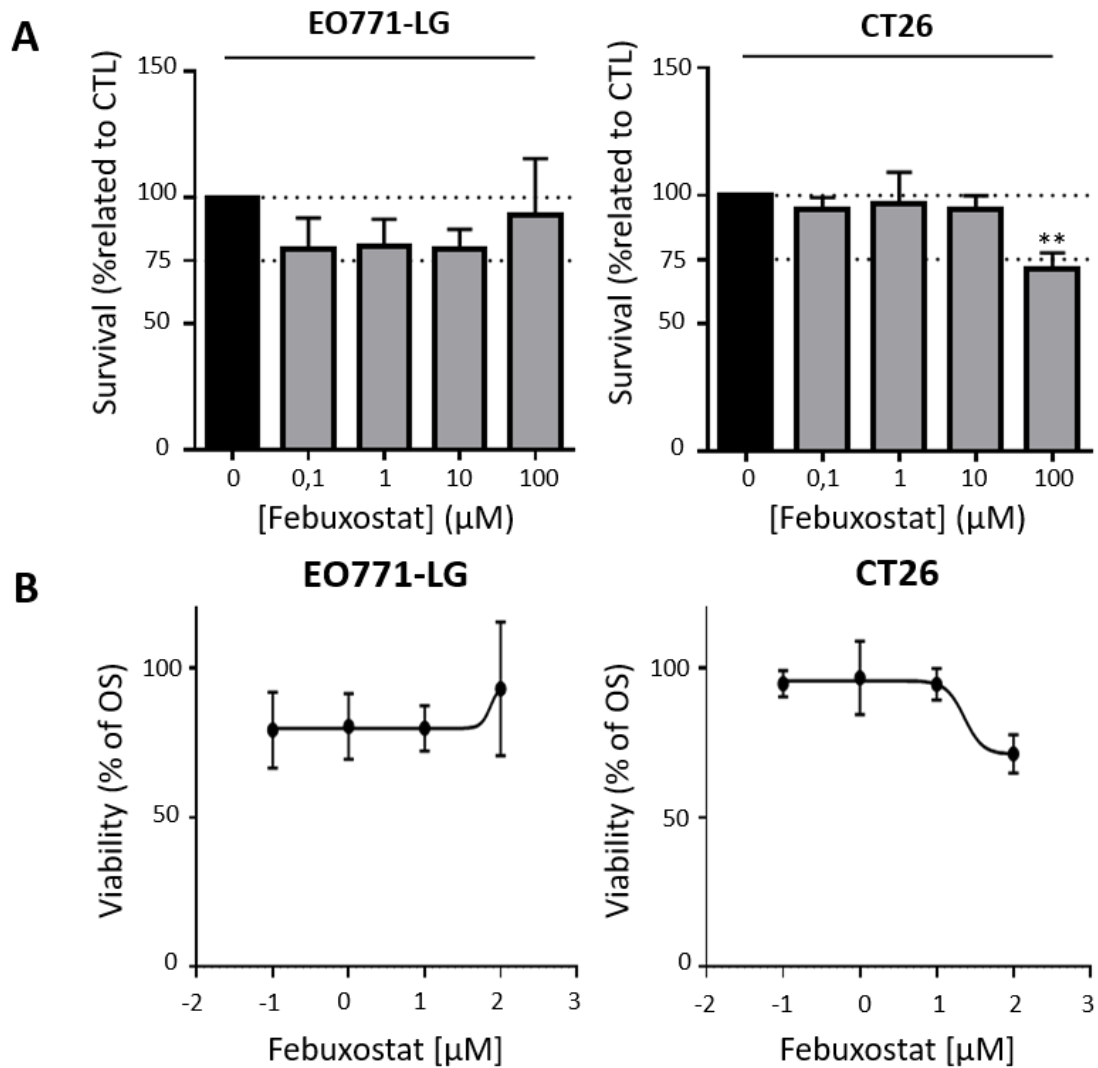


Figure 11: Analysis of EO771-LG and CT26 treated with Xdh-i.

(A) MTT showing cell survival after stimulation with Xdh-i at different concentrations for 72 h (mean + SD, $n = 3$; student's t-test, $**p < 0.01$). **(B)** IC₅₀ curves of Xdh-i in EO771-LG and CT26 (OS = overall survival, mean + SD, $n = 3$).

In order to assess the impact of Xdh-i treatment on protein expression of Xdh in EO771-LG and CT26, we performed a Western Blot. After 0, 4, and 24 h of incubation with the Xdh-i, we saw no significant changes (Fig. 12 A). The effect of the Xdh-i on the gene expression was also not significant after incubation times of 0, 4, and 24 h, as seen in Figure 14 B.

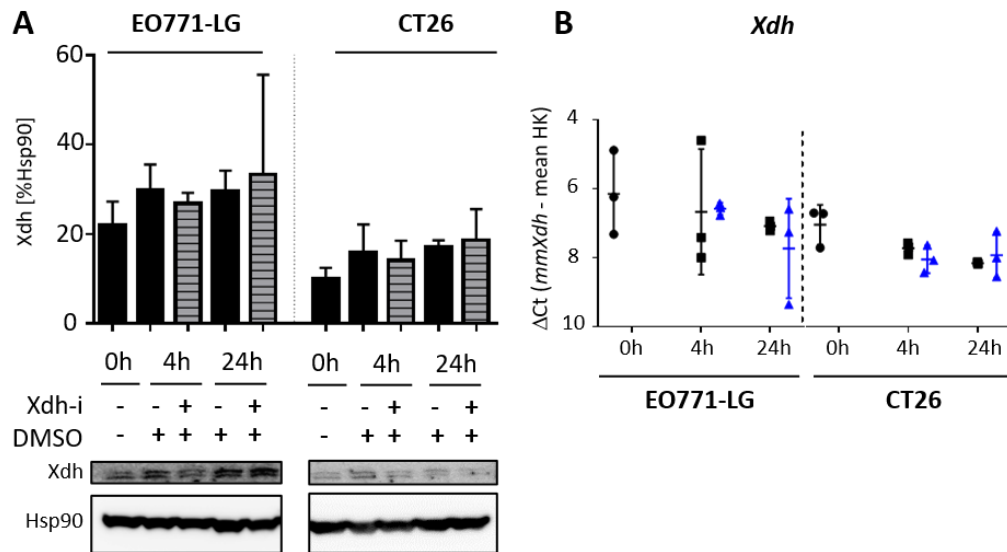


Figure 12: Influence of Febuxostat on protein and gene expression of Xdh.

(A) Representative Western Blot images and corresponding quantification of Xdh after inhibition with Febuxostat (10 μ M) (mean + SD, $n = 3$, ordinary one-way ANOVA). **(B)** qRT-PCR analysis of Xdh expression after inhibition with Febuxostat (10 μ M, blue) vs DMSO control (black) (mean + SD, $n = 3$, ordinary one-way ANOVA).

Subsequently, we wanted to assess the changes in ROS production after Xdh inhibition with Febuxostat. It is known that xanthine oxidase and xanthine dehydrogenase catalyze the reaction of hypoxanthine to xanthine and xanthine to uric acid with the help of NAD⁺ and O₂, respectively, generating NADH and ROS metabolites (Battelli et al. 2016b). The uric acid produced in this reaction has shown to be a non-enzymatic ROS scavenger (Ames et al. 1981). We assumed that inhibiting xanthine oxidase in tumor cells would lead to a reduction of uric acid and thus to an increase of ROS production under stress conditions (in this case, Xdh inhibition). To assess this, we performed a DCFDA assay with the cells treated with the inhibitor after 24 h. To test this, we incubated the cells with tBHP, a potent ROS stimulator, which served as the positive control and to compare the maximum ROS production and with DCFDA, which visualized ROS in the flow cytometer. The determined naïve ROS showed no significant differences after 24 h of Xdh-i treatment compared to the control (Fig. 13 A). Additionally, we did not observe significant deviations of the maximum ROS production after Xdh-i treatment for 24 h, neither in EO771-LG nor in CT26 (Fig. 13 B).

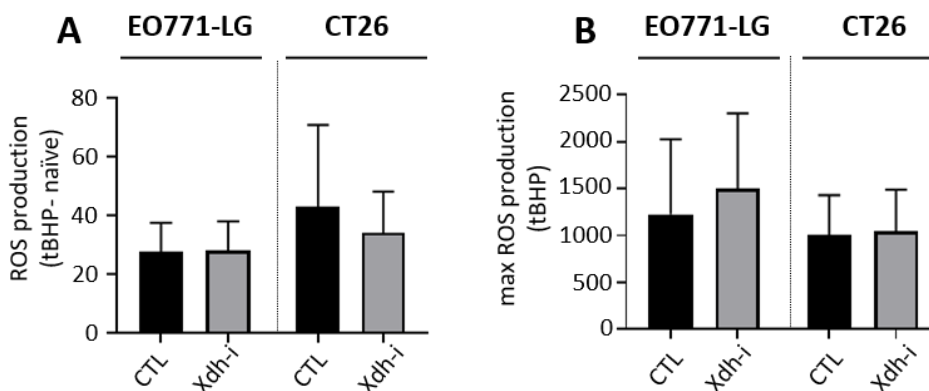


Figure 13: ROS-measurement after Febuxostat inhibition.

EO771-LG and CT26 were incubated with Febuxostat (10 μM, grey) and DMSO (black) as a control for 24 h. (A) Detection of naïve ROS after 1 h of incubation with DCFDA, making ROS measurable by flow cytometry. (B) Detection of maximum ROS production after ROS stimulation with tBHP for 1 h (mean + SD, $n = 3$, student's t-test).

3.1.3 Effect of Blvrb inhibition on EO771-LG and CT26 in vitro

Parallely, we investigated the impact of the Blvrb inhibitor Phloxine B (Li et al. 2018) on the aggressive breast and colon cancer cells. Blvrb is an enzyme, which catalyzes the reduction of biliverdin to bilirubin. Bilirubin is an enzyme linked to the protection of lipids from oxidation, therefore acting as an endogenous ROS quencher (Morita et al. 2019).

Similar to the experiments with the Xdh inhibitor, we began with an MTT assay to determine cell metabolic activity and indirectly cell survival after treatment with Blvrb-i. We treated the cells with concentrations of up to 10 μM for 72 h and saw no significant differences in survival compared to the control in none of the cell lines tested (Fig 14).

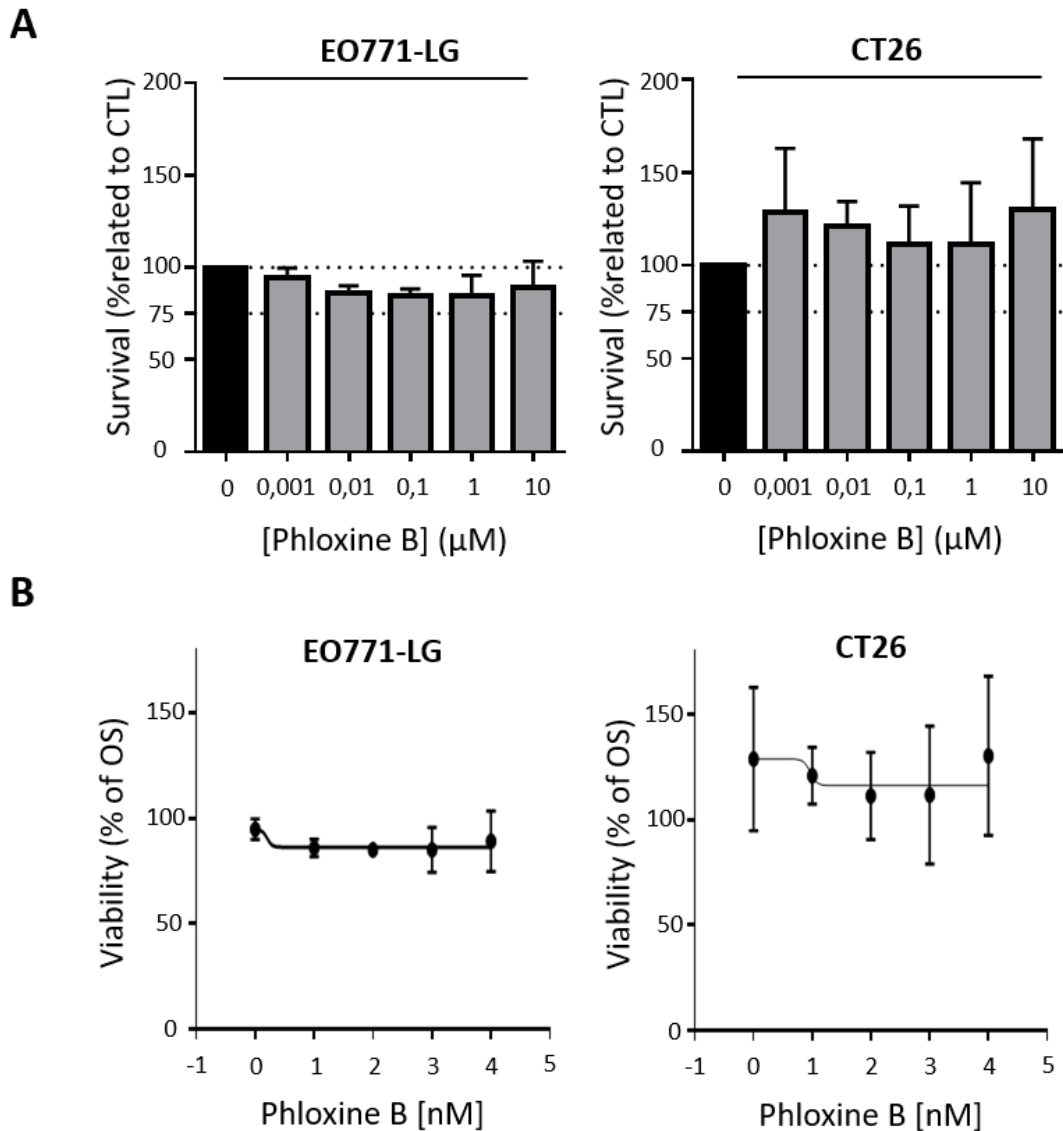


Figure 14: Analysis of EO771-LG and CT26 treated with Blvr-b-i.

(A) MTT showing cell survival after stimulation with Blvr-b-i at different concentrations for 72 h (mean + SD, $n = 3$; student's t-test, $**p < 0.01$). **(B)** IC50 curves of Blvr-b-i in EO771-LG and CT26 (OS = overall survival, mean + SD, $n = 3$).

Therefore, we continued further experiments with concentrations of 10 μM . Similar to the experiments with the Xdh-i, we checked whether a difference in protein expression of Blvr-b could be detected after 0, 4, and 24 hours of treatment with the Blvr-b-i. We saw no significant changes in Blvr-b protein expression compared to the control. Parallely, we checked the Blvr-b gene expression through qRT-PCR and saw no significant changes as well (Fig. 15).

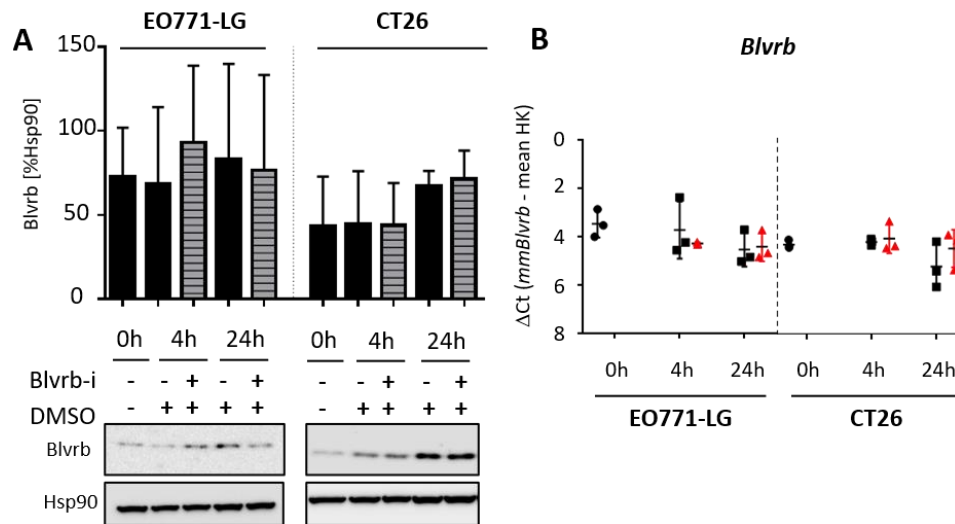


Figure 15: Influence of Phloxine B on protein and gene expression of BlvrB.

(A) Representative Western Blot images and corresponding quantification of BlvrB after inhibition with Phloxine B (10 μ M) (mean + SD, $n = 3$, ordinary one-way ANOVA). **(B)** qRT-PCR analysis of BlvrB expression after inhibition with Phloxine B (mean + SD, $n = 3$, ordinary one-way ANOVA).

As we could not generate BlvrB knock-out clones (see below), we discontinued both the experiments with the BlvrB gRNA clones and parallelly the ROS measurements of the pharmacological inhibitor of BLVRB, since there would be no comparable data of the two methods in the future of this project.

3.2 Genetic inhibition of Xdh and BlvrB

Since the pharmacological inhibition of the target enzymes did not work as expected, we next tried to reduce their expression with the CRISPR/Cas9 gene editing system.

3.2.1 CRISPR/Cas9- transfection is more efficient in CT26 than in EO771-LG

Cells were transfected with lipofectamine and the transfection efficiency was determined by FACS analysis. The cells that incorporated the RNP complex showed a fluorescent signal for ATTO550 since the tracrRNA was tagged with this dye. Therefore, 24 h after transfection, we sorted the ATTO550-positive cells in a 96-well-

plate. As can be seen in Figure 16, the transfection efficacy for both target genes Xdh and Blvrb was higher in the colon cancer cell line CT26 compared to the breast cancer cells EO771-LG (Xdh=1.4% vs 0.193; and Blvrb=1.97% vs 0.089, respectively). Moreover, the few EO771-LG single cell clones that could be recovered after sorting anyhow grew insufficiently in a 96-well-plate, so that we continued our work only with the murine colon cancer cell line CT26.

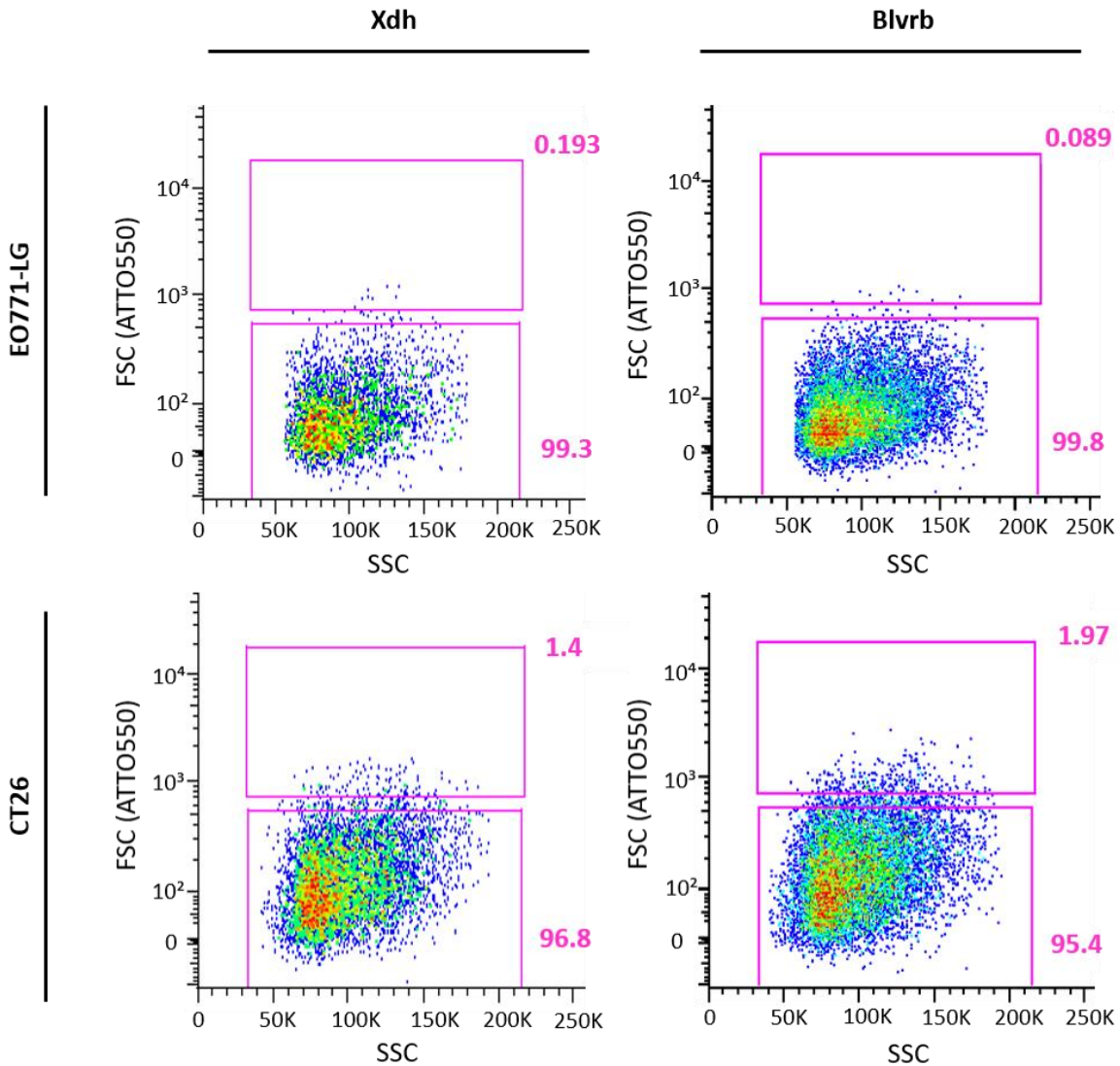


Figure 16: FACS results of EO771-LG and CT26 after transfection.

EO771-LG and CT26 were transfected with RNP complexes containing different gRNAs tagged with ATTO550. ATTO550-positive cells were detected in the upper field, whereas the ATTO550-negative cells were detected in the lower field. Depicted above are representative examples of transfection efficiency in EO771-LG and CT26 (FSC = forward scatter, SSC = sideward scatter).

3.2.2 Xdh-knockout via CRISPR/Cas9 is more efficient than Blvrb-knockout

To simply and efficiently scan multiple samples that we retrieved from the single cell sorting for mutations induced by CRISPR/Cas9, we chose to start with the T7E1 assay. As a cost-efficient and fast method, the assay can visualize mismatched DNA after T7E1 digestion. The assay was carried out as described in 2.2.5.1. To ensure reproducible and reliable results, we chose to test each sample of the Xdh-KO clones and the Blvrb-KO clones with two or three primer pairs, respectively.

The analysis with the T7E1 assay of the single cell clones with a Blvrb gRNA showed less clear transfection, as described below, and presumably, more off-target and no on-target effects (Figure 17).

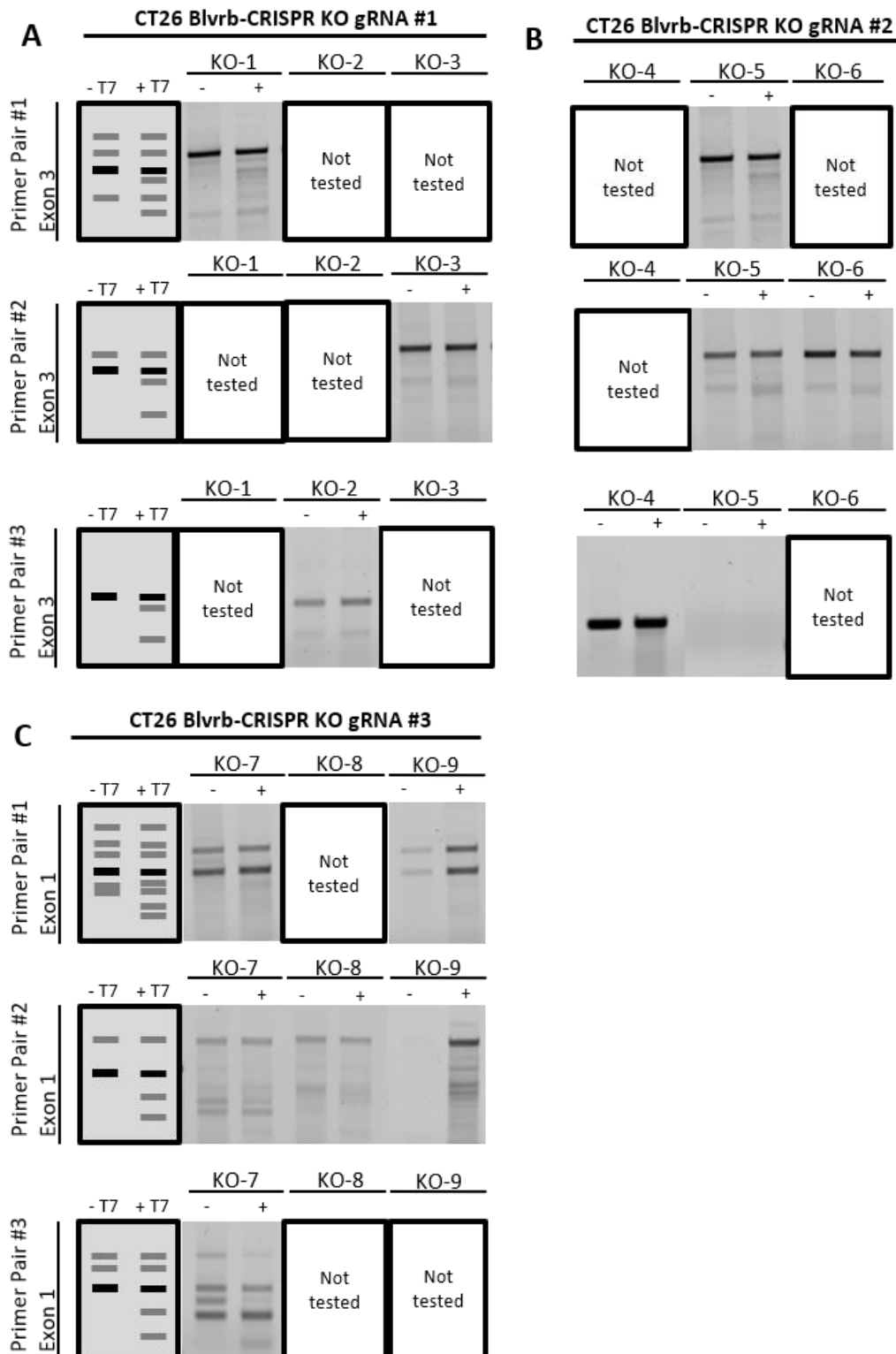


Figure 17: Summary of T7 Endonuclease 1 Assay for Blvrb-KO.

Amplicon of DNA containing the gRNA was cleaned-up, samples were either digested or not with T7E1 (+/-) and resolved on gel. Expected results of positive digestion shown before each row. gRNA#1 and gRNA#2 are located on the same exon, whereas gRNA#3 is on a different exon, therefore different primers were used. Samples stated as "not tested" were not clean and therefore not applied to the gel. Positive clones are marked with "✓".

For this reason, we discontinued the experiments with the Blvrb gRNA clones and decided to continue only with the CT26 Xdh-KO cells for further analyses.

Regarding the Xdh-KO clones, the endonuclease cut 17 out of 23 samples in at least one of the two primer amplicons, indicating that the CRISPR/Cas9 complex induced NHEJ at the site of the specific gRNA. However, six of the sorted single cell clones that were ATTO550 positive did not show a positive digestion band (Figure 18).

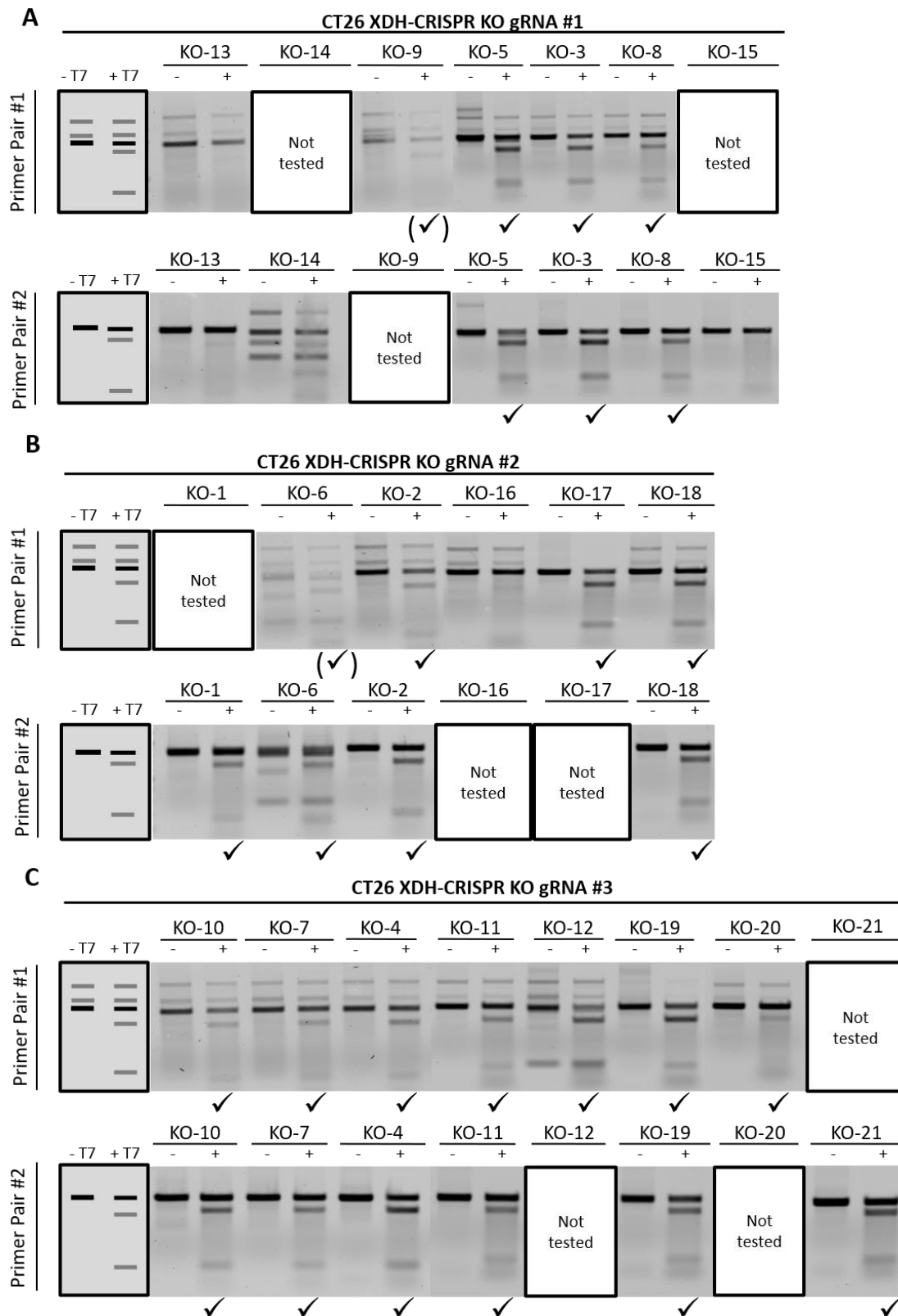


Figure 18: Summary of T7 Endonuclease 1 Assay for Xdh-KO.

Amplicon of DNA containing the gRNA was cleaned-up, samples were either digested or not with T7E1 (+/-) and resolved on gel. Expected results of positive digestion shown before each row. Samples stated as "not tested" were not clean and therefore not applied to the gel. Positive clones are marked with "✓".

3.2.3. Sanger Sequencing of Xdh-KO clones

To further characterize the knockout induced by CRISPR/Cas9 in our samples, we performed Sanger sequencing. This method provides a more detailed information about the homozygosity of the alleles present in each sample and also about the DNA sequence.

The sequencing results showed a heterogenous subtype (e.g., in Figure 19 A) in almost all the samples, meaning that at the CRISPR/Cas9 cut site (2 nt from the PAM of the specific gRNA) an overlap of nucleotides was detected. This heterogeneity is explained by different INDELS (INsertion/DELetion) on the two alleles usually present in the cell. The overlap renders it impossible to judge the sequences any further. Only two of the sequenced samples were homozygous (see Figure 19 B), one of them not showing a mutation near the CRISPR/Cas9 cut site, which means no INDEL has been introduced.

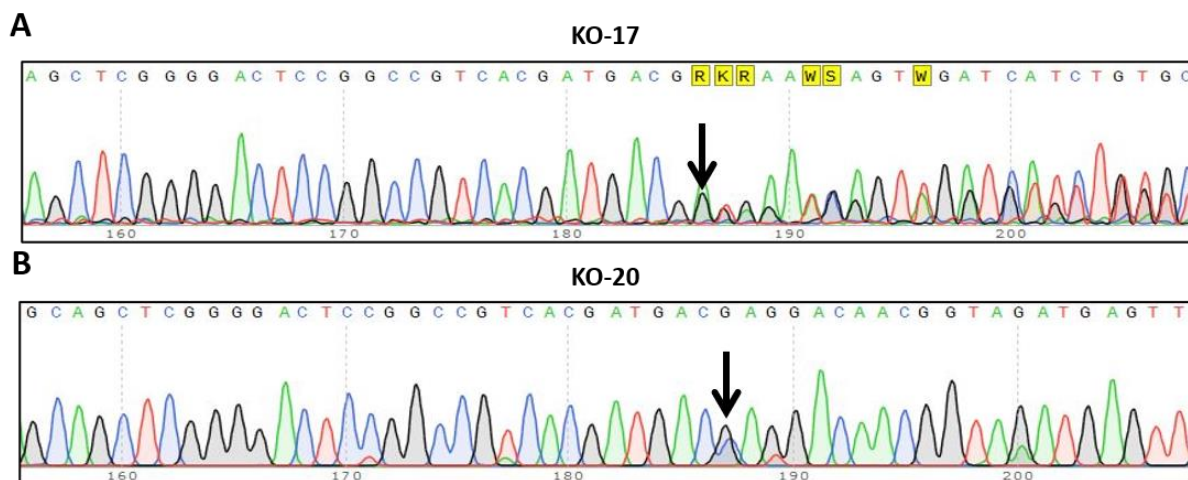


Figure 19: Sanger Sequencing results of CRISPR/Cas9 samples.

(A) Sanger sequencing revealed the heterozygous character of the examined samples. The arrow points to the cut site of CRISPR/Cas9, where the alleles present in the sample vary, depicted by the repeated overlap of two waves. **(B)** Homozygous sample showing no detectable overlap of nucleotides.

3.2.4. Next-Generation-Sequencing of Xdh-KO clones

Since the evaluation of most of the samples' sequences was not realizable through Sanger sequencing, the next approach was to deep sequence the DNA of the cells.

For this, we used amplicon sequencing through synthesis (in contrast to whole genome sequencing), which means that only a predetermined amplicon of the whole DNA was sequenced. In our case, this was the amplicon containing the gRNAs.

The analysis of this data revealed the molecular base pattern of the different alleles of each sample. Interestingly, in most of the samples, the Next-Generation-Sequencing (NGS) indicated that more than two alleles were present in the cell, in contrast to the expectation. Initially, the mutations were judged whether they were in-frame (IF) or out-of-frame (OOF) (see Figure 20), by checking whether the INDEL was a multiple of three. In-frame mutations were assumed not to lead to a KO, whereas out-of-frame mutations supposedly led to a KO. However, some out-of-frame INDELs were not in the exon, therefore, considered as “no KO” while other in-frame INDELs deleted the start codon and were considered to lead to a KO. Out of 14 tested samples (including the negative control and the WT), we have identified one compound heterozygous mutant (full KO, two different mutations on its two alleles, both presumably leading to a KO), two heterozygous mutants, eight clones showing more than two alleles (including the negative control), and three wildtypes or mutations with no effect on the transcription. Unfortunately, INDELs were detected in the negative control (NC), which is discussed below. The details of the mutations in each sample are listed in Table 11 and are discussed below.

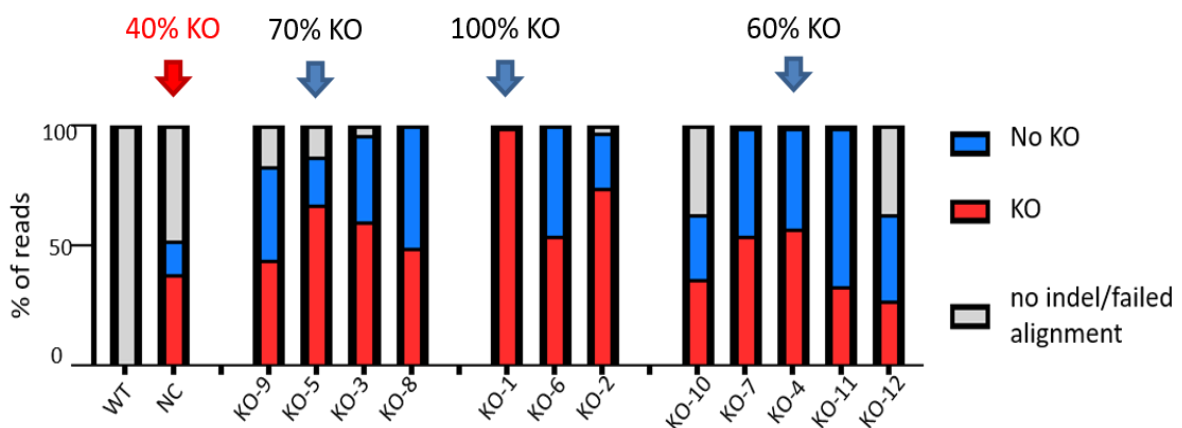


Figure 20: Summary of NGS.

Next-Generation-Sequencing was performed on the CT26 Xdh-KO samples. Plotted is the summary of in-frame, out-of-frame and no INDELs for each sample. IF INDELs including the start codon were counted as KO, OOF INDELs in introns were counted as no KO.

3.3. Functional characterization of Xdh-KO clones

3.3.1 RNA

Subsequently, we wanted to see, whether the Xdh-KO could be also assessable at the RNA level. For this we performed qRT-PCR analysis (Fig. 21). The qRT-PCR revealed significant changes in the expression of *Xdh* in gRNA #2 clone #1, gRNA #3 clone #4 and #6. This might be due to the different mutations in each clone. Whereas some might influence the transcription of the whole gene, others might not, which will be discussed below. Either way, there were no differences between WT and NC.

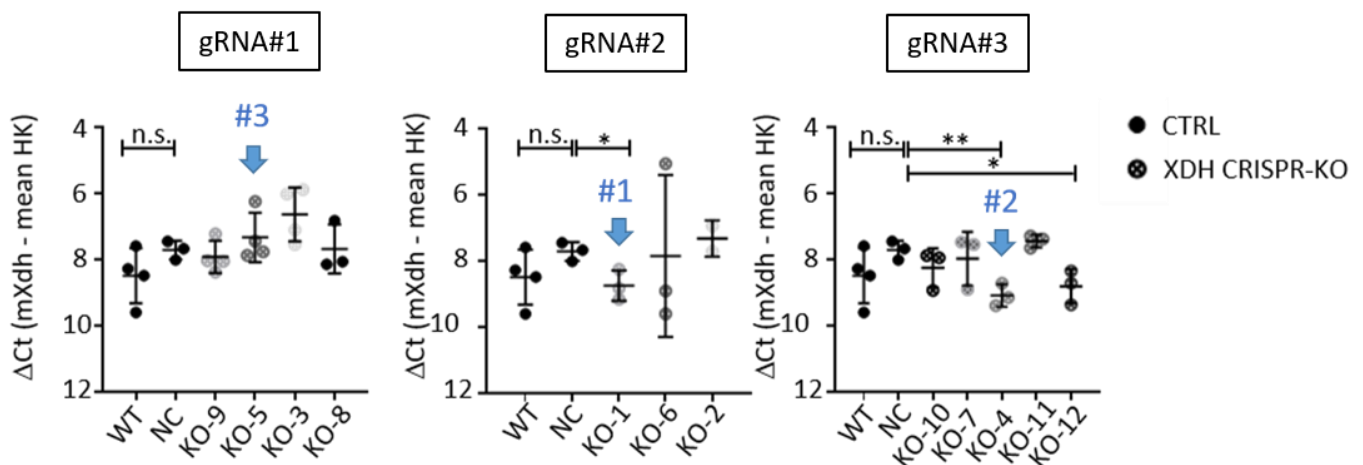


Figure 21: qRT-PCR of CT26 Xdh-KO clones.

Quantitative RT-PCR analysis of *Xdh* (mean + SD, $n = 3$, student's t-test; $*p < 0.05$, $**p < 0.01$, $***p < 0.001$, $****p < 0.0001$, n.s. = not significant).

3.3.2 Protein

Next, to see whether the Xdh-KO could be also detected at the protein level, we performed a Western Blot. The Western Blot revealed that Xdh was significantly downregulated in the CRISPR/Cas9 treated cells (Figure 22). It also revealed that the WT CT26 did not express XDH as highly as the NC. To focus on the most promising clones, we continued with three clones, KO-1, KO-4, and KO-5, which in the following will be called #1, #2, and #3, respectively.

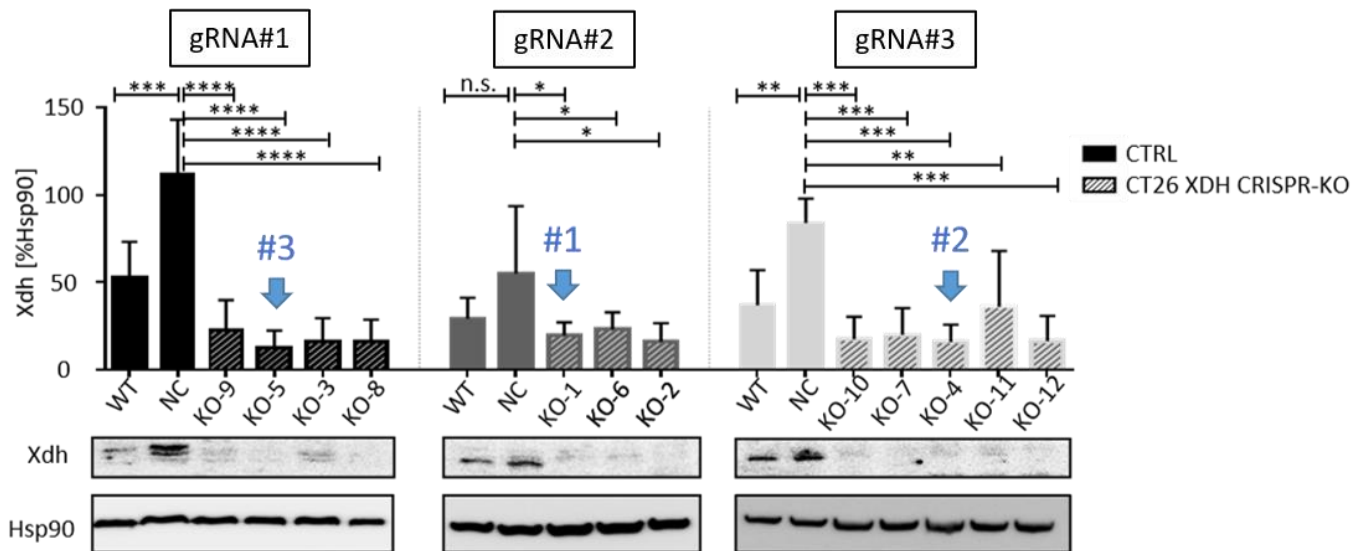


Figure 22: Western Blot and quantification comparing the CRISPR-treated CT26 KO cells with the controls.

Representative Western Blot images and corresponding quantification of Xdh. Controls (monochrome) and Xdh-KO (striped) were measured. Shades representing gRNA#1, #2 and #3 (mean + SD, $n = 3$, student's t-test; * $p < 0.05$, ** $p < 0.01$, *** $p < 0.001$, **** $p < 0.0001$, n.s. = not significant).

3.3.3 The CRISPR/Cas9-treated cells show no difference in morphology and cell metabolic activity

For further experiments we decided to work with the most promising clones, indicated as #1, #2 and #3 in the previous figures.

Apparently, the knockout of *Xdh* in CT26 cells does not change their morphological features. The cells show a diffuse phenotype and, as can be seen in Figure 23, show no difference in morphology compared to the wild type or negative control cells.

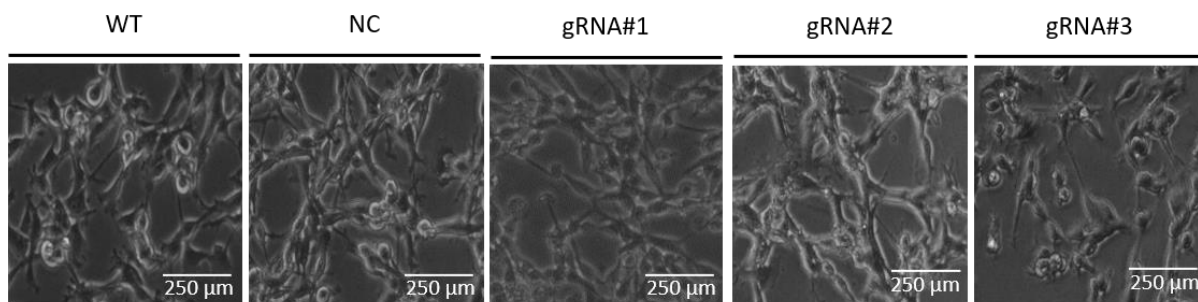


Figure 23: Morphology of CT26 Xdh-KO cells.

Representative pictures of each gRNA compared to the controls. Pictures were taken after 48 h of incubation.

The KO cell lines were tested in an MTT assay. Based on the MTT results, the Xdh-KO doesn't affect the metabolic activity of the CT26 cells at any of the time points tested (24, 48 or 72 h) (Fig. 24).

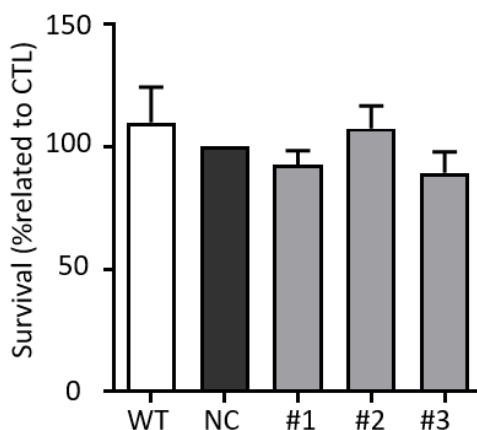


Figure 24: MTT analysis of CT26 Xdh-KO and controls.

MTT assay reveals no differences between controls (WT and NC, black bars) and Xdh-KO (grey bars). Representative results after 24 h (mean + SD, $n = 3$, ordinary one-way Anova).

3.3.3 Xanthine oxidase assay shows no difference in KO cells compared to controls

To date, there is no test available measuring the isolated XDH activity. For that reason, we chose to analyze the XO activity, seeing that it is partly targeted as well in the CRISPR-mediated approach.

A xanthine oxidase (XO) assay was performed to determine the functionality of XO in the CRISPR/Cas9 treated cells compared to the WT and the negative control. The test we performed measures the XO activity through the enzymatic reduction of xanthine to uric acid and the hydrogen peroxide produced in the process, which is then transformed stoichiometrically into a colorimetric substance, read by a photometer. As can be seen in Figure 25, the results showed no difference in the activity of XO in the Xdh-KO cells compared to the negative control and the WT.

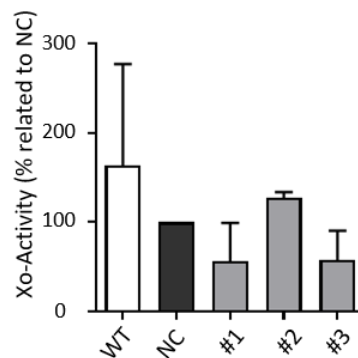


Figure 25: XO activity assay of CT26 Xdh-KO cells.

XO activity measured in the samples and the WT and plotted in relation to the negative control (mean + SD, $n = 2$, ordinary one-way Anova).

3.3.4 ROS-measurement

Re-evaluating our hypothesis stating that Xdh-deprived cells fail to catalyze a reaction that enables ROS quenching, we analyzed the effect of the Xdh-KO on the ROS production of the cells compared to the controls. We used the DCFDA assay as described in 2.2.4.2 to stimulate and measure ROS production.

The first results that can be derived from the experiment are that the basic ROS production (naïve) after 1 h is significantly different in the WT and the NC. After 4 h of incubation with DCFDA, there is no significant difference visible in the two controls.

The KO clones show different results. Only Xdh KO#1 has a significantly higher ROS compared to the WT after 1h stimulation, while the other two clones do not. This difference is lost when compared with the NC, probably due to the mutations carried by the NC as stated before (Figure 26 A). The differences also disappear after 4 h (enzyme saturation, see discussion).

Considering only the net ROS production after 1 h (Fig. 26 B), we see clearly that the clone #1 (Xdh knock-out) is producing a significantly higher amount of ROS compared to the controls and the other two Xdh knock-down clones #2 and #3. The NC is again producing more ROS than the WT, which is explained below.

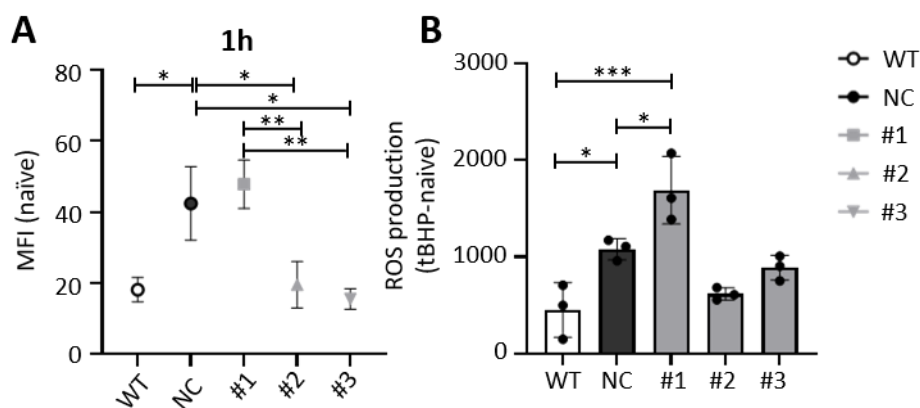


Figure 26: Analysis of ROS production through DCFDA assay.

(A) Plotted are the naïve ROS values of the KO-clones compared to the controls after 1 h. **(B)** Comparison of net ROS production after 1 h (mean + SD, $n = 3$, ordinary one-way ANOVA, MFI = mean fluorescent intensity).

4 Discussion

This project aims at the investigation of the role of ROS-related enzymes (Xdh and Blvrb) in the control of the ROS defense of tumor cells, especially in brain metastasis. One of the major accomplishments to reach this goal has been the establishment of a

stable CRISPR/Cas9 Xdh-KO clone, which allows us to further investigate the role of XDH *ex vivo* and *in vivo*.

4.1 Xdh and Blvrb confirmed as targets

ROS metabolism had been previously identified by our group as a key feature of highly metastasizing cell lines compared to less aggressive counterparts in a breast cancer brain metastasis model. Xdh and Blvrb were two of the seven GSH-related enzymes identified by a proteomic analysis in the highly colonizing cells (Blazquez et al. 2020b)). Thus, the first aim of this work was to confirm this hypothesis. For this, the expression of these two ROS-related enzymes was measured in a set of murine carcinoma cells and compared concerning their metastatic potential (measured by the CI). As expected, the breast and colon cancer cell lines with the highest CI (EO771-LG and CT26, respectively) also displayed the highest Xdh and Blvrb expression (Figure 10).

This finding likely points to an important role of the two enzymes during (brain) metastasis. Which impact it has, however, was not clear yet and therefore subject to our study.

4.2 CRISPR/Cas9 knock-out as a stable model for Xdh-deprivation

What we have confirmed so far is the generation of a model with an Xdh-KO mutation which is integrated into the genome of the cell line of interest, allowing us to test the importance of Xdh-deprivation in that specific cell line in a reliable model. Confirmation was acquired through Next-Generation-Sequencing and Western Blot. However, the results observed through data analysis of NGS has brought up questions regarding the molecular mechanism of CRISPR/Cas9. By using the evaluation tool Outknocker (Schmid-Burgk et al. 2014), we were able to further specify the mutations in every sample in a relatively fast and simple way. Out of 14 tested samples (including the negative control and the WT), we have identified one compound heterozygous mutant, two heterozygous mutants, eight clones showing more than two alleles (including the negative control), and three wildtypes or mutations with no effect on the transcription. It remained unclear at first, as to why eight clones had more than two alleles present.

We concluded that there might be a rest-activity of the Cas9 machinery in the daughter cells, which might be the reason for four or more alleles present in the samples.

Furthermore, it could have been caused during the FACS sort process, in a manner that instead of one cell, two or more cells could have been distributed into one well of a 96-well plate. Those findings are relatively common as they have been observed by other groups using this method of transfection (Bell et al. 2014). It also needs to be recognized, that the cells used in this study are highly aggressive tumor cells. Therefore, further spontaneous mutations are not unlikely.

However, the effect on the NC remains unclear. It is possible that during the FACS sort process, a positive clone was sorted into the 96-well plate instead of a negative one or additionally to the negative clone. This could be due to contaminations in the flow cytometer itself or to contaminations in the preparation or the following experiments with this sample. The NGS results confirm the presence of Xdh-KO sequences in the NC; however, the majority of present alleles in the sample consists of non-KO-sequences.

The WT and NC also vary in their protein expression of Xdh. This difference might be due to the mutations present in the NC that possibly enhance the translation of Xdh. However, it could also be due to a slightly different confluence of the cells when the protein was isolated, leading to different expressions of proteins.

Another limitation would be the data evaluation of the Outknocker tool used to assess the quality of knock-outs in the deep-sequenced samples. The tool is mostly based on evaluating the out-of-frame or in-frame quality of an INDEL, consequently being displayed as a knock-out or no knock-out, respectively. However, the specific amino acid switch in the samples induced by the given insertions or deletions is not further specified, meaning that a 3-base deletion which results in a methionine deletion, for instance, is being treated the same (3 bases equalling an in-frame mutation, but also a deletion of the start codon) as a 3-base deletion of any other amino acid. This leads to an underrepresentation of molecular knock-outs and thus a possible misinterpretation of the actual quality of the INDEL. Therefore, we have summarized the indel patterns more closely and re-evaluated the quality of out-of-frame and in-frame mutations for each sample. In consequence, we consider out-of-frame INDELS that are in the exon and in-frame mutations that delete or change the presence of the

start codon Methionine to lead to a KO. In contrast, out-of-frame mutations that were not in the exon and in-frame mutations which are not affecting the start codon Methionine are considered to not lead to a KO. However, this assumption also serves as a possible underrepresentation of actual KOs, considering INDELS that are not in the exon can also influence transcription, e.g., by altering promoters or enhancers. Additionally, the in-frame INDELS could potentially be changing the tertiary and quaternary structure of the enzyme, which could lead to a functional knock-out as well.

This could also be responsible for the varying results observed in the analysis of RNA expression through qRT-PCR. The various INDELS detected in the samples suggests that the RNA is not being transcribed equally. Whereas some mutations possibly enhance transcription (KO-3), others might reduce it (#1, KO-12) by, e.g., deleting the promoter, which could be the cause for differentially expressed Xdh in the samples.

4.3 XDH expression – survival advantage or highway to hell?

It is known that XOR plays a role in the oxidation of hypoxanthine to xanthine and xanthine to uric acid, which is a non-enzymatic ROS scavenger (Boueiz et al. 2008; Glantzounis et al. 2005). XOR is linked to GSH metabolism and focusses mostly on the antioxidant role in water-soluble proteins. However, it also plays an essential role in producing ROS metabolites. During the two main reactions mentioned above, among others, H_2O_2 and O_2^- are generated as a side product. Both are radicals and a part of the reactive oxygen species in the human organism. The xanthine dehydrogenase (XDH), however, is just one isoform of the enzyme xanthine oxidoreductase (XOR), which is mostly involved in the generation of NADH, while XO mostly generates ROS species as a side product. XOR, depending on the state of the coenzymes molybdenum and FAD and its substrates, can act as a reducing (XDH) or oxidizing (xanthine oxidase, XO) enzyme.

Interestingly, different research groups have studied Xdh in more than one type of cancer, reaching different conclusions concerning the most important functions of the enzyme in cancer cells (Xu et al. 2019; Konno et al. 2012). Xu et al., for example, studied Xdh in prostate cancer, showing convincing data which highlight the ROS-producing parts of the reaction, while Xdh was expressed at a very low level in this cell

line and was not considered of high importance for this cancer type in general. For the adenocarcinoma of the lung, however, Konno et al. pointed out the correlation of high XDH levels in the malignant cells and poor prognosis.

In the experiments confirming our targets, the importance of Xdh was highlighted. Thus, we planned to investigate the impact of the Xor isoform Xdh as isolated as possible. Unfortunately, this goal was limited in our pharmacological approach due to the lack of Xdh inhibitors. In the genetic approach, we generated several clones with large INDELS, rendering it possible that both Xdh and Xo functions have been compromised. Nonetheless, the impact of the Xor, and in particular, the isolated functions of Xo and Xdh on tumor growth, have been investigated by Kusano et al. (Kusano et al. 2019). They concluded that isolated Xo expression in mice enhances tumor growth, which confirms the importance of both isoforms of the enzyme Xor. Therefore, the obtained results are described as Xdh-manipulated but can be considered to be partly Xo-manipulated as well, as can be suspected by the results received in the Xo activity assay, which show a tendency to reduced Xo activity in the KO-cells (Figure 25). However, to make a reliable assumption concerning Xo activity, more biological replicates need to be tested.

Concerning the survival of the Xdh-KO cells, we performed an MTT assay after 72 h of incubation. The Xdh-manipulated cells did not show a survival advantage, nor did they show impairments of survival compared to the WT and NC. This could be due to Xor not being facilitated as much under non-stressful situations for the cell. It can be suspected that the Xdh-KO and the Xdh knock-down cells react differently when confronted with oxidative stress. This will be tested in future experiments.

Through the inhibition of Xor with the Xdh-i Febuxostat, we achieved similar results. Compared to the DMSO control, we only saw a decrease in survival in the MTT at high concentrations of 100 μ M. This effect is supposedly due to toxic effects of Febuxostat (Jordan 2017). In all other concentrations, there was no visible effect on survival. This confirms our suspicion that Xor-depletion has no crucial effect on viability as long as the cell is facing a physiological level of ROS production.

4.4 XDH as ROS quencher or ROS producer?

In several experiments, we analyzed the consequences of pharmacological Xor inhibition. For that, we chose the inhibitor Febuxostat. It is a non-purine inhibitor of XOR. The inhibitor has several advantages compared to more common inhibitors like Allopurinol or Oxypurinol, which are purine inhibitors. On the one hand, it inhibits the xanthine dehydrogenase as well as the xanthine oxidase. Allopurinol inhibits the molybdopterin part of the enzyme, meaning it does not inhibit all its functions. On the other hand, it is also being used in mice, making it a good choice for possible future experiments. It has a subnanomolar K_i and is a very selective inhibitor of XOR compared to Allopurinol or Oxypurinol, which also inhibit other enzymes that are part of the purine and pyrimidine metabolism (Takano et al. 2005).

After inhibiting Xor with Xdh-i for several incubation times, we did not see a change in protein expression of Xdh in the Western Blot, nor did we see significant changes in gene expression in the qRT-PCR. This could be subject to the form of inhibition. Febuxostat, working as an inhibitor of both forms of the enzyme, does not need to come with a change of the amount of enzyme. The inhibition happens posttranslationally through the binding of Febuxostat to a molecular channel, leading to a binding site of the enzyme. This could be an explanation for not seeing changes in gene and protein expression. Furthermore, Allopurinol binding results in a suicide inhibition of XO, which Febuxostat does not enhance (Takano et al. 2005).

The functionality of the enzyme after being inhibited by Xdh-i for several incubation periods, however, is something we examined partly through the ROS stimulation assay. The products of XDH, especially ROS and uric acid, and their role in cancer have been widely discussed in literature (Battelli et al. 2016a; Mi et al. 2020). It is known that systemic ROS is associated with prooncogenic processes like inflammation and DNA damage. It has also been known for a long time now that uric acid can work as an antioxidant (Ames et al. 1981), thus implying uric acid might have an antioncogenic potential by scavenging harmful reactive species. However, there have also been studies describing uric acid as a potential prooncogenic substance, associated with earlier mortality in several metastasized cancerous diseases and activation of prooncogenic cytokines and pathways (Fini et al. 2012). It remains unclear, in which context uric acid serves as a scavenger and in which as a potential threat. To evaluate the impact of Xdh on the ROS metabolism of CT26 and EO771-LG, we started to assess the capability and intensity of ROS production in the cells

inhibited by Xdh-i for several incubation periods (1/4/24 h). The significance of this experiment is limited since only the results of 24 h of incubation with Xdh-i have been tested in a statistically relevant manner.

However, at 24 h of Xdh-i treatment, we observed no significant changes after 1 h and 4 h of incubation with DCFDA and tBHP in naïve ROS production, in maximum ROS production, and most importantly, no significant changes between the control group and the treated group (Fig. 26). Thus, through this experiment, we did not gain insight into the nature of Xdh in the highly aggressive cancer cell lines CT26 and EO771-LG and whether it serves as a ROS scavenger or ROS producer. Therefore, we had to further inspect this mechanism with the Xdh-KO cells compared to the WT and Xdh knock-down cells we generated in our genetic approach.

We observed several interesting changes in the naïve ROS levels as well as in the net ROS production of each sample. First, the NC and the WT showed significantly different results. This is an observation that fits in with the results obtained in the NGS (discussed below). The NC seems to have been mixed with clones containing several alleles with a CRISPR-induced INDEL.

Still, several parts of the ROS measurement are noteworthy. The #1 (Xdh-KO) shows a higher basic ROS production after 1 h of incubation than the other generated clones (all Xdh knock-down). The deprivation of Xdh seems to influence the cell in a way, that either ROS production is now being increased by compensating mechanisms or the ROS-scavenging impact of Xdh through uric acid being gone, the cancer cell has a harder time coping with the basic ROS that is produced under physiological oncogenic conditions. The NC, however, also shows this kind of behaviour. What varies between the NC and #1 is the net ROS production after 1 h. The clone #1 reacts to tBHP with an extreme increase in ROS after 1 h with a 36.1-fold increase in ROS compared to the WT (23.9-fold) and NC (27.1-fold). However, the increase of #2 and #3 is even higher with 48.5-fold and 41.1-fold, respectively, thus implying the potential to produce ROS has amplified in the Xdh-KO and Xdh knock-down cells. Most importantly, Xdh-KO clone #1 has the highest net ROS production. This further strengthens the hypothesis that Xdh is involved in the ROS scavenging process, since the clone without Xdh generates the highest ROS levels when challenged.

The dynamics of the maximum ROS production should be investigated further as well (Supplementary). The samples all seem to reach a plateau of maximum ROS production after 4 h. Remarkably, the #1 clone is the only clone, which is not increasing its maximum ROS production, but reducing it. This is very important, considering that #1 is the only clone with a confirmed full KO.

Xdh does not seem to be of immense importance for ROS generation at first (1 h tBHP). In fact, it seems to be the opposite. Initially, the production of ROS in the cells without Xdh shoots the highest, suggesting an early involvement of Xdh in its ROS scavenging function when reacting to oxidative stress.

In the further process (4h tBHP) Xdh seems to have more prominent effects on ROS production. The samples with Xdh (WT, NC, #2, #3) produce more ROS in the process. Clone #1, however, shows a net reduction of ROS (Supplementary).

One possible explanation could be the saturation of Xdh at a certain time point. In turn, less uric acid would be produced, and thus the loss of ROS scavenging could be the consequence. In #1, Xdh is not present and therefore its main product, uric acid, cannot scavenge ROS. The reduction of ROS after more prolonged stimulation in this Xdh^{-/-} sample could thus be caused by other enzymes or non-enzymatic ROS scavengers present in the cell that compensate for Xdh. The limitation of this explication is the steady rise of ROS in the Xdh-carrying samples. If there is no Xdh present in the clone #1 and it still decreases in ROS, then the compensating mechanisms seem to be very strong, stronger even than the functioning Xdh in the other samples. Since there are only two points in time inspected in this experiment, it is hard to say, whether the compensating mechanisms would also arise and show this kind of ROS reduction in the process when there is obviously a need for ROS coping mechanisms due to the saturation of Xdh. It remains unclear, whether those compensating mechanisms only ascend when the increase in ROS is very sudden (e.g., after 1 h of tBHP stimulation in #1) or if there might be a certain threshold of ROS that, when being reached, activates other coping mechanisms.

Another explanation could be that, at this point, i.e., after 4 h of tBHP stimulation, Xdh is the main ROS producing agent, meaning it changes its function from a ROS scavenger at first, to a ROS producer later on. Permanent ROS stimulation comes with a change in several metabolic and inflammatory pathways. Those pathways are often

responsible for the pH varying or more oxygen being consumed, thus possibly reducing the oxygen tension. It is known that especially under hypoxic conditions, the NADH-dependent XDH produces ROS (Battelli et al. 2016b). Since the expression of Xdh is supposedly the only difference between #1 and the other samples, the reduction of ROS in #1 after 4 h of tBHP could also be caused by the lack of Xdh-dependent ROS production.

These hypotheses remain to be investigated further. Designing an experiment with an even longer ROS stimulation could reveal the actual character of Xdh-dependent ROS production and reduction in the examined cell lines.

Derived from the above-discussed results, XDH is most likely a very important ROS scavenger in the initial phase of defense. Translated to the condition of cancer cells in the human brain, this means that carrying a high load of XDH could be a possible survival advantage when confronted with high amounts of ROS from, e.g., macrophages/microglia, which is the case during the process of brain metastasis. The fact that there is a stable Xdh-KO cell line present will hopefully make further examination on the role of Xdh more realizable and reliable.

4.5 Pharmacological inhibition of BLVRB still uncertain

Biliverdin-reductase α (BVR-A or BLVRA) and β (BVR-B or BLVRB) are subject to recent studies, especially concerning their importance in the metabolism of oxidative stress. Our findings suggest that Blvrb is of vast importance in the metabolism of CT26 and EO771-LG. However, targeting this protein, both pharmacologically and genetically, has proven to be a challenge we have not yet succeeded at in our recent study. The protein expression has not changed after stimulation with the Blvrb inhibitor Phloxine B (Blvrb-i). Nor have we seen significant differences in gene expression after stimulation, which suggests that the inhibition has not been successful yet. This might be due to the type of inhibitor we chose. Phloxine B is a small molecule cell stain, which showed BLVRB inhibition with an IC^{50} of $0.7 \pm 0.36 \mu\text{M}$ in a previous study (Nesbitt et al. 2018). The cells used in that study were BLVRB-overexpressing promyelocytic HL-60 cells. It is possible, that our cells (CT26 and EO771-LG), derived from murine cancer entities, are less sensitive for Blvrb-i, e.g., due to structural varieties in human and murine BLVRB.

Overall, the recent findings in literature are indicating a strong association of both BLVRA and BLVRB to oxidative stress regulation (Chen et al. 2018) through heme oxygenase 1 (HO-1) (Gordon et al. 2019; Ahmad et al. 2002) but also independently of the HO-1 pathway, in a cytoprotective manner (Miralem et al. 2005). These results of different research groups highlight the necessity to further investigate the role of Blvrb in tumor cells, especially concerning the reaction to oxidative stress. The current possibilities of pharmacologically inhibiting the protein are limited since potential inhibitors might interfere with colorimetric assays or could not be specific enough; still, it is a promising target for further experiments.

As well as the pharmacological approach, we investigated the genetic knock-out of Blvrb with CRISPR/Cas9 as described above. We received plenty of ATTO550-positive clones with the lipofection. Most of these clones were growing sufficiently in a 96-well plate. Unfortunately, after analyzation of these clones in the T7 Endonuclease 1 assay, we received not one positive result at the expected cut site induced by CRISPR but several cutting products that let us conclude that mismatches were produced at various DNA sites. This could be subject to low specificity of the introduced gRNAs, meaning even though they were successfully brought into the cell and were able to interact with the DNA, they only settled in low amounts at the *Blvrb* gene site and had a higher binding affinity to different DNA sites. However, by choosing the RNP method of transfection, we chose the method with the least off-target effects in comparison to plasmid transfection according to recent findings confirmed in various studies (Kim et al. 2014; Ramakrishna et al. 2014). The predicted on-target score for the three Blvrb gRNA's was 49, 67 and 89 percent, respectively, while the off-target score was a little higher in comparison with 83, 88 and 67 percent, respectively. This being an explanation for the results observed in the T7E1 assay, we are strongly ambitious to retry the CRISPR/Cas9-induced knock-out of *Blvrb* with different gRNAs in the highly expressing and aggressive cell lines CT26 and EO771-LG for further studies.

4.6 Outlook

In order to further evaluate the consequences of the Xdh knock-out, we need to further characterize the generated cell lines with regard to their migration, invasion,

proliferation and colonization potential. This can be achieved by performing Boyden chamber assays, BrdU assays and colony formation assays (CFAs), respectively.

In a more clinical approach, we want to stimulate the cells with the chemotherapeutic agent 5-FU, which is not only a potent ROS inducer but also working in the pyrimidine metabolism, by inhibiting thymidylate synthase (Longley et al. 2003). We want to measure ROS production in the Xdh-KO cells compared to the WT and Xdh knock-down cells, and compare their behaviour concerning survival (MTT), proliferation, migration, invasion and colonization with the cell lines before 5-FU stimulation. The results of those experiments will lead to insight into the coping of the Xdh-KO cells with oxidative stress induced by chemotherapy *in vitro*.

Furthermore, it is necessary to examine the cells in an *ex vivo* setting. For this, previous work of the group has established a brain slice co-culture model (Blazquez und Pukrop 2017), imitating the physiological environment during the process of infiltration. This model will be of immense importance for the planning of further experiments in an *in vivo* setting.

Considering the importance of uric acid as a ROS quencher, Kusano et al. concluded that uric acid is not part of tumorigenesis (Kusano et al. 2019). However, those results were obtained in uricase carrying mice, an enzyme that converts uric acid to allantoin. This minimizes the validity of the assumptions made by the results they received concerning the function of uric acid. Thus, the impact of the main XOR product uric acid on tumor growth and survival needs to be assessed further. However, for future *in vivo* experiments in mice, it should be noted that a mouse line with a uricase (Uox) knock-out should be chosen to ensure the results and observations are translationally valid and representative. The uricase or uric oxidase is an enzyme present in most mammals, but not in humans. It is considered to oxidize uric acid to allantoin, which is excreted in the urine effortlessly (Maiuolo et al. 2016). Inazawa et al. have shown that uricase knock-out mice are an excellent potential model for research of the purine metabolism in humans (Inazawa et al. 2016).

5 Summary and conclusions

In this thesis, I have generated a clone of the colon cancer cell line CT26 carrying a full knock out on the Xdh gene. This has been achieved via a CRISPR/Cas9-mediated

approach. By doing so, I have established this method in our laboratory. Additionally, through the pharmacological inhibition of Xor and Blvrb, we have assessed the impact of these inhibitors on protein and gene expression and therefore, further characterized them in this context. Furthermore, we evaluated the impact of inhibition of Xor on ROS production in the cells. In order to study the impact of Xdh on oxidative species in the cancer cell more thoroughly, we analyzed the ROS production of the CT26 Xdh-KO cells and their capability to produce or quench ROS. We have seen significant differences in the KO-cells and the WT, highlighting the influence of Xdh in the ROS metabolism. It remains to be inspected, which impact falls on the Xo and which on Xdh subtype of the enzyme Xor.

The clinical importance of these findings lies in the lack of proper therapeutic strategies so far, that target the colonization process. Since disease progression is mainly determined in this step of metastasis, it is clear that new emerging strategies need to be inspected. Targeting the ROS metabolism of highly aggressive colon and breast cancers is a possible mechanism of interfering with colonization.

In conclusion, we have confirmed parts of our hypothesis and enabled the hypothesis to be further examined with an Xdh-deprived clone. It will be crucial to evaluate the Xdh-KO cells in an ex vivo manner as described above, especially in order to examine the brain infiltration and the reaction of immune cells when being confronted with the manipulated cells. Xdh remains to be a promising target for therapy against highly aggressive brain metastases, which are to date insufficiently treatable.

6 Literaturverzeichnis

- Achrol, Achal Singh; Rennert, Robert C.; Anders, Carey; Soffiatti, Riccardo; Ahluwalia, Manmeet S.; Nayak, Lakshmi et al. (2019): Brain metastases. In: *Nature reviews. Disease primers* 5 (1), S. 5. DOI: 10.1038/s41572-018-0055-y.
- Ahmad, Zulfiqar; Salim, Mohammad; Maines, Mahin D. (2002): Human biliverdin reductase is a leucine zipper-like DNA-binding protein and functions in transcriptional activation of heme oxygenase-1 by oxidative stress. In: *The Journal of biological chemistry* 277 (11), S. 9226–9232. DOI: 10.1074/jbc.M108239200.
- Amaya, Y.; Yamazaki, K.; Sato, M.; Noda, K.; Nishino, T. (1990): Proteolytic conversion of xanthine dehydrogenase from the NAD-dependent type to the O₂-dependent type. Amino acid sequence of rat liver xanthine dehydrogenase and identification of the cleavage sites of the enzyme protein during irreversible conversion by trypsin. In: *The Journal of biological chemistry* 265 (24), S. 14170–14175.
- Ames, B. N.; Cathcart, R.; Schwiers, E.; Hochstein, P. (1981): Uric acid provides an antioxidant defense in humans against oxidant- and radical-caused aging and cancer: a hypothesis. In: *Proceedings of the National Academy of Sciences of the United States of America* 78 (11), S. 6858–6862. DOI: 10.1073/pnas.78.11.6858.
- Andreyev, A. Y.; Kushnareva, Y. E.; Murphy, A. N.; Starkov, A. A. (2015): Mitochondrial ROS Metabolism: 10 Years Later. In: *Biochemistry. Biokhimiia* 80 (5), S. 517–531. DOI: 10.1134/S0006297915050028.
- Balaban, Robert S.; Nemoto, Shino; Finkel, Toren (2005): Mitochondria, oxidants, and aging. In: *Cell* 120 (4), S. 483–495. DOI: 10.1016/j.cell.2005.02.001.
- Battelli, Maria Giulia; Polito, Letizia; Bortolotti, Massimo; Bolognesi, Andrea (2016a): Xanthine oxidoreductase in cancer: more than a differentiation marker. In: *Cancer medicine* 5 (3), S. 546–557. DOI: 10.1002/cam4.601.
- Battelli, Maria Giulia; Polito, Letizia; Bortolotti, Massimo; Bolognesi, Andrea (2016b): Xanthine Oxidoreductase-Derived Reactive Species: Physiological and Pathological Effects. In: *Oxidative medicine and cellular longevity* 2016, S. 3527579. DOI: 10.1155/2016/3527579.
- Bell, Charles C.; Magor, Graham W.; Gillinder, Kevin R.; Perkins, Andrew C. (2014): A high-throughput screening strategy for detecting CRISPR-Cas9 induced mutations using next-generation sequencing. In: *BMC genomics* 15, S. 1002. DOI: 10.1186/1471-2164-15-1002.
- Blazquez, R.; Sparrer, D.; Wendl, C.; Evert, M.; Riemenschneider, M. J.; Krahn, M. P. et al. (2020a): The macro-metastasis/organ parenchyma interface (MMPI) - A hitherto unnoticed area. In: *Seminars in cancer biology* 60, S. 324–333. DOI: 10.1016/j.semcancer.2019.10.012.

- Blazquez, Raquel; Pukrop, Tobias (2017): 3D Coculture Model of the Brain Parenchyma-Metastasis Interface of Brain Metastasis. In: *Methods in molecular biology (Clifton, N.J.)* 1612, S. 213–222. DOI: 10.1007/978-1-4939-7021-6_16.
- Blazquez, Raquel; Rietkötter, Eva; Wenske, Britta; Wlochowicz, Darius; Sparrer, Daniela; Vollmer, Elena et al. (2020b): LEF1 supports metastatic brain colonization by regulating glutathione metabolism and increasing ROS resistance in breast cancer. In: *International journal of cancer* 146 (11), S. 3170–3183. DOI: 10.1002/ijc.32742.
- Blazquez, Raquel; Wlochowicz, Darius; Wolff, Alexander; Seitz, Stefanie; Wachter, Astrid; Perera-Bel, Julia et al. (2018): PI3K: A master regulator of brain metastasis-promoting macrophages/microglia. In: *Glia* 66 (11), S. 2438–2455. DOI: 10.1002/glia.23485.
- Boire, Adrienne; Brastianos, Priscilla K.; Garzia, Livia; Valiente, Manuel (2020): Brain metastasis. In: *Nature reviews. Cancer* 20 (1), S. 4–11. DOI: 10.1038/s41568-019-0220-y.
- Boueiz, Adel; Damarla, Mahendra; Hassoun, Paul M. (2008): Xanthine oxidoreductase in respiratory and cardiovascular disorders. In: *American journal of physiology. Lung cellular and molecular physiology* 294 (5), L830-40. DOI: 10.1152/ajplung.00007.2008.
- Brown, Paul D.; Ballman, Karla V.; Cerhan, Jane H.; Anderson, S. Keith; Carrero, Xiomara W.; Whitton, Anthony C. et al. (2017): Postoperative stereotactic radiosurgery compared with whole brain radiotherapy for resected metastatic brain disease (NCCTG N107C/CEC-3): a multicentre, randomised, controlled, phase 3 trial. In: *The Lancet Oncology* 18 (8), S. 1049–1060. DOI: 10.1016/S1470-2045(17)30441-2.
- Chen, Weiyu; Maghzal, Ghassan J.; Ayer, Anita; Suarna, Cacang; Dunn, Louise L.; Stocker, Roland (2018): Absence of the biliverdin reductase-a gene is associated with increased endogenous oxidative stress. In: *Free radical biology & medicine* 115, S. 156–165. DOI: 10.1016/j.freeradbiomed.2017.11.020.
- Christodoulou, Christos; Bafaloukos, Dimitrios; Linardou, Helen; Aravantinos, Gerassimos; Bamias, Aristotelis; Carina, Maria et al. (2005): Temozolomide (TMZ) combined with cisplatin (CDDP) in patients with brain metastases from solid tumors: a Hellenic Cooperative Oncology Group (HeCOG) Phase II study. In: *Journal of neuro-oncology* 71 (1), S. 61–65. DOI: 10.1007/s11060-004-9176-0.
- Chuang, Han-Ning; van Rossum, Denise; Sieger, Dirk; Siam, Laila; Klemm, Florian; Bleckmann, Annalen et al. (2013): Carcinoma cells misuse the host tissue damage response to invade the brain. In: *Glia* 61 (8), S. 1331–1346. DOI: 10.1002/glia.22518.
- Chung, Ling-Yen; Tang, Shye-Jye; Wu, Yi-Ching; Yang, Kai-Chi; Huang, Hui-Ju; Sun, Guang-Huan; Sun, Kuang-Hui (2020): Platinum-based combination chemotherapy triggers cancer cell death through induction of BNIP3 and ROS,

- but not autophagy. In: *Journal of cellular and molecular medicine* 24 (2), S. 1993–2003. DOI: 10.1111/jcmm.14898.
- Culemann, Stephan; Grüneboom, Anika; Nicolás-Ávila, José Ángel; Weidner, Daniela; Lämmle, Katrin Franziska; Rothe, Tobias et al. (2019): Locally renewing resident synovial macrophages provide a protective barrier for the joint. In: *Nature* 572 (7771), S. 670–675. DOI: 10.1038/s41586-019-1471-1.
- D'Andrea, Giancarlo; Palombi, Lucia; Minniti, Giuseppe; Pesce, Alessandro; Marchetti, Paolo (2017): Brain Metastases: Surgical Treatment and Overall Survival. In: *World neurosurgery* 97, S. 169–177. DOI: 10.1016/j.wneu.2016.09.054.
- Davalos, Dimitrios; Grutzendler, Jaime; Yang, Guang; Kim, Jiyun V.; Zuo, Yi; Jung, Steffen et al. (2005): ATP mediates rapid microglial response to local brain injury in vivo. In: *Nature neuroscience* 8 (6), S. 752–758. DOI: 10.1038/nn1472.
- Davis, Alexander; Gao, Ruli; Navin, Nicholas (2017): Tumor evolution: Linear, branching, neutral or punctuated? In: *Biochimica et biophysica acta. Reviews on cancer* 1867 (2), S. 151–161. DOI: 10.1016/j.bbcan.2017.01.003.
- Dixon, Scott J.; Stockwell, Brent R. (2014): The role of iron and reactive oxygen species in cell death. In: *Nature chemical biology* 10 (1), S. 9–17. DOI: 10.1038/nchembio.1416.
- Fidler, I. J. (1970): Metastasis: Quantitative Analysis of Distribution and Fate of Tumor Emboli Labeled With ¹²⁵I-5-Iodo-2'-deoxyuridine. In: *JNCI: Journal of the National Cancer Institute*. DOI: 10.1093/jnci/45.4.773.
- Fidler, Isaiah J.; Kozlowski, James M. (1984): The heterogeneous nature of metastatic neoplasms: Implications for the treatment of cancer. In: *Urology* 23 (4), S. 29–38. DOI: 10.1016/s0090-4295(84)80064-3.
- Fini, Mehdi A.; Elias, Anthony; Johnson, Richard J.; Wright, Richard M. (2012): Contribution of uric acid to cancer risk, recurrence, and mortality. In: *Clinical and translational medicine* 1 (1), S. 16. DOI: 10.1186/2001-1326-1-16.
- Focusing on brain tumours and brain metastasis (2020). In: *Nature reviews. Cancer* 20 (1), S. 1.
- Forrester, Steven J.; Kikuchi, Daniel S.; Hernandez, Marina S.; Xu, Qian; Griendling, Kathy K. (2018): Reactive Oxygen Species in Metabolic and Inflammatory Signaling. In: *Circulation research* 122 (6), S. 877–902. DOI: 10.1161/CIRCRESAHA.117.311401.
- Franklin, Edward M.; Browne, Seamus; Horan, Anne M.; Inomata, Katsuhiko; Hammam, Mostafa A. S.; Kinoshita, Hideki et al. (2009): The use of synthetic linear tetrapyrroles to probe the verdin sites of human biliverdin-IXalpha reductase and human biliverdin-IXbeta reductase. In: *The FEBS journal* 276 (16), S. 4405–4413. DOI: 10.1111/j.1742-4658.2009.07148.x.
- Ganesh, Karuna; Massagué, Joan (2021): Targeting metastatic cancer. In: *Nature medicine* 27 (1), S. 34–44. DOI: 10.1038/s41591-020-01195-4.

- Glantzounis, G. K.; Tsimoyiannis, E. C.; Kappas, A. M.; Galaris, D. A. (2005): Uric acid and oxidative stress. In: *Current pharmaceutical design* 11 (32), S. 4145–4151. DOI: 10.2174/138161205774913255.
- Gordon, Darren M.; Adeosun, Samuel O.; Ngwudike, Somtochukwu I.; Anderson, Christopher D.; Hall, John E.; Hinds, Terry D., JR; Stec, David E. (2019): CRISPR Cas9-mediated deletion of biliverdin reductase A (BVRA) in mouse liver cells induces oxidative stress and lipid accumulation. In: *Archives of biochemistry and biophysics* 672, S. 108072. DOI: 10.1016/j.abb.2019.108072.
- Hille, Frank; Richter, Hagen; Wong, Shi Pey; Bratovic, Majda; Ressel, Sarah; Charpentier, Emmanuelle (2018): The Biology of CRISPR-Cas: Backward and Forward. In: *Cell* 172 (6), S. 1239–1259. DOI: 10.1016/j.cell.2017.11.032.
- Hohensee, Ina; Chuang, Han-Ning; Grottke, Astrid; Werner, Stefan; Schulte, Alexander; Horn, Stefan et al. (2017): PTEN mediates the cross talk between breast and glial cells in brain metastases leading to rapid disease progression. In: *Oncotarget* 8 (4), S. 6155–6168. DOI: 10.18632/oncotarget.14047.
- Inazawa, K.; Yamaguchi, S.; Hosoyamada, M.; Fukuuchi, T.; Tomioka, N. H.; Yamaoka, N.; Kaneko, K. (2016): Urinary excretion of uric acid, allantoin, and 8-OH-Deoxyguanosine in uricase-knockout mice. In: *Nucleosides, nucleotides & nucleic acids* 35 (10-12), S. 559–565. DOI: 10.1080/15257770.2016.1163376.
- Jay Forman, H. (2001): Redox signaling in macrophages. In: *Molecular Aspects of Medicine* 22 (4-5), S. 189–216. DOI: 10.1016/s0098-2997(01)00010-3.
- Jordan, Andreas (2017): Nebenwirkungen und Interaktionen des Xanthinoxidasehemmers Febuxostat. Auswertung der wissenschaftlichen Literatur. Unter Mitarbeit von Ursula Gresser. München: Universitätsbibliothek der Ludwig-Maximilians-Universität.
- Kann, Benjamin H.; Park, Henry S.; Johnson, Skyler B.; Chiang, Veronica L.; Yu, James B. (2017): Radiosurgery for Brain Metastases: Changing Practice Patterns and Disparities in the United States. In: *Journal of the National Comprehensive Cancer Network : JNCCN* 15 (12), S. 1494–1502. DOI: 10.6004/jnccn.2017.7003.
- Kienast, Yvonne; Baumgarten, Louisa von; Fuhrmann, Martin; Klinkert, Wolfgang E. F.; Goldbrunner, Roland; Herms, Jochen; Winkler, Frank (2010): Real-time imaging reveals the single steps of brain metastasis formation. In: *Nature medicine* 16 (1), S. 116–122. DOI: 10.1038/nm.2072.
- Kim, Sojung; Kim, Daesik; Cho, Seung Woo; Kim, Jungeun; Kim, Jin-Soo (2014): Highly efficient RNA-guided genome editing in human cells via delivery of purified Cas9 ribonucleoproteins. In: *Genome Research* 24 (6), S. 1012–1019. DOI: 10.1101/gr.171322.113.
- Kusano, Teruo; Ehrchiou, Driss; Matsumura, Tomohiro; Chobaz, Veronique; Nasi, Sonia; Castelblanco, Mariela et al. (2019): Targeted knock-in mice expressing the oxidase-fixed form of xanthine oxidoreductase favor tumor growth. In: *Nature communications* 10 (1), S. 4904. DOI: 10.1038/s41467-019-12565-z.

- Larkin, J. M. G.; Hughes, S. A.; Beirne, D. A.; Patel, P. M.; Gibbens, I. M.; Bate, S. C. et al. (2007): A phase I/II study of lomustine and temozolomide in patients with cerebral metastases from malignant melanoma. In: *British journal of cancer* 96 (1), S. 44–48. DOI: 10.1038/sj.bjc.6603503.
- Le Scodan, Romuald; Jouanneau, Ludivine; Massard, Christophe; Gutierrez, Maya; Kirova, Youlia; Cherel, Pascal et al. (2011): Brain metastases from breast cancer: prognostic significance of HER-2 overexpression, effect of trastuzumab and cause of death. In: *BMC cancer* 11, S. 395. DOI: 10.1186/1471-2407-11-395.
- Li, Jie; Cao, Feng; Yin, He-Liang; Huang, Zi-Jian; Lin, Zhi-Tao; Mao, Ning et al. (2020): Ferroptosis: past, present and future. In: *Cell death & disease* 11 (2), S. 88. DOI: 10.1038/s41419-020-2298-2.
- Li, Zongdong; Nesbitt, Natasha M.; Malone, Lisa E.; Gnatenko, Dimitri V.; Wu, Song; Wang, Daifeng et al. (2018): Heme degradation enzyme biliverdin IXbeta reductase is required for stem cell glutamine metabolism. In: *The Biochemical journal* 475 (6), S. 1211–1223. DOI: 10.1042/BCJ20180016.
- Longley, Daniel B.; Harkin, D. Paul; Johnston, Patrick G. (2003): 5-fluorouracil: mechanisms of action and clinical strategies. In: *Nature reviews. Cancer* 3 (5), S. 330–338. DOI: 10.1038/nrc1074.
- Lorger, Mihaela; Felding-Habermann, Brunhilde (2010): Capturing changes in the brain microenvironment during initial steps of breast cancer brain metastasis. In: *The American Journal of Pathology* 176 (6), S. 2958–2971. DOI: 10.2353/ajpath.2010.090838.
- Maiuolo, Jessica; Oppedisano, Francesca; Gratteri, Santo; Muscoli, Carolina; Mollace, Vincenzo (2016): Regulation of uric acid metabolism and excretion. In: *International journal of cardiology* 213, S. 8–14. DOI: 10.1016/j.ijcard.2015.08.109.
- Marusyk, Andriy; Polyak, Kornelia (2010): Tumor heterogeneity: causes and consequences. In: *Biochimica et biophysica acta* 1805 (1), S. 105–117. DOI: 10.1016/j.bbcan.2009.11.002.
- Mi, Shuyi; Gong, Liang; Sui, Ziqi (2020): Friend or Foe? An Unrecognized Role of Uric Acid in Cancer Development and the Potential Anticancer Effects of Uric Acid-lowering Drugs. In: *Journal of Cancer* 11 (17), S. 5236–5244. DOI: 10.7150/jca.46200.
- Miralem, Tihomir; Hu, Zhenbo; Torno, Michael D.; Lelli, Katherine M.; Maines, Mahin D. (2005): Small interference RNA-mediated gene silencing of human biliverdin reductase, but not that of heme oxygenase-1, attenuates arsenite-mediated induction of the oxygenase and increases apoptosis in 293A kidney cells. In: *The Journal of biological chemistry* 280 (17), S. 17084–17092. DOI: 10.1074/jbc.M413121200.
- Morita, Mayuko; Naito, Yuji; Itoh, Yoshito; Niki, Etsuo (2019): Comparative study on the plasma lipid oxidation induced by peroxynitrite and peroxy radicals and its

- inhibition by antioxidants. In: *Free radical research* 53 (11-12), S. 1101–1113. DOI: 10.1080/10715762.2019.1688799.
- Nesbitt, Natasha M.; Zheng, Xiliang; Li, Zongdong; Manso, José A.; Yen, Wan-Yi; Malone, Lisa E. et al. (2018): In silico and crystallographic studies identify key structural features of biliverdin IX β reductase inhibitors having nanomolar potency. In: *The Journal of biological chemistry* 293 (15), S. 5431–5446. DOI: 10.1074/jbc.RA118.001803.
- Nieder, Carsten; Spanne, Oddvar; Mehta, Minesh P.; Grosu, Anca L.; Geinitz, Hans (2011): Presentation, patterns of care, and survival in patients with brain metastases: what has changed in the last 20 years? In: *Cancer* 117 (11), S. 2505–2512. DOI: 10.1002/cncr.25707.
- Obenauf, Anna C.; Zou, Yilong; Ji, Andrew L.; Vanharanta, Sakari; Shu, Weiping; Shi, Hubing et al. (2015): Therapy-induced tumour secretomes promote resistance and tumour progression. In: *Nature* 520 (7547), S. 368–372. DOI: 10.1038/nature14336.
- Patel, Girijesh Kumar; Khan, Mohammad Aslam; Bhardwaj, Arun; Srivastava, Sanjeev K.; Zubair, Haseeb; Patton, Mary C. et al. (2017): Exosomes confer chemoresistance to pancreatic cancer cells by promoting ROS detoxification and miR-155-mediated suppression of key gemcitabine-metabolising enzyme, DCK. In: *British journal of cancer* 116 (5), S. 609–619. DOI: 10.1038/bjc.2017.18.
- Pukrop, Tobias; Dehghani, Faramarz; Chuang, Han-Ning; Lohaus, Raphaela; Bayanga, Kathrin; Heermann, Stephan et al. (2010): Microglia promote colonization of brain tissue by breast cancer cells in a Wnt-dependent way. In: *Glia* 58 (12), S. 1477–1489. DOI: 10.1002/glia.21022.
- Quail, Daniela F.; Joyce, Johanna A. (2017): The microenvironmental landscape of brain tumors. In: *Cancer cell* 31 (3), S. 326–341. DOI: 10.1016/j.ccell.2017.02.009.
- Ramakrishna, Suresh; Kwaku Dad, Abu-Bonsrah; Beloor, Jagadish; Gopalappa, Ramu; Lee, Sang-Kyung; Kim, Hyongbum (2014): Gene disruption by cell-penetrating peptide-mediated delivery of Cas9 protein and guide RNA. In: *Genome Research* 24 (6), S. 1020–1027. DOI: 10.1101/gr.171264.113.
- Robinson, James T.; Thorvaldsdóttir, Helga; Winckler, Wendy; Guttman, Mitchell; Lander, Eric S.; Getz, Gad; Mesirov, Jill P. (2011): Integrative genomics viewer. In: *Nature biotechnology* 29 (1), S. 24–26. DOI: 10.1038/nbt.1754.
- Schmid-Burgk, Jonathan L.; Schmidt, Tobias; Gaidt, Moritz M.; Pelka, Karin; Latz, Eicke; Ebert, Thomas S.; Hornung, Veit (2014): OutKnocker: a web tool for rapid and simple genotyping of designer nuclease edited cell lines. In: *Genome Research* 24 (10), S. 1719–1723. DOI: 10.1101/gr.176701.114.
- Sentmanat, Monica F.; Peters, Samuel T.; Florian, Colin P.; Connelly, Jon P.; Pruett-Miller, Shondra M. (2018): A Survey of Validation Strategies for CRISPR-Cas9 Editing. In: *Scientific reports* 8 (1), S. 888. DOI: 10.1038/s41598-018-19441-8.

- Steeg, Patricia S. (2006): Tumor metastasis: mechanistic insights and clinical challenges. In: *Nature medicine* 12 (8), S. 895–904. DOI: 10.1038/nm1469.
- Stocker, R.; Yamamoto, Y.; McDonagh, A. F.; Glazer, A. N.; Ames, B. N. (1987): Bilirubin is an antioxidant of possible physiological importance. In: *Science (New York, N.Y.)* 235 (4792), S. 1043–1046. DOI: 10.1126/science.3029864.
- Takano, Yasuhiro; Hase-Aoki, Kumiko; Horiuchi, Hideki; Zhao, Lin; Kasahara, Yoshinori; Kondo, Shiro; Becker, Michael A. (2005): Selectivity of febuxostat, a novel non-purine inhibitor of xanthine oxidase/xanthine dehydrogenase. In: *Life sciences* 76 (16), S. 1835–1847. DOI: 10.1016/j.lfs.2004.10.031.
- Tawbi, Hussein A.; Forsyth, Peter A.; Algazi, Alain; Hamid, Omid; Hodi, F. Stephen; Moschos, Stergios J. et al. (2018): Combined Nivolumab and Ipilimumab in Melanoma Metastatic to the Brain. In: *The New England journal of medicine* 379 (8), S. 722–730. DOI: 10.1056/NEJMoa1805453.
- Uderhardt, Stefan; Martins, Andrew J.; Tsang, John S.; Lämmermann, Tim; Germain, Ronald N. (2019): Resident Macrophages Cloak Tissue Microlesions to Prevent Neutrophil-Driven Inflammatory Damage. In: *Cell* 177 (3), 541-555.e17. DOI: 10.1016/j.cell.2019.02.028.
- Valko, M.; Rhodes, C. J.; Moncol, J.; Izakovic, M.; Mazur, M. (2006): Free radicals, metals and antioxidants in oxidative stress-induced cancer. In: *Chemico-biological interactions* 160 (1), S. 1–40. DOI: 10.1016/j.cbi.2005.12.009.
- van Zijl, Franziska; Krupitza, Georg; Mikulits, Wolfgang (2011): Initial steps of metastasis: cell invasion and endothelial transmigration. In: *Mutation research* 728 (1-2), S. 23–34. DOI: 10.1016/j.mrrev.2011.05.002.
- Xue, Danfeng; Zhou, Xiongming; Qiu, Jiakuan (2020): Emerging role of NRF2 in ROS-mediated tumor chemoresistance. In: *Biomedicine & pharmacotherapy = Biomedecine & pharmacotherapie* 131, S. 110676. DOI: 10.1016/j.biopha.2020.110676.
- Yap, Y. S.; Cornelio, G. H.; Devi, B. C. R.; Khorprasert, C.; Kim, S. B.; Kim, T. Y. et al. (2012): Brain metastases in Asian HER2-positive breast cancer patients: anti-HER2 treatments and their impact on survival. In: *British journal of cancer* 107 (7), S. 1075–1082. DOI: 10.1038/bjc.2012.346.

Acknowledgements

Zuerst möchte ich mich beim gesamten Team bedanken und allen, die mir so viel persönliche und fachliche Entwicklung in den letzten Jahren ermöglicht haben.

Ein besonderer Dank geht an dich, Dr. Raquel Blázquez, ohne deine Hilfe und ständige Erreichbarkeit wäre ich an den einfachsten Aufgaben gescheitert. Du hast mir immer gezeigt, dass es sich lohnt, hart zu arbeiten und mich in meinen Vorhaben ermutigt und unterstützt. Du warst eine tolle Betreuerin und bist für mich zu einem Vorbild geworden. Vielen Dank dafür.

Weiterhin möchte ich mich bei meinem Doktorvater, Prof. Tobias Pukrop, für die unermüdliche Geduld und Unterstützung bedanken. Ich habe mich von Anfang an wohl gefühlt und gemerkt, dass nicht nur die professionelle, sondern auch die persönliche Ebene im Team stimmt. Dazu hast du durch die Zeit, die du dir Woche für Woche genommen hast, und den Humor, den du in unsere Laborbesprechungen gebracht hast, enorm viel beigetragen. Danke für die Chancen und die Förderung, die du mir ermöglicht hast.

Naturally, I have to mention you in my acknowledgements, Laura! What would the last 1,5 years have been without you? I don't even want to think about it. You have helped (and entertained) me so much, through you I have learned a lot about research and about life. I'm so glad I got to meet you and call you a friend!
Muchísimas gracias chica.

Liebe Dani, auch ohne dich wäre das hier alles nicht möglich gewesen. Sei es ein Moment der Bewunderung für deine Power-Point-Skills, eine Antwort auf jede noch so kleine Frage oder doch ein schönes Gespräch über Harry Potter – du hast meinen Laboralltag definitiv bereichert!

Ein großer Dank geht auch an Gunnar und Elena, die ich beide jeden Moment mit Fragen löchern konnte und die mir so viel Geduld entgegengebracht haben. Ein Glück, dass ihr beide im Team seid, ohne euch wäre ich wohl jetzt noch dabei die Zellkultur und Western Blots zu lernen. Gunnar, für deine absolut zuverlässige Hilfe, die langen Stunden am FACS und deine Unterstützung bei etlichen Experimenten kann ich dir nicht genug danken.

Zu guter Letzt möchte ich mich bei meinen Freunden und meiner Familie bedanken. Danke Konstantin, danke Papa, danke Moma, ihr habt mich immer ermutigt, meine Ziele zu verfolgen und auch in meinen weniger ambitionierten Phasen unterstützt und weiterhin motiviert. Ich habe während meiner gesamten Doktorarbeit immer an Mama gedacht und bin so froh, in so einer tollen Familie groß geworden zu sein. Ich bin mir sicher, dass sie genau so stolz ist wie ihr und genau das motiviert mich jeden Tag wieder, eine tolle Ärztin zu werden und an meinen Werten festzuhalten.

Curriculum Vitae

Ellinor Görgen

Born on June 2nd, 1997 in Hildesheim, Germany.

E-Mail: ellinor.goergen@googlemail.com

EDUCATION

10/2015 – 12/2022 Medical studies at University of Regensburg, Germany
Degree: state examination 2022

Doctoral thesis:
“Targeting the ROS-defense of tumor cells as a potential target against brain metastasis”

10/2021 – 12/2022 Working student at iuvando Health GmbH

11/2021 USMLE Step 2 CK

07/2021 USMLE Step 1

02/2017 - 04/2019 Tutor at the dissection course of human anatomy

2007 - 2015 Wildermuth-Gymnasium Tübingen, Abitur

AWARDS AND SCHOLARSHIPS

10/2019 - present

Scholar of German National Academic Foundation

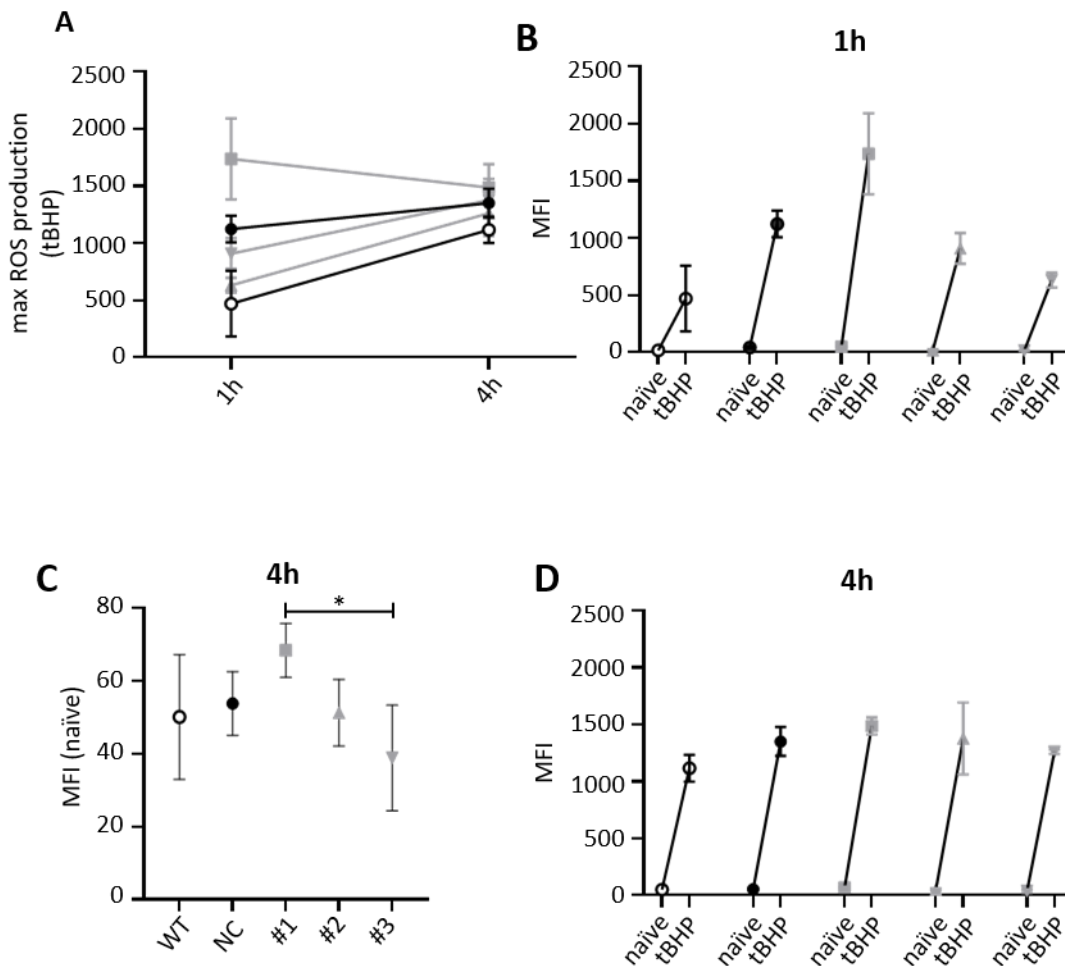
Supplemental material

Sample		INDEL	DNA	Protein
X1.3	Allele No.#1	1nt deletion, A->G	c.1005A>G; c.1004delC;	p.Glu8>Ser (generation of a stop codon after 5 (Ser-Leu-Ser-Ser-Leu-Stop) aminoacids)
	Allele No.#2	3nt deletion	c.1005_1007del;	p.Asp7del
	Allele No.#3			
	Allele No.#4			
	Allele No.#5			
X1.4	Allele No.#1	79nt deletion	c.967_1046+?del; not completely sequenced	
	Allele No.#2	1nt deletion	c.1004delC	(generation of a stop codon after 5 (Ser-Leu-Ser-Ser-Leu-Stop) aminoacids)
	Allele No.#3	6nt deletion, C>A	c.1004C>A; c.998_1003del;	p.Glu8Leu9del
	Allele No.#4	SNP C>G	c.1004C>G;	p.Glu8>Gln
	Allele No.#5	5nt deletion	c.1004_1008del;	p.Asp7del+Glu8>Val (generation of stop codon 50 aminoacids later)
	Allele No.#6			
X1.5	Allele No.#1	20nt deletion	c.1004_1023del;	p.Met1>Ile; p.Thr2Arg3Thr4Thr5Val6Asp7Glu8del
	Allele No.#2	6nt deletion, T>A; A>T	c.1006T>A; c.1005A>T; c.999_1004del;	p.Glu8Leu9del; p.Asp7>Val
	Allele No.#3	7nt deletion, T>A	c.1003T>A; c996_1002del;	p. Glu8>Val; p.Leu9Val10del (generation of stop codon 50 aminoacids later)
	Allele No.#4	36nt deletion	c.976_1011del;	p.Val6Asp7Glu8Leu9Val10Phe11Phe12Val13Asn14Gly15Lys16Lys17del
	Allele No.#5	23nt deletion; G>T; A>T;C>T	c.984_1006del; c.1007C>T; c.1009A>T; c.1012G>T;	p.Asp7>Arg; p.Glu8Leu9Val10Phe11Phe12Val13Asn14; p.Val6>Glu; p.Thr5>Lys
	Allele No.#6			
X1.6	Allele No.#1	9nt deletion	c.999_1007del;	p.Asp7Glu8Leu9del
	Allele No.#2	1nt deletion	c.1003del;	p.Glu8>Gly (generation of stop codon 5 (Gly-Trp-Ser-Ser-Leu-Stop) aminoacids later)
	Allele No.#3			
	Allele No.#4			
	Allele No.#5			
X2.1	Allele No.#1	52nt deletion; C>T	c.990_1041del; c.1042C>T;	p.Met1>del
	Allele No.#2	1nt deletion	c.1015del;	p.Thr4>Lys (generation of stop codon 3 (Thr-Lys-Arg-Stop) aminoacids later)
	Allele No.#3			
	Allele No.#4			
	Allele No.#5			
X2.2	Allele No.#1	84nt deletion	c.968_1052+?del; breakpoint not sequenced;	p.Met1del
	Allele No.#2	3nt deletion	c.1014_1016del;	p.Thr4del
	Allele No.#3			
	Allele No.#4			
	Allele No.#5			
X2.3	Allele No.#1	2nt deletion	c.1014_1015del;	p.Thr4>Asn (generation of stop codon 3 (Asn-Gly-Arg-Stop) aminoacids later)
	Allele No.#2	8nt deletion	c.1011_1018del;	p.Arg3>Ser (generation of stop codon 2 (Ser-Ser-Stop) aminoacids later)
	Allele No.#3	1nt deletion	c.1015del;	p.Thr4>Lys (generation of stop codon 2 (Lys-Arg-Stop) aminoacids later)
	Allele No.#4	9nt deletion	c1014_1022del;	p.Thr2Arg3Thr4del
	Allele No.#5			
X3.1	Allele No.#1	15nt deletion	c.1022_1036del;	p.Met1del
	Allele No.#2	SNP G>T	c.1027G>T;	
	Allele No.#3	3nt deletion	c.1026_1028del	
	Allele No.#4			
	Allele No.#5			
X3.3	Allele No.#1	8nt deletion; G>A	c.1025_1032del; c.1033G>A;	p.Met1>Leu
	Allele No.#2	11nt deletion	c.1022_1032del;	p.Met1del
	Allele No.#3	9nt deletion	c.1028_1036del	
	Allele No.#4	4nt insertion; A>T; G>A; T>C	c.1027_1028insGAGT; c.1028T>C; c.1029G>A; c.1030A>T	p.-3_-2insMetThrPro
	Allele No.#5			
X3.4	Allele No.#1	17nt deletion	c.1019_1035;	p.Met1del
	Allele No.#2	24nt deletion	c.1019_1042;	p.Met1del
	Allele No.#3	1nt deletion	c.1028del	
	Allele No.#4	3nt deletion	c.1026_1028del	
	Allele No.#5		c.1028del	
	Allele No.#6			
X3.5	Allele No.#1	1nt deletion	c.1028del	
	Allele No.#2	24nt deletion	c.1013_1036del	p.Met1del
	Allele No.#3	1nt deletion	c.1027del	
	Allele No.#4			
	Allele No.#5			
X3.6	Allele No.#1	9nt deletion	c.1028_1036del	
	Allele No.#2	33nt deletion	c.1013_1045del	p.Met1del
	Allele No.#3			
	Allele No.#4			
	Allele No.#5			

Sample		% of reads	OOF/IF/no Indel	Aminoacid switch	resulting in KO	summary Xdh
X1.3	Allele No.#1	44	OOF	Substitution no, deletion yes (Glu>Ser oof)	yes	0,56
	Allele No.#2	39	IF	one Aminoacid deletion	unclear	
	Allele No.#3	17	no INDEL			
	Allele No.#4					
	Allele No.#5					
X1.4	Allele No.#1	34	OOF	Aminoacid deletion	yes	0,46
	Allele No.#2	24	OOF	yes (Glu>Ser oof)	yes	
	Allele No.#3	20	IF	Glu and Leu deletion	unclear	
	Allele No.#4	13	IF	yes (Glu>Gln)	unclear	
	Allele No.#5	9	OOF	Asp del; Glu>Val oof	yes	
	Allele No.#6	13	no INDEL			
X1.5	Allele No.#1	25	OOF	Met>Ile(no start codon), deletion 7 aminoacids	yes	0,4
	Allele No.#2	24	IF	Glu and Leu deletion	unclear	
	Allele No.#3	23	OOF	Leu and Val deletion; Glu>Val oof	yes	
	Allele No.#4	12	IF	12 aminoacid deletion	likely	
	Allele No.#5	12	OOF	Asp>Arg, 7 aminoacid deletion, Val>Glu, Thr>Lys	yes	
	Allele No.#6	4	no INDEL			
X1.6	Allele No.#1	51	IF	3 Aminoacid deletion	unclear	0,51
	Allele No.#2	49	OOF	Glu>Gly oof	yes	
	Allele No.#3					
	Allele No.#4					
	Allele No.#5					
X2.1	Allele No.#1	55	OOF	Met1 deletion (no start codon)	yes	0,01
	Allele No.#2	44	OOF	Thr>Lys oof	yes	
	Allele No.#3	1	no INDEL			
	Allele No.#4					
	Allele No.#5					
X2.2	Allele No.#1	54	IF	Met1 deletion (no start codon)	yes	0,46
	Allele No.#2	46	IF	Thr4 deletion	unclear	
	Allele No.#3					
	Allele No.#4					
	Allele No.#5					
X2.3	Allele No.#1	26	OOF		yes	0,26
	Allele No.#2	25	OOF		yes	
	Allele No.#3	23	OOF		yes	
	Allele No.#4	23	IF	3 aminoacid deletion	unclear	
	Allele No.#5	3	no INDEL			
X3.1	Allele No.#1	36	IF	Met1 deletion (no start codon)	yes	0,67
	Allele No.#2	36		SNP not in exon	unclear	
	Allele No.#3	27	IF	Deletion not in exon	unclear	
	Allele No.#4	1	no INDEL			
	Allele No.#5					
X3.3	Allele No.#1	28	OOF	Met1 deletion (no start codon)	yes	0,46
	Allele No.#2	26	OOF	Met1 deletion (no start codon)	yes	
	Allele No.#3	24	IF	Deletion not in exon	unclear	
	Allele No.#4	21	IF	Insertion of start codon-Thr-Pro-normal enzyme	unclear	
	Allele No.#5	1	no INDEL			
X3.4	Allele No.#1	33	OOF	Met1 deletion (no start codon)	yes	0,85
	Allele No.#2	24	IF	Met1 deletion (no start codon)	yes	
	Allele No.#3	22	OOF	Deletion not in exon	unclear	
	Allele No.#4	20	IF	Deletion not in exon	unclear	
	Allele No.#5	42	OOF	Deletion not in exon	unclear	
	Allele No.#6	1	no INDEL			
X3.5	Allele No.#1	42	OOF	Deletion not in exon	unclear	0,67
	Allele No.#2	33	IF	Met1 deletion (no start codon)	yes	
	Allele No.#3	24	OOF	Deletion not in exon	unclear	
	Allele No.#4	1	no INDEL			
	Allele No.#5					
X3.6	Allele No.#1	36	IF	Deletion not in exon	unclear	0,73
	Allele No.#2	27	IF	Met1 deletion (no start codon)	yes	
	Allele No.#3	37	no INDEL			
	Allele No.#4					
	Allele No.#5					

Detailed summary of mutations in each sample.

Legend: unclear: amino acid switch/deletion ≤ 3 amino acids; likely: amino acid switch/deletion ≥ 4 ; yes: oof INDEL or Met1 deletion; no Indel: no Indel or failed alignment; summary Xdh: unclear+likely+no INDEL



Analysis of ROS production through DCFDA assay.

(A) Comparison of dynamics of maximum ROS value after 1 h and 4 h of tBHP stimulation **(B)** Plotted are the naïve ROS values of the KO-clones compared to the controls after 4 h of incubation with DCFDA. **(C and D)** Comparison of the inclination of naïve vs stimulated (tBHP) ROS values after 1 h (C) and 4 h (D) of DCFDA and tBHP treatment (mean + SD, $n = 3$, ordinary one-way ANOVA, MFI = mean fluorescent intensity).